PLOS ONE

RESEARCH ARTICLE

Pressure regulated basis for gene transcription by delta-cell micro-compliance modeled in silico: Biphenyl, bisphenol and small molecule ligand models of cell contraction-expansion

Hemant Sarin *

Freelance Investigator in Translational Science and Medicine, Charleston, West Virginia, United States of America

* hsmd74@hotmail.com

Citation: Sarin H (2020) Pressure regulated basis for gene transcription by delta-cell micro-compliance modeled in silico: Biphenyl, bisphenol and small molecule ligand models of cell contraction-expansion. PLoS ONE 15(10): e0236446. https://doi.org/10.1371/journal.pone.0236446

Editor: Esra Bozgeyik, Tekirdag Namik Kemal University, TURKEY

Received: April 3, 2020

Accepted: July 6, 2020

Published: October 6, 2020

Data Availability Statement: All relevant data are within the paper.

Funding: The author(s) received no specific funding for this work.

Competing interests: The authors have declared that no competing interests exist.

Abbreviations: P, octanol-to-water partition coefficient; vdWD, van der Waals diameter; Log *P*/vdWD, Log *P*/vdWD; $L_{external/internal\ struct}$ ·

Abstract

Molecular diameter, lipophilicity and hydrophilicity exclusion affinity limits exist for small molecule carrier-mediated diffusion or transport through channel pores or interaction with the cell surface glycocalyx. The molecular structure lipophilicity limit for non-specific carrier-mediated transmembrane diffusion through polarity-selective transport channels of the cell membrane is $L_{external\ structure} \cdot H_{polar\ group}^{-1}$ of ≥ 1.07. The cell membrane channel pore size is > 0.752 and < 0.758 nm based on a 3-D ellipsoid model (biphenyl), and within the molecular diameter size range 0.744 and 0.762 nm based on a 2-D elliptical model (alkanol). The adjusted van der Waals diameter (vdWD, adj; nm) for the subset of halogenated vapors is predictive of the required MAC for anesthetic potency at an initial (-) Δ C_{micro} effect. The molecular structure $L \cdot H_{polar\ group}^{-1}$ for Neu5Ac is 0.080, and the $L \cdot H_{polar\ group}^{-1}$ interval range for the cell surface glycocalyx hydrophilicity barrier interaction is 0.101 (Saxitoxin, Stx; $L_{internal\ structure} \cdot H_{polar\ group}^{-1}$) - 0.092 (*m*-xylenediamine, $L_{external\ structure} \cdot H_{polar\ group}$). Differential predictive effective pressure mapping of gene activation or repression reveals that *p*-dioxin exposure results in activation of AhR-Erβ (Arnt)/Nrf-2, Pparδ, Errγ (LxRα), Dio3 (Dio2) and Trα limbs, and due to high affinity Dio2 and Dio3 (OH-TriCDD, $L_{ext} \cdot H^{-1}$: 1.91–4.31) exothermy-antagonism (Δ contraction) with high affinity T_4/rT_3-TRα-mediated agonism (Δ expansion). *co*-planar PCB metabolite exposure ($L_{ext} \cdot H^{-1}$: 1.95–3.91) results in activation of AhR (Erα/β)/Nrf2, Rev-Erbβ, Errα, Dio3 (Dio2) and Trα limbs with a Δ C_{micro} contraction of 0.89 and Δ C_{micro} expansion of 1.05 as compared to *p*-dioxin. *co*-, *ortho*-planar PCB metabolite exposure results in activation of Car/PxR, Pparα (Srebf1,—Lxrβ), Arnt (AhR-Erβ), AR, Dio1 (Dio2) and Trβ limbs with a Δ C_{micro} contraction of 0.73 and Δ C_{micro} expansion of 1.18 (as compared to *p*-dioxin). Bisphenol A exposure ($L_{ext\ struct} \cdot H^{-1}$: 1.08–1.12, BPA–BPE, Errγ; BPAF, $L_{ext\ struct} \cdot H^{-1}$: 1.23, CM Erα, β) results in increased duration at P_{eff} for *Timm8b* (P_{eff} 0.247) transcription and in indirect activation of the AhR/Nrf-2 hybrid pathway with decreased duration at P_{eff} 0.200 (*Nrf1*) and increased duration at P_{eff} 0.257 (*Dffa*). The Bpa/Bpaf convergent pathway C_{micro} contraction-expansion response increase

$H_{polar\ group}^{-1}$, internal or external lipophilicity per vdWD per polar group hydrophilicity per vdWD; IS, insufficiently separated in space; SS, sufficiently separated in space; *esebssiwaago*T_Q, episodic sub-episode block sums split-integrated weighted average-averaged gene overexpression tropy quotient (P_{eff}); P_{eff}, effective intracellular pressure; Σ min·count, summed $t_{1/2}$ at receptor · receptor count product; K_d, dissociation constant; ARE, anti-oxidant response element (Nrf-2/Nrf-1); AHRE, androgen receptor response element; ERE, estrogen response element; GRE, glucocorticoid receptor response element; PPRE, peroxisome proliferator response element; PBREM, constitutive androstane receptor response element, phenobarbital-inducible; PXRE, pregnane receptor response element; TRE, half-site TRE, thyroid hormone receptor response element, retinoid X receptor response element, AP-1 response element (Jun/Fos); XRE, DRE, xenobiotic response element; CM, cell membrane; SCM, subcellular membrane; TCDD, 3,7,8-tetrachlorodibenzo-p-dioxin; PCB, polychlorinated biphenyl; PDBE, polybrominated ether; AhR, aryl hydrocarbon receptor; Arnt, AhR-related nuclear translocator; TCPOBOP, 1,4-Bis[2-(3,5-Dichloropyridyloxy)] benzene; REF, RPF, relative potency factor; TEF, toxicity equivalency factor; BPA, bisphenol A; DBP, dibutylphthalate; DES, diethylstilbesterol; MBP, BP, monobutylphthalate; SRC-1, steroid receptor coactivator-1.

in the lower P_{eff} interval is 0.040; in comparison, small molecule hormone Δ C_{micro} contraction-expansion response increases in the lower P_{eff} intervals for gene expression $\leq$ 0.168 (Dex· GR) $\geq$ 0.156 (Dht · AR), with grade of duration at P_{eff} (*min·count*) of 1.33x10^5 (Dex/Cort) and 1.8–2.53x10^5 (Dht/R1881) as compared to the (-) coupled (+) Δ C_{micro} P_{eff} to 0.136 (*Wnt5a*, *Esr2*) with applied DES (1.86x10^6). The subtype of trans-differentiated cell as a result of an applied toxin or toxicant is predictable by delta-C_{micro} determined by P_{eff} mapping. Study findings offer additional perspective on the basis for pressure regulated gene transcription by alterations in cell micro-compliance (Δ contraction-expansion, C_{micro}), and are applicable for the further predictive modeling of gene to gene transcription interactions, and small molecule modulation of cell effective pressure (P_{eff}) and its potential.

Introduction

The mechanism of detoxification in human cells is induction of the phase I aryl hydrocarbon receptor (*AHR*)/AhR nuclear translocator (*ARNT*) pathway by transcriptional activation of P450 monooxygenase system enzyme genes (*CYP1A1*, *CYP1B1*) inseries with phase II nuclear respiratory factor-2 (NRF-2, *NFE2L2*) activation of UDP-glucoronosyl transferases (ie *UGT1A6*, *UGT1A7*), glutathione synthesis (*GCLC*) and NAD(P)H-quinone acceptor oxidoreductase (*NQO1*), and glutathione S-transferases (ie *GSTA1*) [1–3], within which the constitutive androstane receptor pathway (CAR, *NR3C1*) also plays a role in phase I/II metabolism (ie *CYP3A4*, *UGT1A1*) [4]. *z*, *x*-plane alignment establishes the reading frame for transcriptional factor binding and activation or repression of genes with or without recruitment [5], which results in the differentially-increased activation of *CYP1A1* and *CYP1B1* genes by co-activator adapter RIP140 recruited to the AhR/ARNT binding affinity xenobiotic response element (XRE) or to the 15mer full-site estrogen response element sequences (ERE) by liganded ERα/β dimers [6–8], transcriptional regulation of *SREBF1* by a functional CAR and LXRα or LXRβ interaction [4], or activation of the cell membrane *DIO1* gene by SRC-1 co-adapter recruited to T_3-liganded TRβ [9].

These pathways are activated by a spectrum of small molecule lipophiles of variable affinity either directly or indirectly, including in response to the classic high-affinity agonists, 2,3,7,8-tetrachlorodibenzo-*p*-dioxin (TCDD) at 10^{-12} M concentration for activity *in vivo* [1], as compared to bisphenols such as BPA with bioavailable concentration approaching 2 ng/mL levels in blood for involvement of high- and mid-affinity binding to ERRγ and GPR30 receptors respectively for those well-characterized [10–12]. Furthermore, since such exotoxicants have bioaccumulated in the ecosystem, toxicity relative potency factor (REP)-adjusted additive TEF TEQs have been developed on the basis of combinatory data of *in vivo* dose escalation (ie ED_{50}) and competitive assay studies (EC_{50}, K_D) such as from kinetic *in silico* models as fractional measures of planar (*co*-, *ortho*-) atom structural affinity (TCDD K_{CALC} 10^{-10}; TEF 1) [13, 14]. With serum globulin-binding being high affinity for endogenous ligands, and OH-, $MeS(O_4)$-PCB metabolites (Σ) present in the 0.3–30 nM to 0.07–0.7 μM range in local tissue resident adipocytes (ng/g lipid) [15, 16], it can be hypothesized that there is high-affinity pharmacokinetic non-competition at the cell membrane (CM) or subcellular membrane (SCM) enzyme/receptor, and/or nuclear receptor (AhR/ARNT) for exogenous lipophile and metabolite bioaccumulants such as OH-, $MeS(O_4)$-PCBs, as in prior study it has been noted that dioxin-like *co*-planar PCB-77 alters membrane fluidity less than *ortho*-substituted PCB-52 [17].

Polarity-specific transmembrane channels of varying pore sizes exist for facilitated diffusion of water, electrolytes, saccharides and amino acids into eukaryotic cells [18–20], though which

non-polar small molecules will diffuse, both endogenous and exogenous. The permeation thresholds for small molecule hydrophile micro-molecular permeability across respiratory epithelial (macula occludens, adherens; non-pericytotic) and brain endothelial barriers (zona occludens) are lower than predictable based on molecular diameter of equivalently-sized neutral small molecules due to greater hydrophilicity for size (-Log *P*/vdWD, nm^{-1}), limit interval van der Waals diameters (vdWD) for anionic, neutral and cationic small molecule hydrophiles are 0.50–0.63 nm, between 0.66–0.73/0.81 nm, and at around 0.55 nanometers, respectively [21]. With small molecule hydrophile plasma half-life and lipophile tissue biodistribution as determinants, it deserves to be considered that there exist various molecular exclusion and/or philicity affinity limits for exogenous ligands of receptors and channels (ie Saxitoxin, Tetrodotoxin, 1,2-diaminocyclohexane) and small molecule hormones of various classes (ie Cortisol, Aldosterone, E_2, DHT), which include: 1, a structural hydrophilicity for interactions with the epicellular proteoglycan matrix; 2, interval range of electropolarity at channel pore entry zone for endocytic transport; 3, a transition to selective facilitated diffusion and from polarity-selective to non-specific facilitated diffusion, and 4, the limit at which molecular diameter becomes the determinant of transmembrane channel transport subcellularly.

In this study, the 2,3,7,8-tetrachlorodibenzo-p-dioxin (TCDD), *co*-planar and *ortho*-planar PCB-activated, diethylstilbesterol (DES) and bisphenol (BPA, BPAF) gene regulation pathways are further characterized by differential effective intracellular pressure (P_{eff}) mapping of delta-cell micro-compliance in response to exposure *in silico*, these being model toxicant-mediated gene activation molecular pathways, as are activation pathways of small molecule lipophiles (ie halogenate ethers), hydrophile channel substrates or receptor agonists (ie lactate, mannitol; *m*-xylenediamine) as compared to those of endogenous steriod axis ligands (ie Estradiol, E_2; Dht). The $L_{external/internal} \circ H_{external}^{-1}$ quotient, isomerism-adjusted $L_{external/internal} \circ H_{external}^{-1}$ quotient for acyclic hydroxylates, and vdWD (nm; sub-Å) are applied as measures to model cellular interactions by affinity and molecular size; correlative differential P_{eff} mapping of gene expression in *esebssiwaagoT*$_Q$ units is applied to determine the delta (Δ)-range of P_{eff} as a measure of cell micro-compliance (C_{micro},); and the Σ *min·count* is determined by power regression as a measure of the pressure grade of effect for a subset of molecular size-excluded steroid axis ligands. Therefore, in this study the transcriptional regulation effects will be studied by differential predictive (pred) effective intracellular pressure (P_{eff}) mapping of delta (Δ)-cell micro-compliance to further explore the underlying basis for cell type-specific alterations in gene transcription as it has been determined that *x*, *z*-plane alignment of intergene tropy results in gene transcription in response to applied small molecule inverse agonists over a range of molecular diameter and philicity modeled *in silico*.

Methods

Selection of small molecules for study and determination of molecular size exclusion and hydrophilicity affinity interaction limits

Representative classes of small molecules of increasing complexity with non-chiral carbons (2-D elliptical) and/or a chiral carbon (3-D ellipsoid) with halogen-substituted atoms (*para*-, *ortho*- and *co*-/*meta*-) or functional group charge separation (sufficiently separated in space, SS; insufficiently separated in space, IS) were sampled for the study inclusive of small molecules of sedimentary origin (C_1-C_{13} alkanes: methane, ethane, propane, butane), biosynthetic small molecules (C_2-C_{13} alcohols: nonalol, decanol, undecanol, dodecanol, tridecanol; saxitoxin (Stx), tetradotoxin (Ttx); *trans*-retinol, α-tocopherol; aldosterone (Ald), cortisol (Cort), dexamethasone (Dex), 17β-estradiol E_2, dihydroxytestosterone (Dht), and thyroxine T_4), and synthetic molecules (tetraethyllead, cyclononalol, acetochlor; diethylstilbestrol (DES),

methyltrienolone; polybrominated diphenyl ether-209; 2,3,7,8-tetrachlorodibenzo-*para*-dioxin, Tcdd; *co*-planar polychlorinated biphenyls Pcb-77, Pcb-126; *co*-planar, *ortho*-planar Pcb-106, -153, -172, -180; *ortho*-planar Pcb-54, -95, -132 and metabolites; bisphenols A, C, E and AF (chiral); branched C_2-C_4 halogenates: halothane, desflurane, isoflurane, enflurane, sevoflurane; *m*-xylenediamine; phthalate (mono-, di-*n*-butyl)). The predicted values of Log *P* (unitless), molecular weight (Da), van der Waals molecular volume ($Å^3$) and polar surface area ($Å^2$) were applied (www.chemicalize.org) for determinations of molecular diameter (vdWD; nm), and whole or part-molecular lipophilicity or hydrophilicity per diameter (Log *P*/vdWD; nm^{-1}) inclusive of functional groups as previously reported [21]. Additional parameters were determined inclusive of i) molecular exterior or interior structural lipophilicity per diameter (vdWD, 3-digit sub-Å; $L_{external\ (or\ internal)}$; nm^{-1}) and exterior structural hydrophilicity per diameter ($H_{external}$; nm^{-1}) with determinations of ii) polar surface area (psa) Log *P*/vdWD (nm^{-1}) for intervening single atoms, and iii) the intermediate values of Log *P*/vdWD for part-molecular structures, as:

$$\frac{L\text{external (internal)}}{H\text{external}} = \frac{10^{(L\text{part})n} + 10^{(L\text{isophile part})n}}{10^{(H\text{part})n} + 10^{(H\text{isophile polar part})n}}$$

When the isophile is an external or intervening ether, the polar part *P* is 0.3319 (-0.479 nm^{-1}) for mono-oxygen and 1.8197 (0.260 nm^{-1}) for the mono-ether adjustment; and for a 2^{ary} amine, the polar part *P* is 0.2048 (-0.624 nm^{-1}) for mono-nitrogen with no additional adjustment. The calc $L_{external/internal}$ ˚ $H_{external}^{-1}$ is normalized to methanol as the reference standard, 2.75 (Ch_3oh nl).

Determination of molecular structure-polar group substituted lipophilicity limit for non-specific transmembrane transport

The Log P_{alkane}/vdWD $_{alkane}$ ($L_{external\ structure}$)]/[Log P_{OH}/$vdWD_{OH}$ ($H_{polar\ group}$)] ratio quotient (abs value) was determined for the subset of 1- to 4-C simple alkane hydroxylates (methanol, 1-ethanol, 1-propanol, 1,2-propanol, 1,3-propandiol, 1,2-butanediol, 1,2-ethandiol and 2,3-glycer-1-ol). The unadjusted for isomerism Log *P*/vdWD was applied for presence of single hydroxyl (OH) group of -1.05 nm^{-1} (methanol, 1-ethanol), and the adjusted for external isomerism hydrophilic moiety Log *P*/vdWD was applied for the presence of dual hydroxyl group isomerism, as:

$$L_{external} \cdot H_{OH\ group}{}^{-1}\ (\text{adj}) = \frac{L_{external}}{-1.05\ nm^{-1} + (1/i+1)(0.437)}$$

$i + 1$ is the number of carbon bonds in-between the initial hydroxylated position and the subsequent hydroxylated position for a polar group functionalized simple aliphatic. Based on the calc nl $L_{external/internal}$ ˚ $H_{external}^{-1}$ limit for non-specific carrier-mediated diffusion, the interval range limits of molecular hydrophilicity for endocytosis and channel wall domain affinity interactions for the remainder of the molecules of the study sample.

Determination of the gradient of effect for duration at P_{eff} for steroid axis ligands at cell membrane receptors

The minute-receptor counts for corticosteroid axis receptor ligands at GR and MR (Cortisol, Cort; Dexamethasone, Dex; Aldosterone, Ald), estrogen axis receptor ligands at ERα (17β-Estradiol; Diethylstilbestrol, DES), androgen axis receptor ligands (Dihydroxytestosterone, DHT; methyltrienolone, R1881) and macromolecular marker as standard (Insulin-like growth factor II) for negative $\Delta\ C_{micro}$ shift at lower limit of P_{eff}. The $t_{1/2}$ at receptor·receptor count

(min·count) was determined as a product sum of half-lives at receptor and the cell membrane receptor count, and as Σ *min·count* in case of co-axis receptor system expression (MR, GR). The $t_{1/2}$ at receptor for DES, DHT and R1881 were determined by *x*, *y*-plotting of radiolabeled hormone disassociation constants (K_D, *x*-axis) and known $t_{1/2}$ at receptor (min, *y*-axis). The grade of P_{eff} was stratified by hormone ligand and receptor subtype, positive to negative by *min·count*, as determined by the semi-exponential power regression, and adjusted for cell receptor count:

$$[f(\mathrm{x}) = 3.0\mathrm{E} - 05 \cdot (\mathrm{K_d})^{0.6784}] \cdot n \qquad R^2 = 0.955$$

Selection of genes for study and effective intracellular pressure mapping of pathway genes

Representative genes were selected for effective intracellular pressure (P_{eff}) mapping of cellular pathway regulation by small molecules of the study sample (ie acyclic C_2-C_4 halogenates; 2,3,7,8-tetrachlorodibenzo-*para*-dioxin (*p*-dioxin); *co*-planar PCB-126; *co*-, *ortho*-planar PCB-153; bisphenol A, bisphenol AF; biosynthetic, ie tetradotoxin), which includes the following genes, which fall into the following categories:

i. Transcription factor/adapter [*AHR*, *AR*, *ARNT*, *ARNTL*, *ATF3; CEBPD*, *DDIT3 (CHOP)*, *CREB1*, *ESR1*, *ESR2*; *ESRRG*, *ESRRA*; *FOSB*, *FOS*, *FOXA1*; *GTF2IRD1*, *HNF4A*, *JUN*; *NCOR1*, *NCOR2*; *NFE2L2* (NRF-2), *NR1D1* (Rev-Erbα), *NRID2* (Rev-Erbβ), *NR3C1* (GR), *NR3C2* (MR); *NR1H3* (LXRα), *NR1H2* (LXRβ); *NR1I2* (PXR), *NR1I3* (CAR), *NRF1*; *PPARA*, *PPARD*, *PPARG*; *PER1*, *RXRA*, *RXRB*, *RARA*, *RARB*, *RARG*, *SIM1*, *SIN3A*, *SREBF1*, *TGIF1*, *THRA*, *THRB*; *DBP; HOXA9*, *HOXA10*, *HOXA11*, *HOXA13*; *KLF4*; *WNT5A*];

ii. Transcription factor co-adapter/co-adapter [*PPARGC1A* (PGC1α), *NRIP1*, *NCOA1* (SRC-1), *GADD45A*; *GADD45B*, *CIDEA*; *DFFA*];

iii. Cell membrane enzymes/proteins or channels/subunits [*ADAM8*, *EXOC7*, *NOS1*; *DIO1*, *DIO3*; *MBP*; *SLC9A1* (NHE-1), *SLC2A4* (Glut-4)];

iv. Cell membrane antigen/receptor (*CEACAM1*, *CEACAM5*; *TSPAN14*; *TRFC*);

v. Cell membrane receptor ligand [*DLK1* (PREF-1)];

vi. Cytochrome P450 monooxygenases [*CYP1A1*, *CYP1B1*, *CYP1A2*, *CYP2B6*, *CYP2E1*, *CYP3A5*, *CYP3A7*, *CYP5A*, *CYP11B1* (11-β-hydroxylase), *CYP11B2* (aldosterone synthase), *CYP17A1* (17, 20-lysase)];

vii. Cytosolic/nuclear enzyme, DNA or mRNA adapter (*PPP1R9B*, *CUL2*, *PLEKHG4*, *RAP-GEFL1*; *CCND1*, *CDKN1A*; *CIDEA*; *DFFA*, *CASP3*; *MEG3*, *MIAT*, *MIR132*);

viii. Intracellular enzymes [*ALAS1*, *ALAS2*; *ACSM2A*, *ALDH3A1*, *CAT*, *DAO*, *DUSP1*; *FABP4* (aP2), *FABP5*, *FABP6*; *FASN*, *GSTM2*, *ME1*, *MT1A*, *NQO1*, *PCK1*, *PER1*, *TIPARP*; *SCD*, *SCD5*; *LGAL1*, *UGT1A_* locus (*UGT1A1*, *UGT1A6*, *UGT1A7*)];

ix. Mitochondrial-specific membrane-associated (*COX6C*, *COX8C*, *CYCS*; *TIMM8B*);

x. Mitochondrial-specific protein synthesis/cell cycle regulation (*TFB2M*);

xi. Rough endoplasmic reticulum enzyme/receptor (*DIO2*, *GPR30*, *RESP18*, *OLFM1*); and

xii. Secretory peptides/hormones [*COL1A1*, *TFF1* (pS2), *SFTPC*, *PMCH*, *A2M*].

The gene/gene loci positions of protein coding and non-coding genes/gene loci were utilized as previously reported (www.genecards.org; lncipedia.org) for determinations of the episodic sub-episode block sums split-integrated weighted average-averaged gene overexpression tropy quotient as previously reported. The sub-episode block sums and averages were determined for gene loci as categorized by episode and initial SEB structure [5, 22], 1) Episode 3 ($\leq$ 11,864, 7 SEB); 2) Episode 2 ($>$ 11,864 $\leq$ 265,005, 5 SEB); 3) Episode 4 ($>$ 265,095 $<$ 521,757; 9 SEB); 4) Episode 5 ($\geq$ 521,757 $<$ 784,883; 11 SEB); and 5) Episode 5 ($\geq$ 784,883; 13 SEB). The upstream and downstream part anisotropic sub-episode block sum (*uppasebs*, *dppasebs*) and correlate upstream and downstream part anisotropic sub-episode block sum split integrated weighted average (*uppasebssiwa*, *dppasebssiwa*) were determined for further calculation of the weighted average upstream and downstream part mesotropic sub-episode block sum split integrated weighted average (*uppmsebssiwa*, *dppasebssiwa*) and the final *esebssiwaagoT*$_{Q}$ quotient as a measure of effective intracellular pressure (P_{eff}). The increase (plus %; ratio Δ) or decrease (minus %; ratio Δ) in the differential P_{eff} mapping duration response was determined for the subset of marker genes as standards, based on which the placement of additional genes of study sample was determined, as either an increase (or decrease) in duration at P_{eff}, as:

$$\sum_{0}^{n}(uppaseb, dppaseb), \sum_{0}^{m}(uppmseb, dppmseb) \quad \text{(i)}$$

$$\int_{0}^{h}(dppasebssiwa, dppmsebssiwa)\, dt$$

$$\int_{0}^{d}(uppasebssiwa, uppmsebssiwa)\, dt \quad \text{(ii)}$$

$$esebssiwaagoT_{Q}, \quad \text{(iii)}$$

$$\%\text{inc, dec } (+, -\Delta \text{ ratio}), \geq 2\text{−x } P \text{ for std marker mRNA}$$

Determination of range of cell micro-compliance response by correlative differential gene expression P_{eff} mapping

Representative gene overexpression range of cell micro-compliance P_{eff} mapping upper and lower bounds were determined for applied TCDD, *co*-planar PCB (ie OH-PCB-77; OH-PCB-126), and *ortho*-, *co*-, *ortho*-planar (ie OH-PCB-54; OH-PCB-95; OH-PCB-153) *in silico*, as follows:

$$C_{micro} = \frac{k}{\begin{matrix} P_{eff\ TCDD\ upper} & P_{eff\ TCDD\ \ lower} \\ P_{eff\ co-planar\ upper} & P_{eff\ co-planar\ lower} \\ P_{eff\ co-,\ ortho-planar\ upper} & P_{eff\ co-,\ ortho-planar\ lower} \end{matrix}}$$

The P_{eff} for activation of gene marker standards (std) in addition to predicted differential P_{eff} gene expression of exposure-modeled cell(s) was determined on the basis of intracellular *esebssiwaagoT*$_{Q}$ pressure units (P_{eff}). The upper and lower bounds of the expansion response were determined as subtractive residuals of the upper direction maxima from the lower direction contraction responses from the respective minima in each direction of the.PCB-95 or

PCB-153 exposed normal cell modeled *in silico*. The contraction-expansion response range of cell micro-compliance (C_{micro}) was then determined as the difference between max and min bounds of range (BoR) in C_{micro} P_{eff} range units. Pairwise delta (Δ) micro-compliance (C_{micro}) comparisons between the range of the cellular contraction-expansion response to *p*-dioxin exposure (TCDD, std; bracket 1), and *co*-planar PCB-126 (bracket 2 vs 1) and *co*-, *ortho*-planar PCB-95/-153 (bracket 3 vs 1) were performed [Δ, ratio expansion; a.u.].

Results

van der Waals diameter and external structural lipophilicity per polar group hydrophilicity of small molecule hydroxylates that are polarity-specific transport channel substrates

Methane (CH_4) has a Log *P* of 1.08, and a vdWD of 0.373 nm with a Log *P*/vdWD of 2.89 nm^{-1}. Methanol (CH_4O) has a calc $L_{external\ structure}/H_{polar\ group}$ ratio of 2.75 (reference, 0 or 1) (Table 1).

Ethane (C_2H_6) has a Log *P* of 1.35, and a vdWD of 0.437 nm with a Log *P*/vdWD of 3.09 nm^{-1}. Ethan-1-ol (C_2H_6O) has a calc $L_{external\ structure}/H_{polar\ group}$ ratio of 2.94, calc Δ $L_{external\ structure}/H_{polar\ group}$ of 0.19, and a nl calc $L_{external\ structure}/H_{polar\ group}$ quotient of 1.069. 2-ethan-1-ol ($C_2H_6O_2$) has a calc $L_{external\ structure}/H_{polar\ group}$ ratio of 1.47, calc Δ $L_{external\ structure}/H_{polar\ group}$ of 1.28, and a nl calc $L_{external\ structure}/H_{polar\ group}$ quotient of 0.535 (Table 1).

Propane (C_3H_8) has a Log *P* of 1.80, and a vdWD of 0.485 nm with a Log *P*/vdWD of 3.71 nm^{-1}. Propan-1-ol (C_3H_8O) has a calc $L_{external\ structure}/H_{polar\ group}$ ratio of 3.53, calc Δ $L_{external\ structure}/H_{polar\ group}$ of 0.78, and a nl calc ratio $L_{external\ structure}/H_{polar\ group}$ quotient of 1.280. Propan-1,2-diol ($C_3H_8O_2$) has a calc $L_{external\ structure}/H_{polar\ group}$ ratio of 2.90, calc Δ $L_{external\ structure}/H_{polar\ group}$ of 0.13, and a nl calc $L_{external\ structure}/H_{polar\ group}$ quotient of 1.047. Propan-1,3-diol ($C_3H_8O_2$) has a calc $L_{external\ structure}/H_{polar\ group}$ ratio of 3.08, calc Δ $L_{external\ structure}/H_{polar\ group}$ of 0.31, and a nl calc $L_{external}/H_{polar\ group}$ quotient of 1.113. 2,3-glyercer-1-ol ($C_3H_8O_3$) has a calc $L_{external\ structure}/H_{polar\ group}$ ratio of 1.18, calc Δ $L_{external\ structure}/H_{polar\ group}$ of 1.57, and a nl calc $L_{external}/H_{polar\ group}$ quotient of 0.428. Mannitol ($C_6H_{14}O_6$) has a calc $L_{internal\ structure}/H_{polar\ group}$ ratio of 0.838, calc Δ $L_{internal\ structure}/H_{polar\ group}$ of 1.91, and a nl calc $L_{internal}/H_{polar\ group}$ quotient of 0.304 (Table 1).

Table 1. Molecule structural hydrophilicity limit for non-specific diffusion into cells through polarity-specific transmembrane transport channels.

Hydroxylate external structure	Formula	Log *P*	Molecular weight (Da)	Size ($Å^3$)	vdWD (nm)	Log *P*/vdWD (nm^{-1})	$L_{external\ structure} \cdot H_{polar\ group}^{-1}$ ^, & [calc, calc Δ; Δ·ref^{-1}] ◊
Hexane	C_6H_{12}	3.13	86.1	113.2	0.593	5.28	Mannito1 [0.838, 1.91; 0.304]
Butane	C_4H_{10}	2.24	58	79.1	0.526	4.26	1,2-butanediol [3.34, 0.57; 1.21]
Propane	C_3H_8	1.80	44	62.2	0.485	3.71	1-propanol [3.53, 0.78; 1.28]
							1,3-propanediol [3.08, 0.31; 1.11]
							1,2-propanediol [2.90, 0.13; 1.05]
							2,3-glycer-1-ol [1.18, 1.57; 0.428]
Ethane	C_2H_6	1.35	30	45.2	0.437	3.09	1-ethanol [2.94, 0.19; 1.07]
							1,2-ethanediol [3.09, 1.28; 0.535]
Methane	CH_4	1.08	16	28.3	0.373	2.89	Methanol [ref]*

^ hydroxyl group hydrophilicity is Log *P*/vdWD of -1.05 nm^{-1} (Log *P*: -0.33; vdWD: 0.316 nm)

& dual hydroxylate isomerism adjustment for 1,2-propanediol, 1,3-propanediol and 1,2-butanediol is Log *P*·vdWD^{-1}/[1.05 + (1/*i* + 1)(0.437)], where *i* = no. of C bonds in-between the initial OH position and the subsequent hydroxylate for a simple aliphatic or cycloaliphatic

*Δ, calc -ref; nl calc, calc—ref/ref when calc > ref, and 1 –(calc -ref/ref) when ref > calc Note(s): Polarity-specific transport occurs at a nl calc ratio < 1.07 (1,2-propanediol, 1,2-ethanediol and 2,3-glycer-1-ol)

◊ Reference is methan-1-ol with a $L_{internal\ structure} \cdot H_{polar\ group}^{-1}$ of 2.75 (1.00).

https://doi.org/10.1371/journal.pone.0236446.t001

Lactate ($C_3H_5O_3$) has a Log *P* of -0.47 (Log *D*, -3.7), and a vdWD of 0.526 nm with a Log *P*/vdWD of -0.893 nm^{-1} (Log *D*/vdWD, -7.04 nm^{-1}). Lactate (lactic acid) has a calc $L_{external\ structure}/H_{polar\ group}$ of 0.309 (0.901), calc $\Delta\ L_{external\ structure}/H_{polar\ group}$ of 1.85 (2.44), and a nl calc $L_{external}/H_{polar\ group}$ quotient of 0.112 (0.328) (Table 1).

Butane (C_4H_{10}) has a Log *P* of 2.24, and a vdWD of 0.526 nm with a Log *P*/vdWD of 4.26 nm^{-1}. 1,2-butanediol ($C_4H_{10}O_2$) has a calc $L_{external\ structure}/H_{polar\ group}$ of 3.54, calc $\Delta\ L_{external\ structure}/H_{polar\ group}$ of 0.57, and a nl calc $L_{external}/H_{polar\ group}$ quotient of 1.207 (Table 1).

van der Waals diameter and external structural lipophilicity per polar group hydrophilicity parameters of small molecule halogenates that are non-specific transport channel substrates

Halothane ($C_2HBrClF_3$) has a Log *P* of 2.12, and a vdWD of 0.554 nm with a Log *P*/vdWD of 3.82 nm^{-1} (Table 2).

Desflurane ($C_3H_2F_6O$) has a Log *P* of 2.40, and a vdWD of 0.571 nm with a Log *P*/vdWD of 4.21 nm^{-1}. Part-halogenate 1,1,1-trifluoro-2-fluoroethane ($C_2H_2F_4$) has a Log *P* of 1.33, and a vdWD of 0.493 nm with a Log *P*/vdWD of 2.70 nm^{-1}. Part-halogenate fluoromethane (CH_3F) has a Log *P* of 0.370, and a vdWD of 0.394 nm with a Log *P*/vdWD of 0.939 nm^{-1}. Desflurane has a calc $L_{external\ structure}/H_{polar\ group}$ ratio of 9.62, and a nl calc $L_{external\ structure}/H_{polar\ group}$ quotient of 3.50 (Table 2).

Isoflurane ($C_3H_2ClF_5O$) has a Log *P* of 2.84, and a vdWD of 0.588 nm with a Log *P*/vdWD of 4.83 nm^{-1}. Part-halogenate 1,1,1-trifluoro-2-chloroethane ($C_2H_2ClF_3$) has a Log *P* of 1.79, and a vdWD of 0.515 nm with a Log *P*/vdWD of 3.48 nm^{-1}. Part-halogenate difluoromethane (CH_2F_2) has a Log *P* of 0.677 (calc), and a vdWD of 0.413 nm with a Log *P*/vdWD of 1.65 nm^{-1}. Isoflurane has a calc $L_{external\ structure}/H_{polar\ group}$ ratio of 11.25, and a nl calc $L_{external\ structure}/H_{polar\ group}$ quotient of 4.09 (Table 2).

Enflurane ($C_3H_2ClF_5O$) has a Log *P* of 2.80, and a vdWD of 0.588 nm with a Log *P*/vdWD of 4.77 nm^{-1}. Part-halogenate 1-chloro-1,2,2-trifluoroethane ($C_2H_2ClF_3$) has a Log *P* of 1.54, and a vdWD of 0.515 nm with a Log *P*/vdWD of 2.99 nm^{-1}. Part-halogenate difluoromethane

Table 2. Small molecule halogenates with affinity interactions at inner mitochondrial membrane P450 cytochromes.

Halogenate/Part-halogenate	Formula	Log *P*	Molecular Weight (Da)	Size (Ang^3)	vdWD (nm) ^	Polar SA (Ang^2)	Log *P*/vdWD (nm^{-1}); $L_{external\ structure} \cdot H_{polar\ group}^{-1}$ (Ch_3OH nl)
Halothane	$C_2HBrClF_3$	2.12	196	92.6	0.554	-	3.82; n/a
Desflurane	$C_3H_2F_6O$	2.40	168	101	0.571	9	4.21; 3.50
1,1,1-trifluoro-2-fluoroethane	$C_2H_2F_4$	1.33	102	65	0.493	-	2.70; n/a
Isoflurane	$C_3H_2ClF_5O$	2.84	184	110	0.588	9	4.83; 4.09
1,1,1-trifluoro-2-chloroethane	$C_2H_2ClF_3$	1.79	118	74.2	0.515	-	3.48; n/a
Enflurane	$C_3H_2ClF_5O$	2.80	184	110	0.588	9	4.77; 3.72
1-chloro-1,2,2-trifluoroethane	$C_2H_2ClF_3$	1.54	118	74.2	0.515	-	2.99; n/a
Sevoflurane	$C_4H_3F_7O$	2.27	200	123	0.610	9	3.72; 3.83
1,1,1,3,3,3-hexaflouropropane	$C_3H_2F_6$	2.13	152	92.05	0.553	-	3.85; n/a

^ The molecular diameter (vdWD, nm) is predictive of end-tidal minimum alveolar concentration (MAC, vol %), y = 10.41x -4.707 (R^2 = 0.73) in comparison to molecular weight (Da), y = 0.0081x – 0.214 (R^2 = 0.29), when trichloromethane (0.72%, 0.505 nm), halothane (0.75%), isoflurane (1.17%), enflurane (1.63%) and sevoflurane (1.80%) are *x*, *y*-plotted; and & lower non-polar part-structural lipophilicity Log *P*/vdWD is predictive of deviation from measured minimum alveolar concentration (MAC) *Difluoromethane ($C_3H_{1\text{-}2}F_2$), common part-structure moiety to Isoflurane, Enflurane and Desflurane (Log *P* 0.677, vdWD 0.413 nm, 1.65 nm^{-1}; y = 16.154x – 5.995, R^2 = 1); and Fluoromethane ($CH_{2\text{-}3}F$), part-structure moiety of Sevoflurane (Log *P* 0.37, vdWD 0.394 nm, 0.939 nm^{-1}).

https://doi.org/10.1371/journal.pone.0236446.t002

(CH_2F_2) has a Log *P* of 0.677 (calc), and a vdWD of 0.413 nm with a Log *P*/vdWD of 1.65 nm^{-1}. Enflurane has a calc $L_{external\ structure}/H_{polar\ group}$ ratio of 10.23, and a nl calc $L_{external\ structure}/H_{polar\ group}$ quotient of 3.72 (Table 2).

Sevoflurane ($C_4H_3F_7O$) has a Log *P* of 2.27, and a vdWD of 0.610 nm with a Log *P*/vdWD of 3.72 nm^{-1}. Part-halogenate 1,1,1,3,3,3-hexaflouropropane ($C_3H_2F_6$) has a Log *P* of 2.13, and a vdWD of 0.553 nm with a Log *P*/vdWD of 3.85 nm^{-1}. Sevoflurane has a calc $L_{external\ structure}/H_{polar\ group}$ ratio of 10.54, and a nl calc $L_{external\ structure}/H_{polar\ group}$ quotient of 3.83 (Table 2).

Gene expression effective pressure mapping for small molecule halogenates that are outer mitochondrial transmembrane channel substrates

CYP2E1 is a 2 A 2 q terminal final SEB gene at *x*-, *y*-vertical axis angulation 48.4°. *CYP2E1* has an *uppasebssiwa*, *dppasebssiwa*, *uppmsebssiwa* and *dppmsebssiwa* of 1.6445E + 04, 7.3717E + 04, 2.7927E + 04 and 5.5415E + 04 intergene bases. *CYP2E1* has an *uppesebssiwaa* and *dppesebssiwaa* of 2.2186E + 04 and 6.4566E + 04 intergene bases with a P_{eff} of 0.344 *esebssiwaagoT*$_Q$ units (Table 3).

CYP2B6 is a 2 M 5 initial and final SEB gene at *x*-, *y*-vertical axis angulation of 50.9°. *CYP2B6* has an *uppasebssiwa*, *dppasebssiwa*, *uppmsebssiwa* and *dppmsebssiwa* of 1.4887E + 04, 3.2241E + 04, 3.224E + 03, 2.3693E + 04 intergene bases. *CYP2B6* has an *uppesebssiwaa* and *dppesebssiwaa* of 2.7170E + 04 and 3.1800E + 04 intergene bases with a P_{eff} of 0.324 *esebssiwaagoT*$_Q$ units (Table 3).

JUN is a 3 M 5 NCA ACM final SEB gene at *x*-, *y*-vertical axis angulation 57.8°. *JUN* has an *uppasebssiwa*, *dppasebssiwa*, *uppmsebssiwa* and *dppmsebssiwa* of 6.8635E + 04, 1.32597E + 05, 1.5679E + 04 and 1.83485E + 05 intergene bases. *JUN* has an *uppesebssiwaa* and *dppesebssiwaa* of 4.2157E + 04 and 1.58041E + 05 intergene bases with a P_{eff} of 0.267 *esebssiwaagoT*$_Q$ units (Table 3).

TFB2M is a 2 A 5 initial and final SEB gene at *x*-, *y*-vertical axis angulation 57.8°. *TFB2M* has an *uppasebssiwa*, *dppasebssiwa*, *uppmsebssiwa* and *dppmsebssiwa* of 1.4509E + 04, 1.64443E + 05, 6.7711E + 04 and 1.43918E + 05 intergene bases. *TFB2M* has an *uppesebssiwaa*

Table 3. Effective intracellular pressure mapping of gene activation by small molecule halogenates.

Human gene (no. of bases, locus bases or n/a)	Gene locus (ch, strand)	Angle (°)	Episode category (final, initial SEB structure)[&]	*uppesebssiwaa*, *dppesebssiwaa* (P_{eff}, fract)	P_{eff} direction (inc, dec or n/a)[*]
CYP2E1, cytochrome P450 Family 2 Subfamily E Member 1 (107,293; n/a)	10q26.3 (+)	48.4	2 A 2 q term (2 A 5)	2.2186E + 04, 6.4566E + 04 (*0.344*)	inc
JUN, c-jun proto-oncogene, AP-1 (3,540; n/a)	1p32.2 (-)	57.8	3 M 7 nca acm (3 M 5)	4.2157E + 04, 1.58041E + 05 [0.2667 (*0.267*)]	n/c
TFB2M, transcription factor B2, mitochondrial (2.5759E + 04, n/a)	1q44 (-)	-	2 A 5 (-)	4.110E + 03, 1.54180E + 05 [0.2666 (*0.267*)]	-
SFTPC, surfactant protein C (7,567; n/a)	8p21.3 (+)	59.0	3 A 7 (-)	3.3516E + 04, 1.30616E + 05 (*0.257*)	dec (inc)[1,2]
FOSB, fosB proto-oncogene, AP-1 transcription factor subunit (7,185; 7,187)	19q13.32 (+)	65.6	3 A 8 acm (3 A 7)	8.092E + 03, 4.1656E + 04 (*0.194*)	dec
HMOX1, heme oxygenase 1 (13,854; n/a)	22q12.3 (+)	71.5	2 M 5 (-)	9.305E + 03, 6.0788E + 04 (*0.153*)	inc

inc, increase; n/c, no Δ; atm, atmospheric pressure (atm)

[1)] delta (Δ) increase in P_{eff} to 0.344, P_{eff} 0.257 (*SFTPC*) and to epi-nadir P_{eff} 0.153 (*HMOX1*) *esebssiwaagoT*$_Q$ units; and

[2)] *in vitro*, P_{eff} decreases from ≥ 0.344 to 0.257 units in atm pressure (mmHg)

[&] gene loci sub-episode block structure (SEB) variations include non-contributory anisotropy (NCA), anisotropy converted to mesotropy (ACM), and/or 0.5-factor adjusted stabilizing mesotropy or anisotropy converted to stabilizing isotropy for anisotropy or mesotropy (stIAfM, stIMfA or stIMfM).

https://doi.org/10.1371/journal.pone.0236446.t003

and *dppesebssiwaa* of 4.110E + 03 and 1.54180E + 05 intergene bases with a P_{eff} of 0.267 *esebssiwaagoT*$_Q$ units (Table 3).

SFTPC is a 3 A 7 initial and final SEB gene at *x*-, *y*-vertical axis angulation 59.0°. *SFTPC* has an *uppasebssiwa*, *dppasebssiwa*, *uppmsebssiwa* and *dppmsebssiwa* of 2.7644E + 04, 1.79499E + 05, 3.9387E + 04 and 8.1734E + 04 intergene bases. *SFTPC* has an *uppesebssiwaa* and *dppesebssiwaa* of 3.3516E + 04 and 1.30616E + 05 intergene bases with a P_{eff} of 0.257 *esebssiwaagoT*$_Q$ units (Table 3).

FOSB is a 3 A 8 ACM final SEB gene at *x*-, *y*-vertical axis angulation 65.6°. *FOSB* has an *uppasebssiwa*, *dppasebssiwa*, *uppmsebssiwa* and *dppmsebssiwa* of 1.2564E + 04, 2.9210E + 04, 3.621E + 03 and 5.4102E + 04 intergene bases. *FOSB* has an *uppesebssiwaa* and *dppesebssiwaa* of 8.092E + 03 and 4.1656E + 04 intergene bases with a P_{eff} of 0.194 *esebssiwaagoT*$_Q$ units (Table 3).

CREB1 is a 2 A 5 initial and final SEB gene at *x*-, *y*-vertical axis angulation 71.4°. *CREB1* has an *uppasebssiwa*, *dppasebssiwa*, *uppmsebssiwa* and *dppmsebssiwa* of 2.5030E + 04, 4.03885E + 05, 5.2441E + 04 and 9.8597E + 05 intergene bases. *CREB1* has an *uppesebssiwaa* and *dppesebssiwaa* of 3.8736E + 04 and 2.51241E + 05 intergene bases with a P_{eff} of 0.154 *esebssiwaagoT*$_Q$ units (Table 3).

HMOX1 is a 2 M 5 initial and final SEB gene at *x*-, *y*-vertical axis angulation 71.5°. *HMOX1* has an *uppasebssiwa*, *dppasebssiwa*, *uppmsebssiwa* and *dppmsebssiwa* of 1.3974E + 04, 3.8608E + 04, 4.636E + 03 and 8.2968E + 04 intergene bases. *HMOX1* has an *uppesebssiwaa* and *dppesebssiwaa* of 9.305E + 03 and 6.0788E + 04 intergene bases with a P_{eff} of 0.153 *esebssiwaagoT*$_Q$ units (Table 3).

van der Waals diameter and structural lipophilicity parameters of small molecules within the channel molecular size-inclusion range

Biphenyl ($C_{12}H_{10}$) has a Log *P* of 3.62, a vdWD of 0.655 nm and a Log *P*/vdWD of 5.53 nm^{-1} (Table 4).

Cyclononalol ($C_9H_{18}O$) has a Log *P* of 2.61, a vdWD of 0.688 nm and a Log *P*/vdWD of 3.91 nm^{-1} (Table 4).

Nonal-1-ol ($C_9H_{20}O$) has a Log *P* of 3.06, a vdWD of 0.682 nm and a Log *P*/vdWD of 4.48 nm^{-1} (Table 4).

Tetraethyllead ($C_8H_{20}Pb^{\delta+}$) has a Log *P* of 1.94, a vdWD of 0.700 nm and a Log *P*/vdWD of 2.77 nm^{-1} (Table 4).

Bisphenol E (BPE; $C_{14}H_{14}O_2$) has a Log *P* of 3.74, a vdWD of 0.727 nm and a Log *P*/vdWD of 5.14 nm^{-1}. Part-BPE 1,1-diphenylethane ($C_{14}H_{14}$) has a Log *P* of 4.35, a vdWD of 0.701 nm and a Log *P*/vdWD of 6.21 nm^{-1}. Bisphenol E has a calc $L_{external\ structure}/H_{polar\ group}$ ratio of 2.10, and a nl calc $L_{external\ structure}/H_{polar\ group}$ quotient of 1.08 (Table 4).

Decan-1-ol ($C_{10}H_{22}O$) has a Log *P* of 3.47, a vdWD of 0.704 nm and a Log *P*/vdWD of 4.93 nm^{-1} (Table 4).

Bisphenol A (BPA; $C_{15}H_{16}O_2$) has a Log *P* of 4.04, a vdWD of 0.742 nm and a Log *P*/vdWD of 5.44 nm^{-1}. Part-BPA 2-phenylpropan-2-yl benzene ($C_{15}H_{16}$) has a Log *P* of 4.65, a vdWD of 0.722 nm and a Log *P*/vdWD of 6.44 nm^{-1}. Bisphenol A has a calc $L_{external\ structure}/H_{polar\ group}$ ratio of 3.07, and a nl calc $L_{external\ structure}/H_{polar\ group}$ quotient of 1.12 (Table 4).

Undecan-1-ol ($C_{11}H_{24}O$) has a Log *P* of 3.92, a vdWD of 0.724 nm and a Log *P*/vdWD of 5.41 nm^{-1} (Table 4).

Mono-*n*-butylphthalate (BP, MBP; $C_{12}H_{14}O_4$) has a Log *P* (*D*) of 2.96 (-0.55), a vdWD of 0.724 nm and a Log *P* (*D*)/vdWD of 4.09 (-0.76) nm^{-1}(Table 4). MBP has a calc $L_{external\ structure}/H_{polar\ group}$ ratio of 0.886, and a nl calc $L_{external\ structure}/H_{polar\ group}$ quotient of 0.322.

Table 4. Small molecules with intracellular effects at inner mitochondrial membrane ETS cytochromes, rough endoplasmic reticulum deiodinase or at orphan nuclear receptors.

Small molecule [1,2]	Formula	Log *P*/*D*	Molecular Weight (Da)	Size (Ang^3)	vdWD (nm) [3]	Polar SA (Ang^2)	Log *P*/vdWD (nm^{-1}) [4]
Biphenyl	$C_{12}H_{10}$	3.62	154	153	0.655	-	5.53
Cyclononalol	$C_9H_{18}O$	2.61	142	162	0.668	20	3.91
Nonalol	$C_9H_{20}O$	3.06	144	173	0.682	20	4.48
Tetraethyllead	$C_8H_{20}Pb^{\delta+}$	1.94	324	186	0.700	-	2.77
1,1-diphenylethane	$C_{14}H_{14}$	4.35	182	187	0.701	-	6.21
Decanol	$C_{10}H_{22}O$	3.47	158	190	0.704	20	4.93
2-phenylpropan-2-yl benzene	$C_{15}H_{16}$	4.65	196	204	0.722	-	6.44
Undecanol	$C_{11}H_{24}O$	3.92	172	207	0.724	20	5.41
Mono-*n*-butylphthalate	$C_{12}H_{14}O_4$	2.96 (-0.55)	222	206	0.724	64	4.09 (-0.76)
Bisphenol E	$C_{14}H_{14}O_2$	3.74	214	209	0.727	40	5.14
2,2-dichloro-1-phenylethenyl benzene	$C_{14}H_{10}Cl_2$	4.90	248	209	0.727	-	6.74
ortho-planar PCB-54	$C_{12}H_6Cl_4$	5.84	290	209	0.727	-	8.04
2,3,7,8-tetrachlorodibenzo-*p*-dioxin	$C_{12}H_4Cl_4O_2$	5.42	320	216	0.735	18	7.38
ortho-planar PCB-95	$C_{12}H_5Cl_5$	6.76$^{\diamond}$	326	218	0.737	-	9.17
Bisphenol A	$C_{15}H_{16}O_2$	4.04	228	222	0.742	40	5.44
Dodecanol	$C_{12}H_{26}O$	4.36	186	224	0.744[a]	20	5.86
Bisphenol C	$C_{14}H_{10}Cl_2O_2$	4.29	280	224	0.744	40	5.77
Iodothyroxine	$C_{15}H_{11}I_4NO_4$	3.73	777	225*	0.745*	93	5.00*
co-planar PCB-126	$C_{12}H_5Cl_5$	6.69$^{\diamond}$	324	228	0.749	-	8.94
4'-OH-2,3,3',4,5-PCB-106	$C_{12}H_5Cl_5O$	6.34	343	231	0.752[b]	20	8.43

[1)] 1,1-diphenylethane (6.21 nm^{-1}), 2-phenylpropan-2-yl benzene (6.44 nm^{-1}) and 2,2-dichloro-1-phenylethenyl benzene (6.74 nm^{-1}) are the respective internal molecular structures of bisphenol E (BPE, 5.14 nm^{-1}; ERRα, ERRγ), bisphenol A (BPA, 5.44 nm^{-1}; ERRα, ERRγ) and bisphenol C (BPC, 5.77 nm^{-1}; ERα, ERβ)

[3)] [a], lower limit of range for molecular size-inclusion at the transmembrane channel pore as determined by elliptical molecules, vdWD = 0.744 nm; and [b], lower limit of range for molecular size-inclusion at the cell membrane channel pore as determined by ellipsoid (chiral carbon) small molecules, vdWD = 0.752 nm; and [5)] the lower limit of $L_{\text{external structure}} \cdot H_{\text{polar group}}^{-1}$ for biphenyl metabolites is 1.92 (4-OH-biphenyl).

$^{\diamond}$ Log *P* values for *ortho*-planar PCB-95 and *co*-planar PCB-126, calculated weighted average (chemicalize, ACD/Labs or EPI suite at chemspider and PubChem databases)

* Thyroxine (T_4), vdWD is adjusted for *x*, *y*-dimensional molecular aspect, $b = (T_4 \text{ unadjusted vdWD})\ (0.760 \text{ nm}) \cdot (c)^{-1}$, *where* c = 0.874.

https://doi.org/10.1371/journal.pone.0236446.t004

Bisphenol C (BPC; $C_{14}H_{10}Cl_2O_2$) has a Log *P* of 4.29, a vdWD of 0.744 nm and a Log *P*/vdWD of 5.77 nm^{-1}. Part-BPC 2,2-dichloro-1-phenylethenyl benzene ($C_{14}H_{10}Cl_2$) has a Log *P* of 4.90, a vdWD of 0.727 nm and a Log *P*/vdWD of 6.74 nm^{-1}. Bisphenol C has a calc $L_{\text{external structure}}/H_{\text{polar group}}$ ratio of 3.21, and a nl calc $L_{\text{external structure}}/H_{\text{polar group}}$ quotient of 1.17 (Table 4).

2,2',6,6'-*ortho*-planar PCB-54 ($C_{12}H_6Cl_4$) has a Log *P* of 5.84, a vdWD of 0.727 nm and a Log *P*/vdWD of 8.04 nm^{-1} (Table 4).

2,3,7,8-tetrachlorodibenzo-*p*, *p*-dioxin ($C_{12}H_4Cl_4O_2$; *p*-dioxin, TCDD) has a Log *P* of 5.42, a vdWD of 0.735 nm and a Log *P*/vdWD of 7.38 nm^{-1} (Table 4). *p*-dioxin has a calc $L_{\text{external structure}}/H_{\text{polar group}}$ ratio of 11.86, and a nl calc $L_{\text{external structure}}/H_{\text{polar group}}$ quotient of 4.31. 8-OH-2,3,7-TriCDD has a calc $L_{\text{external structure}}/H_{\text{polar group}}$ ratio of 5.25, and a nl calc $L_{\text{external structure}}/H_{\text{polar group}}$ quotient of 1.91 8-*O*-glucoronide-2,3,7-TriCDD has a calc $L_{\text{external structure}}/H_{\text{polar group}}$ ratio of 1.15, and a nl calc $L_{\text{external structure}}/H_{\text{polar group}}$ quotient of 0.419.

2,2',5,5',6-*ortho*-planar PCB-95 ($C_{12}H_5Cl_5$) has a Log *P* of 6.76, a vdWD of 0.737 nm and a Log *P*/vdWD of 9.17 nm^{-1} (Table 4).

3,4,4',5,5'-*co*-planar PCB-126 ($C_{12}H_5Cl_5$) has a Log *P* of 6.69, a vdWD of 0.749 nm and a Log *P*/vdWD of 8.94 nm^{-1} (Table 4).

Dodecan-1-ol ($C_{12}H_{26}O$) has a Log *P* of 4.36, a vdWD of 0.744 nm and a Log *P*/vdWD of 5.86 nm^{-1} (Table 4).

Dodecan-1-ol ($C_{12}H_{26}O$) has a Log *P* of 4.36, a vdWD of 0.744 nm and a Log *P*/vdWD of 5.86 nm^{-1} (Table 4).

3,5,3',5'-Iodothyroxine ($C_{15}H_{11}I_4NO_4$) has a Log *P* of 3.73, a vdWD of 0.745* nm and a Log *P*/vdWD of 5.00 nm^{-1}* (Table 4). Iodothyroxine has a calc $L_{external\ structure}/H_{polar\ group}$ ratio of 1.625, and a nl calc $L_{external\ structure}/H_{polar\ group}$ quotient of 0.591. (4'-hydroxy-3',5'-diiodophenoxy)-1-ethyl-3,5-diiodophenyl (non-zwitterion part T_4) has a calc $L_{external\ structure}/H_{polar\ group}$ ratio of 8.92, and a nl calc $L_{external\ structure}/H_{polar\ group}$ quotient of 3.24.

4'-OH-2,3,3',4,5-PCB-106 ($C_{12}H_5Cl_5O$) has a Log *P* of 6.34, a vdWD of 0.752 nm and a Log *P*/vdWD of 8.43 nm^{-1} (Table 4).

van der Waals diameter and structural lipophilicity parameters of small molecules in the molecular size-exclusion range

2',3,4,4',5',6-PCB-153 ($C_{12}H_4Cl_6$) has a Log *P* of 7.24, a vdWD of 0.758 nm and a Log *P*/vdWD of 9.55 nm^{-1} (Table 5).

Tridecan-1-ol ($C_{13}H_{28}O$) has a Log *P* of 4.81, a vdWD of 0.762 nm and a Log *P*/vdWD of 6.31 nm^{-1} (Table 5).

4'-OH-3,3',4,5,5',6-*ortho*-planar PCB-136 ($C_{12}H_4Cl_6O$) has a Log *P* of 7.04, a vdWD of 0.767 nm and a Log *P*/vdWD of 9.18 nm^{-1} (Table 5).

Bisphenol AF (BFAF, $C_{15}H_{10}F_6O_2$) has a Log *P* of 4.77, a vdWD of 0.774 nm and a Log *P*/vdWD of 6.17 nm^{-1}. 1,1,1,3,3,3-hexafluoro-2-phenylpropan-2-yl ($C_{15}H_{10}F_6$) has a Log *P* of 5.38, a vdWD of 0.756 nm and a Log *P*/vdWD of 7.12 nm^{-1}. Bisphenol AF has a calc $L_{external\ structure}/H_{polar\ group}$ ratio of 3.39, and a nl calc $L_{external\ structure}/H_{polar\ group}$ quotient of 1.23 (Table 5).

Table 5. Small molecules in the molecular size-exclusion range at the cell membrane channel pore with extracellular effects on nuclear pathways via transmembrane receptor or protein affinity interactions.

Small molecule [1,2,3]	Formula	Log *P*	Molecular Weight (Da)	Size (Ang^3)	vdWD (nm) [4]	Polar SA (Ang^2)	Log *P*/vdWD (nm^{-1}) [5]
2',3,4,4',5',6-PCB-153	$C_{12}H_4Cl_6$	7.24	358	236	0.758[b]	-	9.55
Tridecan-1-ol	$C_{13}H_{28}O$	4.81	200	241	0.762[a]	20	6.31
4'-OH-*ortho*-planar PCB-136	$C_{12}H_4Cl_6O$	7.04◇	376	245	0.767	20	9.18
Bisphenol AF	$C_{15}H_{10}F_6O_2$	4.77	336	252	0.774	40	6.17
2,2',4,4',6-PBDE-100	$C_{12}H_{10}Br_5$	7.32	560	271	0.775	9	9.44
Acetochlor	$C_{14}H_{20}Cl_5NO_2$	3.50	269	256	0.778	30	4.50
4'-OH-2,3,3',4,5,5',6'-PCB-172	$C_{12}H_3Cl_7O$	7.55	421	259	0.781	20	9.92
Di-*n*-butyl phthalate	$C_{16}H_{22}O_4$	4.63	278	275	0.797	53	5.81
4'-CH_3-SO_2-*ortho*-planar PCB-132	$C_{13}H_6Cl_6O_2S$	6.09	436	290	0.811	34	7.51
trans-retin-1-ol	$C_{20}H_{30}O$	4.69	286	310	0.829	20	5.66
α-tocopherol	$C_{29}H_{50}O_2$	10.51	430	481	0.960	18	10.95

[1)] Bisphenol AF (BFAP) external structure is 1,1,1,3,3,3-hexafluoro-2-phenylpropan-2-yl within the nl calc $L_{external\ structure}/H_{polar\ group}$ quotient range of 1.17 (BPC)– 1.23 (BPAF) for mid-to-high binding to ERα/ERβ (Acetochlor, $L \cdot H^{-1}$ 1.16)

[2)] *trans*-retin-1-ol with a van der Waals diameter (vdWD) at 0.829 nm is a specific substrate for the cell membrane STRA6 transporter; and

[3)] [a], lower limit of range for molecular size-exclusion at the transmembrane channel pore as determined by elliptical small molecules, range 0.742–0.762 nm, and [b], upper limit of the range for molecular size-exclusion at the cell membrane channel pore as determined by ellipsoid small molecules, range 0.752–0.758 nm; and

[4)] the upper limit of $L_{external\ structure} \cdot H_{polar\ group}^{-1}$ range for PCB metabolites is 3.91 (4'-OH-2,2',3,3',4,5,5'6,6'-PCB-208), UL ◇ Log *P* values for 4'-OH-*ortho*-planar PCB-136 (isomer, 2'-OH-*co*-planar PCB-169), calculated weighted average determined from ACD/Labs, EPI suite, chemicalize and/or PubChem databases as applicable; PBDE, polybrominated diphenyl ether BDE-100.

https://doi.org/10.1371/journal.pone.0236446.t005

2,2',4,4',6-PBDE-100 ($C_{12}H_{10}Br_5$) has a Log *P* of 7.32, a vdWD of 0.775 nm and a Log *P*/vdWD of 9.44 nm^{-1} (Table 5).

Acetochlor ($C_{14}H_{20}Cl_5NO_2$) has a Log *P* of 3.50, a vdWD of 0.778 nm and a Log *P*/vdWD of 4.50 nm^{-1}. n-(1-chloroethyl)-n-(2-ethoxymethyl)-2-methyl-6-ethylaniline has a Log *P* of 4.18, a vdWD of 0.758 nm and a Log *P*/vdWD of 5.43 nm^{-1}. Acetochlor has a calc $L_{external\ structure}/H_{polar\ group}$ ratio of 3.20, and a nl calc $L_{external\ structure}/H_{polar\ group}$ quotient of 1.16 (Table 5).

4'-OH-2,3,3',4,5,5',6'-PCB-172 ($C_{12}H_3Cl_7O$) has a Log *P* of 7.55, a vdWD of 0.781 nm and a Log *P*/vdWD of 9.92 nm^{-1} (Table 5).

Di-*n*-butyl phthalate (DBP; $C_{16}H_{22}O_4$) has a Log *P* of 4.63, a vdWD of 0.797 nm and a Log *P*/vdWD of 5.81 nm^{-1} (Table 5). DBP has a calc $L_{external\ structure}/H_{polar\ group}$ ratio of 4.099, and a nl calc $L_{external\ structure}/H_{polar\ group}$ quotient of 1.491.

4'-CH_3-SO_2-*ortho*-planar PCB-132 ($C_{13}H_6Cl_6O_2S$) has a Log *P* of 6.09, a vdWD of 0.811 nm and a Log *P*/vdWD of 7.51 nm^{-1} (Table 5).

trans-retin-1-ol ($C_{20}H_{30}O$) has a Log *P* of 4.69, a vdWD of 0.829 nm and a Log *P*/vdWD of 5.66 nm^{-1} (Table 5). *trans*-retin-1-ol has a calc $L_{external\ structure}/H_{polar\ group}$ ratio of 6.914, and a nl calc $L_{external\ structure}/H_{polar\ group}$ quotient of 2.54. *trans*-retinoic acid has a calc $L_{external\ structure}/H_{polar\ group}$ ratio of 0.913, and a nl calc $L_{external\ structure}/H_{polar\ group}$ quotient of 0.332.

α-tocopherol ($C_{29}H_{50}O_2$) has a Log *P* of 10.51, a vdWD of 0.960 nm and a Log *P*/vdWD of 10.95 nm^{-1} (Table 5). α-tocopherol has a calc $L_{external\ structure}/H_{polar\ group}$ ratio of 8.018, and a nl calc $L_{external\ structure}/H_{polar\ group}$ quotient of 2.92. 13'-*O*-glucoronide-α-tocopherol ($C_{16}H_{22}O_4$) has a calc $L_{external\ structure}/H_{polar\ group}$ ratio of 1.26, and a nl calc $L_{external\ structure}/H_{polar\ group}$ quotient of 0.459.

Gene expression effective pressure mapping for small molecule chlorinates that are cell membrane, rough endoplasmic membrane enzyme or orphan nuclear receptor substrates

2,3,7,8-tetrachlorodibenzo-p-dioxin (Tcdd). *AHR* is a 5 A 9 ACM final SEB gene at *x*-, *y*-vertical axis angulation 42.3°. *AHR* has an *uppasebssiwa*, *dppasebssiwa*, *uppmsebssiwa* and *dppmsebssiwa* of 7.173E + 03, 7.2908E + 04, 1.71804E + 05 and 3.79987E + 05 intergene bases. *AHR* has an *uppesebssiwaa* and *dppesebssiwaa* of 8.9488E + 04 and 2.26448E + 05 intergene bases with a P_{eff} of 0.395 *esebssiwaagoT*$_Q$ units (Table 6).

COX8C is a 4 M 9 initial and final SEB gene at *x*-, *y*-vertical axis angulation 44.0°. *COX8C* has an *uppasebssiwa*, *dppasebssiwa*, *uppmsebssiwa* and *dppmsebssiwa* of 9.8211E + 04, 1.71795E + 05, 7.786E + 03 and 1.06511E + 05 intergene bases. *COX8C* has an *uppesebssiwaa* and *dppesebssiwaa* of 5.2998E + 04 and 1.39153E + 05 intergene bases with a P_{eff} of 0.381 *esebssiwaagoT*$_Q$ units (Table 6).

CEACAM1 is a 2 M 5 initial and final SEB gene at *x*-, *y*-vertical axis angulation 44.2° (act). *CEACAM1* has an *uppasebssiwa*, *dppasebssiwa*, *uppmsebssiwa* and *dppmsebssiwa* of 6.3332E + 04, 1.31731E + 05, 1.4468E + 04, 7.3384E + 04 intergene bases (act). *CEACAM1* has an *uppesebssiwaa* and *dppesebssiwaa* of 3.8900E + 04 and 1.02558E + 05 intergene bases with a P_{eff} of 0.379 *esebssiwaagoT*$_Q$ units (act) (Table 6).

SLC2A4 is a 2 M 5 initial and final SEB gene at *x*-, *y*-vertical axis angulation 44.6°. *SLC2A4* has an *uppasebssiwa*, *dppasebssiwa*, *uppmsebssiwa* and *dppmsebssiwa* of 1.5426E + 04, 2.7907E + 04, 917 and 1.5607E + 04 intergene bases. *SLC2A4* has an *uppesebssiwaa* and *dppesebssiwaa* of 8.172E + 04 and 2.1757E + 04 intergene bases with a P_{eff} of 0.376 *esebssiwaagoT*$_Q$ units (Table 6).

RXRA is a 2 M 5 initial and final SEB gene at *x*-, *y*-vertical axis angulation 44.8°. *RXRA* has an *uppasebssiwa*, *dppasebssiwa*, *uppmsebssiwa* and *dppmsebssiwa* of 3.7754E + 04, 7.2478E +

Table 6. Effective intracellular pressure mapping of gene activation by 2,3,7,8-tetrachlorodibenzo-p-dioxin (TCDD) via the AhR-Erβ (Arnt): Nrf-2:: Pparδ, Errγ (LxRα): Dio3/Dio2 (Trα) pathway.

Human gene (no. of bases, locus bases or n/a)	Gene locus (ch, strand)	Angle (°)	Episode category (final, initial SEB structure)	*uppesebssiwaa*, *dppesebssiwaa* (P_{eff}, fract)	P_{eff} range effect fract (Δ %)
AHR, aryl hydrocarbon receptor (429,794; 550,898)	7p21.1 (+)	42.3	5 A 9 stIMfM, acm (5 A 11)	8.9488E + 04, 2.26448E + 05 (*0.395*)	(+)
COX8C, cytochrome C oxidase subunit 8C (1,166; 374,660)•	14q32.12 (+)	44.0	4 M 9 (-)	5.2998E + 04, 1.39153E + 05 (*0.381*)	(+10.2)
CEACAM1, carcinoembryonic antigen related cell adhesion molecule 1 (53,931; 54,447)[a,◇,•]	19q13.2 (-)	44.2	2 M 5 (-)	3.8900E + 04, 1.02558E + 05 (*0.379*)	(+20.3)
SLC2A4 (Glut-4), solute carrier family 2 member 4 (6,540; n/a)	17p13.1 (+)	44.6	3 M 7 (-)	8.172E + 03, 2.1757E + 04 (*0.376*)	(+)
RXRA, retinoid X receptor alpha (123,489; n/a)	9q34.3 (+)	44.8	2 M 5 (-)	2.2689E + 04, 6.0662E + 04 (*0.374*)	(+)
NR1D1, nuclear receptor subfamily 1 group D member 1 (7,942; n/a)	17q21.2 (-)	44.9	3 M 7 ext (-)	1.7961E + 04, 4.8106E + 04 (*0.373*)	(+0.16)
DAO, d-amino acid oxidase	12q24.11 (+)	48.9	2 M 5 (-)	3.0313E + 04, 8.6996E + 04 (*0.348*)	(-)[&]
PPARD, peroxisome proliferator-activated receptor delta (85,634; n/a)	6p21.31 (+)	49.0	2 M 5 (-)	1.7924E + 04, 5.2800E + 04 (*0.339*)	(+)
GADD45B, growth arrest and DNA damage inducible beta (275,458; n/a)	19p13.3 (+)	49.9	4 M 5 stIMfa acm, nca acm (4 M 9)	2.0045E + 04, 6.0366E + 04 (*0.332*)	(+)
NFE2L2, nuclear factor, erythroid 2 like 2 (165,103, 880,745)[◇]	2q31.2 (-)	-	-	- (*0.331*)	(+0.07)
ALAS1, 5'-aminolevulinate synthase 1 (16,245;18,054)	3p21.2 (+)	50.9	2 A 5 (-)	1.5772E + 04, 4.8734E + 04 (*0.324*)	(-)[&]
DBP, D-box binding PAR BZIP transcription factor (7,521; n/a)	19q13.33 (-)	55.8	3 A 7 (-)	1.3046E + 04, 4.6054E + 04 (*0.283*)	(+0.3)
SCD, stearoyl-coenzyme A desaturase (17,817; 107,029)•	10q24.2 (+)	56.0	2 M 5 (-)	2.6206E + 04, 9.3046E + 04 [*0.282* (0.2816)]	(+0.16)
RXRB, retinoic acid receptor B (7,269; 328,916)	6p21.8 (-)	56.0	4 A 7 acm (4 A 9)	2.3576E + 04, 8.3743E + 04 [*0.282* (0.2815)]	(+)
PPARGC1A, PPARG coactivator 1 alpha (829,563; n/a)	4p15.2 (-)	56.3	6 M 13 (-)	1.20545E + 05, 4.32277E + 05 (*0.279*)	--[*]
MT1A, metallothionein 1A (1,422; n/a)	16q13 (+)	57.0	3 M 7 (-)	1.0479E + 04, 3.8405E + 04 (*0.273*)	(+0.07)
SREBF1, sterol regulatory element binding transcription factor 1 (26,619; n/a)	17p11.2 (-)	61.4	2 M 5 (-)	1.2714E + 04, 5.3646E + 04 (*0.237*)	--
DIO1, deiodinase I (21,520; 19,848)	1p32.3 (+)	61.5	2 A 4 nca (2 A 5)	1.8591E + 04, 7.8810E + 04 (*0.236*)	--[CM]
FABP5, fatty acid binding protein 5 (4,295; n/a)	8q21.13 (-)	63.0	3 M 7 (-)	3.2236E + 04, 1.44208E + 05 (*0.224*)	(+0.07)
TIPARP, TCDD inducible poly(ADP-ribose) polymerase (33,536; n/a)^	3q25.31 (+)	63.1	2 A 4 nca stIMfM (2 A 5)	1.9209E + 04, 8.6191E + 04 [*0.223* (0.2233)]	(+)
SIN3A, SIN3 transcription regulator family member A (86,464; n/a)	15q24.1 (-)	63.0	2 M 7 acm (2 M 5)	1.3371E + 04, 5.9872E + 04 [*0.223* (0.2229)]	(+)
PPARG, peroxisome proliferator-activated receptor gamma (268,877; n/a)	3p25.2 (+)	63.2	2 M 5 (-)	2.6689E + 04, 1.20354E + 05 (*0.222*)	--[**]
RARB, retinoic acid receptor B (423, 601; n/a)	3p24.2 (+)	63.2	4 A 9 (-)	3.6064E + 04, 1.62543E + 05 (*0.222*)	(+)
CYP1A1, cytochrome P450, family 1, subfamily A, polypeptide 1 (6,069; n/a)^	15q24.1 (-)	63.9	3 A 7 (-)	1.0633E + 04, 4.9247E + 04 (*0.216*)	(+33.5)
NR1H3, nuclear receptor subfamily 1 group H member 3 (20,734: n/a)	11p11.12 (+)	64.7	2 M 7 acm (2 M 5)	1.0224E + 04, 4.8803E + 04 [*0.209* (0.2095)]	(+)
ESRRG, estrogen related receptor gamma (634,510; n/a)	1q41 (-)	64.7	5 A 9 acm (5 A 11)	4.6694E + 04, 2.23137E + 05 *0.209* (0.2093)]	(+, -)[§]
CYP1A2, cytochrome P450, family 1, subfamily A2 (7,765; n/a)	15q24.1 (+)	65.7	3 A 9 acm (3 A 7)	1.5646E + 04, 7.7758E + 04 (*0.201*)	(+0.10)
NRF1, nuclear respiratory factor 1 (145,381; n/a)	7q32.2 (+)	65.8	2 A 5 (-)	2.0850E + 04, 1.04212E + 05 (*0.200*)	(-)
ESRRA, estrogen related receptor alpha (11,220; n/a)	11q13.1 (+)	66.8	3 M 9 acm (3 M 7)	7.796E + 03, 3.9699E + 04 (*0.196*)	(-, +)[■]

(*Continued*)

Table 6. (Continued)

Human gene (no. of bases, locus bases or n/a)	Gene locus (ch, strand)	Angle (°)	Episode category (final, initial SEB structure)	*uppesebssiwaa*, *dppesebssiwaa* (P_{eff}, fract)	P_{eff} range effect fract (Δ %)
ARNTL, ARNT like factor (111,160; n/a)	11p15.3 (+)	66.9	2 M 5 (-)	1.5097E + 04, 7.8855E + 04 (*0.191*)	(+)
EXOC7, exocyst complex component 7 (40,584; 51,507)	17q25.1 (-)	67.1	3 M 9 (3 M 7)	3.692E + 03, 1.9475E + 04 (*0.190*)	(+1.05)
ESR1, estrogen receptor alpha (472,929; n/a)	6q25.1 (+)	68.0	4 A 9 acm nca (4 A 9)	5.0063E + 04, 2.72635E + 05 (*0.184*)	(-)
DIO2, iodothyronine deiodinase 2 (190,233; n/a)	14q31.1 (-)	67.9	2 A 5 (-)	4.8369E + 04, 2.64538E + 05 (*0.183*)	□ (-)[&]
RARA, retinoic acid receptor, alpha (48,473; n/a)	17q21.2 (+)	68.4	2 M 5 (-)	1.9801E + 04, 1.09351E + 05 (*0.181*)	(-)˚˚
NCOR2, nuclear receptor corepressor 2 (243,179; 355,292)	12q24.2 (-)	68.5	4 M 9 (-)	1.5758E + 04, 8.8699E + 04 (*0.178*)	(+)
THRA, thyroid hormone receptor alpha (35,578; 35,846)	17q21.2 (+)	68.6	2 M 7 acm 2 M 5)	1.5557E + 04, 8.7918E + 04 (*0.177*)	(+)
NRIP1, Nuclear receptor interacting protein 1 (104,702; 248,423)	21q11.2 (-)	69.1	2 M 7 acm (2 M 5)	1.41470E + 05, 8.15738E + 05 (*0.173*)	(+)*
CYP1B1, cytochrome P450, family 1, subfamily B, polypeptide 1 (42,930; 565,830)	2p22.2 (-)	69.6	5 M 11 (-)	6.1304E + 04, 3.63307E + 05 (*0.169*)	(+24.3)
ALDH3A1, aldehyde dehydrogenase family, polypeptide A6 (10,960; n/a)	17p11.2 (-)	69.7	2 A 7 (-)	1.0360E + 04, 6.1604E + 04 (*0.168*)	(+1.9)
ACSM2A, acyl-CoA synthetase medium chain family member 2A (36,209; n/a)	16p12.3 (+)	70.9	2 A 5 (-)	1.0522E + 04, 6.6500E + 04 (*0.158*)	(-)[&]
HMOX1				[*0.153* (0.1531)]	(+)
NQO1, NAD(P)H dehydrogenase quinone 1 (19,673; n/a)	16q22.11 (-)	72.2	2 A 5 (-)	1.8473E + 04, 1.25308E + 05 (*0.147*)	(+0.65)
ESR2, estrogen receptor beta (254,319; 254,368)	14q23.2-q23.3 (-)	73.6	2 A 5 (-)	1.3835E + 04, 1.01622E + 05 (*0.136*)	(+)
ME1, malic enzyme 1 (221,353; n/a)	6q14.2 (-)	73.7	2 M 5 (-)	3.9550E + 04, 2.92302E + 05 (*0.135*)	(+0.10)^
CYP3A7, cytochrome P450, family 3, subfamily A, polypeptide 1 (50,244; 50,522)•	7q22.1 (-)	76.6	2 M 5 (-)	2.1824E + 04, 1.97244E + 05 (*0.111*)	(-)[&]
UGT1A7, UDP glucuronosyltransferase family 1 member A7 (81,699; 187,867)	2q37.1 (+)	77.2	2 M 5 ext (2 M 5)	2.9540E + 04, 2.77604E + 05 (*0.106*)	(+2.8)
DIO3, deiodinase type 3 (2,102; n/a)	14q32.3 (+)	78.4	2 A 5 (-)	3.504E + 04, 3.6368E + 04 (*0.096*)	(+)
IGHM, immunoglobulin heavy chain M (4,511; n/a)	14q32.3 (-)	-	-	- (*0.088*)	(-)[□]
ARNT, aryl hydrocarbon receptor nuclear translocator (67,064; n/a)	1q21.3 (-)	82.4	2 A 5	4.287E + 03, 6.7882E + 04 (*0.063*)	--
TSPAN14, tetraspanin 14 (79,316; n/a)	10q23.1 (+)	83.1	2 A 8 acm acm (2 A 5)	1.4992E + 04, 2.63650E + 05 (*0.057*)	--

[&] % dec in effect genes include *DAO1*, -4.1; *ALAS1*, - 0.54; *ACSM2A*, -7.0; *CYP3A7*, -37.6; and *DIO2*, -0.54 (2-fold change threshold)

• *CEACAM1*, *SCD*, *COX8A* and *CYP3A7* are respective orthologs (pred) of rodent *CEACAM10*, *SCD2*, *COX8H* and *CYP3A13*

[a], actual

▪ *ESRRA* initial under-activation during EXOC7 protein expression phase, while *ESRRG* overactivation

□Baseline decrease at P_{eff} duration during acute applied exposure (hours) *in vitro*

**NcoR2 and PPARγ interaction ˚˚ RARA and ERRγ interaction [$] *NFIB* repression of *PCK1* transcription factor decreases (as cited)

^ Activation of *ME1* gene at TRα response element (TRE) increases, as does *DBP* gene activation containing both TRE and ERα/β ERE (not determined, n.d.)

* RIP140 (*NRIP1*) as co-activator for AhR-ERα/β and ERR transcription factors; and * *PPARGC1A* (PGC1α) as co-activator for PPARG and SREBF1 transcription factors Note(s): [1)] Gene loci sub-episode block structure (SEB) variations include: non-contributory anisotropy (NCA), anisotropy converted to mesotropy (ACM), 0.5-factor adjusted stabilizing mesotropy or anisotropy converted to stabilizing isotropy for anisotropy or mesotropy (stIAfM, stIMfA or stIMfM), and/or extended block (ext) SEB; and [2)] gene(s) with previously reported episode and sub-episode block structure include [◊] *CEACAM1* (unadj), NFE2L2 (NRF-2), *NRF1* [22] and *IGHM* [38].

https://doi.org/10.1371/journal.pone.0236446.t006

04, 7.624E + 03 an 4.8816E + 04 intergene bases. *RXRA* has an *uppesebssiwaa* and *dppesebssiwaa* of 2.2689E + 04 and 6.0662E + 04 intergene bases with a P_{eff} of 0.374 *esebssiwaagoT*$_Q$ units (Table 6).

NR1D1 is a 3 M 7 ext final SEB gene at *x*-, *y*-vertical axis angulation 44.9°. *NR1D1* has an *uppasebssiwa*, *dppasebssiwa*, *uppmsebssiwa* and *dppmsebssiwa* of 3.2742E + 04, 6.6932E+ 04, 3.181E + 03 and 2.9279E + 04 intergene bases. *NR1D1* has an *uppesebssiwaa* and *dppesebssiwaa* of 1.7961E + 04 and 4.8106E + 04 intergene bases with a P_{eff} of 0.373 *esebssiwaagoT*$_Q$ units (Table 6).

DAO is a 2 M 5 initial and final SEB gene at *x*-, *y*-vertical axis angulation 47.9°. *DAO* has an *uppasebssiwa*, *dppasebssiwa*, *uppmsebssiwa* and *dppmsebssiwa* of 6.0186E +04, 1.15409E + 05, 440 and 6.0583E + 04 intergene bases. *DAO* has an *uppesebssiwaa* and *dppesebssiwaa* of 3.0313E + 04 and 8.6996E + 04 intergene bases with a P_{eff} of 0.348 *esebssiwaagoT*$_Q$ units (Table 6).

PPARD is a 2 M 5 initial and final SEB gene at *x*-, *y*-vertical axis angulation 49.0°. *PPARD* has an *uppasebssiwa*, *dppasebssiwa*, *uppmsebssiwa* and *dppmsebssiwa* of 3.3902E + 04, 7.5097E + 04, 1.946E + 03 and 3.0504E + 04 intergene bases. *PPARD* has an *uppesebssiwaa* and *dppesebssiwaa* of 1.7924E + 04 and 5.2800E + 04 intergene bases with a P_{eff} of 0.339 *esebssiwaagoT*$_Q$ units (Table 6).

GADD45B is a 4 M 5 stIMfa, ACM, NCA ACM final SEB gene at *x*-, *y*-vertical axis angulation 49.9°. *GADD45B* has an *uppasebssiwa*, *dppasebssiwa*, *uppmsebssiwa* and *dppmsebssiwa* of 3.8061E + 04, 9.8594E + 04, 2.029E + 03 and 2.2138E + 04 intergene bases. *GADD45B* has an *uppesebssiwaa* and *dppesebssiwaa* of 2.0045E + 04 and 6.0366E + 04 intergene bases with a P_{eff} of 0.332 *esebssiwaagoT*$_Q$ units (Table 6).

ALAS1 is a 2 A 5 initial and final SEB gene at *x*-, *y*-vertical axis angulation 50.9°. *ALAS1* has an *uppasebssiwa*, *dppasebssiwa*, *uppmsebssiwa* and *dppmsebssiwa* of 3.929E + 03, 2.9633E + 04, 2.7615E + 04 and 6.7836E + 04 intergene bases. *ALAS1* has an *uppesebssiwaa* and *dppesebssiwaa* of 1.5772E + 04 and 4.8734E + 04 intergene bases with a P_{eff} of 0.324 *esebssiwaagoT*$_Q$ units (Table 6).

DBP is a 3 A 7 initial and final SEB gene at *x*-, *y*-vertical axis angulation 55.8°. *DBP* has an *uppasebssiwa*, *dppasebssiwa*, *uppmsebssiwa* and *dppmsebssiwa* of 2.499E + 03, 4.4612E + 04, 2.3594E + 04 and 4.7496E + 04 intergene bases. *DBP* has an *uppesebssiwaa* and *dppesebssiwaa* of 1.3046E + 04 and 4.6054E + 04 intergene bases with a P_{eff} of 0.283 *esebssiwaagoT*$_Q$ units (Table 6).

RXRB is a 4 A 7 final SEB gene at *x*-, *y*-vertical axis angulation 56.0°. *RXRB* has an *uppasebssiwa*, *dppasebssiwa*, *uppmsebssiwa* and *dppmsebssiwa* of 8.075E + 03, 8.3710E + 04, 3.9078E + 04 and 8.3775E + 04 intergene bases. *RXRB* has an *uppesebssiwaa* and *dppesebssiwaa* of 2.3576E + 04 and 8.3743E + 04 intergene bases with a P_{eff} of 0.282 *esebssiwaagoT*$_Q$ units (Table 6).

PPARGC1A is a 6 M 13 initial and final SEB gene at *x*-, *y*-vertical axis angulation 56.3°. *PPARGC1A* has an *uppasebssiwa*, *dppasebssiwa*, *uppmsebssiwa* and *dppmsebssiwa* of 1.98293E + 05, 4.43060E + 05, 4.2797E + 04 and 4.21495E + 05 intergene bases. *PPARGC1A* has an *uppesebssiwaa* and *dppesebssiwaa* of 1.20545E + 05 and 4.32277E + 05 intergene bases with a P_{eff} of 0.279 *esebssiwaagoT*$_Q$ units (Table 6).

SCD is a 2 M 5 initial and final SEB gene at *x*-, *y*-vertical axis angulation 56.9°. *SCD* has an *uppasebssiwa*, *dppasebssiwa*, *uppmsebssiwa* and *dppmsebssiwa* of 4.0705E + 04, 7.4127E + 04, 1.1708E + 04 and 1.11966E + 05 intergene bases. *SCD* has an *uppesebssiwaa* and *dppesebssiwaa* of 2.6206E + 04 and 9.3046E + 04 intergene bases with a P_{eff} of 0.282 *esebssiwaagoT*$_Q$ units (Table 6).

MT1A is a 3 M 7 initial and final SEB gene at *x*-, *y*-vertical axis angulation 57.0°. *MT1A* has an *uppasebssiwa*, *dppasebssiwa*, *uppmsebssiwa* and *dppmsebssiwa* of 1.9593E + 04, 4.5208E + 04, 1.365E + 03 and 3.1603E + 04 intergene bases. *MT1A* has an *uppesebssiwaa* and *dppesebssiwaa* of 1.0479E + 04 and 3.8405E + 04 intergene bases with a P_{eff} of 0.273 *esebssiwaagoT*$_Q$ units (Table 6).

SREPF1 is a 2 M 5 initial and final SEB gene at *x*-, *y*-vertical axis angulation 61.4°. *SREPF1* has an *uppasebssiwa*, *dppasebssiwa*, *uppmsebssiwa* and *dppmsebssiwa* of 1.6701E + 04, 4.6217E + 04, 8.727E + 03 and 6.1076E + 04 intergene bases. *SREPF1* has an *uppesebssiwaa* and *dppesebssiwaa* of 1.2714E + 04 and 5.3646E + 04 intergene bases with a P_{eff} of 0.237 *esebssiwaagoT*$_Q$ units (Table 6).

DIO1 is a 2 A 4 NCA final SEB gene at *x*-, *y*-vertical axis angulation 60.7°. *DIO1* has an *uppasebssiwa*, *dppasebssiwa*, *uppmsebssiwa* and *dppmsebssiwa* of 3.0841E + 04, 8.6335E + 04, 6.342E + 03 and 7.1284E + 04 intergene bases. *DIO1* has an *uppesebssiwaa* and *dppesebssiwaa* of 1.8591E + 04 and 7.8810E + 04 intergene bases with a P_{eff} of 0.236 *esebssiwaagoT*$_Q$ units (Table 6).

FABP5 is a 3 M 7 initial and final SEB gene at *x*-, *y*-vertical axis angulation 63.0°. *FABP5* has an *uppasebssiwa*, *dppasebssiwa*, *uppmsebssiwa* and *dppmsebssiwa* of 5.2075E + 04, 1.38023E + 05, 1.2397E + 04 and 1.50392E + 05 intergene bases. *FABP5* has an *uppesebssiwaa* and *dppesebssiwaa* of 3.2236E + 04 and 1.44208E + 05 intergene bases with a P_{eff} of 0.224 *esebssiwaagoT*$_Q$ units (Table 6).

TIPARP is a 2 A 4 NCA stIMfM final SEB gene at *x*-, *y*-vertical axis angulation 63.1°. *TIPARP* has an *uppasebssiwa*, *dppasebssiwa*, *uppmsebssiwa* and *dppmsebssiwa* of 2.0872E + 04, 1.44564E + 05, 1.7547E + 04 and 2.7819E + 04 intergene bases. *TIPARP* has an *uppesebssiwaa* and *dppesebssiwaa* of 1.9209E + 04 and 8.6191E + 04 intergene bases with a P_{eff} of 0.223 *esebssiwaagoT*$_Q$ units (Table 6).

SIN3A is a 2 M 7 NCA final SEB gene at *x*-, *y*-vertical axis angulation 63.0°. *SIN3A* has an *uppasebssiwa*, *dppasebssiwa*, *uppmsebssiwa* and *dppmsebssiwa* of 2.2660E + 04, 5.6611E + 04, 4.082E + 03 and 6.3132E + 04 intergene bases. *SIN3A* has an *uppesebssiwaa* and *dppesebssiwaa* of 1.3371E + 04 and 5.9872E + 04 intergene bases with a P_{eff} of 0.223 *esebssiwaagoT*$_Q$ units (Table 6).

PPARG is a 2 M 5 initial and final SEB gene at *x*-, *y*-vertical axis angulation 63.2°. *PPARG* has an *uppasebssiwa*, *dppasebssiwa*, *uppmsebssiwa* and *dppmsebssiwa* of 5.1238E + 04, 9.3514E + 04, 2.140E + 03 and 1.47194E + 05 intergene bases. *PPARG* has an *uppesebssiwaa* and *dppesebssiwaa* of 2.6689E + 04 and 1.20354E + 05 intergene bases with a P_{eff} of 0.222 *esebssiwaagoT*$_Q$ units (Table 6).

RARB is a 4 A 9 initial and final SEB gene at *x*-, *y*-vertical axis angulation 63.2°. *RARB* has an *uppasebssiwa*, *dppasebssiwa*, *uppmsebssiwa* and *dppmsebssiwa* of 2.6685E + 04, 2.28760E + 05, 4.5444E + 04 and 9.6325E + 04 intergene bases. *RARB* has an *uppesebssiwaa* and *dppesebssiwaa* of 3.6064E + 04 and 1.62543E + 05 intergene bases with a P_{eff} of 0.222 *esebssiwaagoT*$_Q$ units (Table 6).

CYP1A1 is a 3 A 7 initial and final SEB gene at *x*-, *y*-vertical axis angulation 63.9°. *CYP1A1* has an *uppasebssiwa*, *dppasebssiwa*, *uppmsebssiwa* and *dppmsebssiwa* of 1.620E + 03, 5.2602E + 04, 1.9646E + 04 and 4.5892E + 04 intergene bases. *CYP1A1* has an *uppesebssiwaa* and *dppesebssiwaa* of 1.0633E + 04 and 4.9247E + 04 intergene bases with a P_{eff} of 0.216 *esebssiwaagoT*$_Q$ units (Table 6).

CYP1A2 is a 3 A 9 ACM final SEB gene at *x*-, *y*-vertical axis angulation 65.7°. *CYP1A2* has an *uppasebssiwa*, *dppasebssiwa*, *uppmsebssiwa* and *dppmsebssiwa* of 1.1688E + 04, 1.11934E + 05, 1.9604E + 04 and 4.3582E + 04 intergene bases. *CYP1A2* has an *uppesebssiwaa* and

dppesebssiwaa of 1.5646E + 04 and 7.7758E + 04 intergene bases with a P_{eff} of 0.210 *esebssiwaagoT*$_Q$ units (Table 6).

ESRRG is a 5 A 9 ACM final SEB gene at *x*-, *y*-vertical axis angulation 64.7°. *ESRRG* has an *uppasebssiwa*, *dppasebssiwa*, *uppmsebssiwa* and *dppmsebssiwa* of 3.8238E + 04, 3.07603E + 05, 5.5149E + 04 and 1.38670E + 05 intergene bases. *ESRRG* has an *uppesebssiwaa* and *dppesebssiwaa* of 4.6694E + 04 and 2.23137E + 05 intergene bases with a P_{eff} of 0.209 *esebssiwaagoT*$_Q$ units (Table 6).

NR1H3 is a 2 M 7 ACM final SEB gene at *x*-, *y*-vertical axis angulation 64.7°. *NR1H3* has an *uppasebssiwa*, *dppasebssiwa*, *uppmsebssiwa* and *dppmsebssiwa* of 1.1881E + 04, 2.3346E + 04, 8.567E + 03 and 7.4260E + 04 intergene bases. *NR1H3* has an *uppesebssiwaa* and *dppesebssiwaa* of 1.0224E + 04 and 4.8803E + 04 intergene bases with a P_{eff} of 0.209 *esebssiwaagoT*$_Q$ units (Table 6).

NRF1 is a 2 A 5 initial and final SEB gene at *x*-, *y*-vertical axis angulation 65.8°. *NRF1* has an *uppasebssiwa*, *dppasebssiwa*, *uppmsebssiwa* and *dppmsebssiwa* of 8.803E + 03, 9.6944E + 04, 3.2897E + 04 and 1.11479E + 05 intergene bases. *NRF1* has an *uppesebssiwaa* and *dppesebssiwaa* of 2.0850E + 04 and 1.04212E + 05 intergene bases with a P_{eff} of 0.200 *esebssiwaagoT*$_Q$ units (Table 6).

ESRRA is a 3 M 9 ACM final SEB gene at *x*-, *y*-vertical axis angulation 64.7°. *ESRRA* has an *uppasebssiwa*, *dppasebssiwa*, *uppmsebssiwa* and *dppmsebssiwa* of 9.619E + 03, 2.5863E + 04, 5.972E + 03 and 5.3534E + 04 intergene bases. *ESRRA* has an *uppesebssiwaa* and *dppesebssiwaa* of 3.9699E + 04 and 3.9699E + 04 intergene bases with a P_{eff} of 0.196 *esebssiwaagoT*$_Q$ units (Table 6).

ARNTL is a 2 M 5 initial and final SEB gene at *x*-, *y*-vertical axis angulation 66.9°. *ARNTL* has an *uppasebssiwa*, *dppasebssiwa*, *uppmsebssiwa* and *dppmsebssiwa* of 1.7408E + 04, 4.4697E + 04, 1.2785E + 04 and 1.13014E + 05 intergene bases. *ARNTL* has an *uppesebssiwaa* and *dppesebssiwaa* of 1.5097E + 04 and 7.8855E + 05 intergene bases with a P_{eff} of 0.191 *esebssiwaagoT*$_Q$ units (Table 6).

EXOC7 is a 2 M 5 initial and final SEB gene at *x*-, *y*-vertical axis angulation 67.1°. *EXOC7* has an *uppasebssiwa*, *dppasebssiwa*, *uppmsebssiwa* and *dppmsebssiwa* of 5.265E + 03, 9.381E + 03, 2.119E + 03 and 2.9570E + 04 intergene bases. *EXOC7* has an *uppesebssiwaa* and *dppesebssiwaa* of 3.692E + 03 and 1.9475E + 04 intergene bases with a P_{eff} of 0.190 *esebssiwaagoT*$_Q$ units (Table 6).

ESR1 is a 4 A 9 ACM (-2) NCA (+2) final SEB gene at *x*-, *y*-vertical axis angulation 67.8°. *ESR1* has an *uppasebssiwa*, *dppasebssiwa*, *uppmsebssiwa* and *dppmsebssiwa* of 2.4317E + 04, 3.26647E + 05, 7.5809E + 04 and 2.18623E + 05 intergene bases. *ESR1* has an *uppesebssiwaa* and *dppesebssiwaa* of 5.0063E + 04 and 2.72635E + 05 intergene bases with a P_{eff} of 0.184 *esebssiwaagoT*$_Q$ units (Table 6).

DIO2 is a 2 A 5 initial and final SEB gene at *x*-, *y*-vertical axis angulation 67.9°. *DIO2* has an *uppasebssiwa*, *dppasebssiwa*, *uppmsebssiwa* and *dppmsebssiwa* of 3.1126E + 04, 4.10031E + 05, 6.5612E + 04 and 1.19045E + 05 intergene bases. *DIO2* has an *uppesebssiwaa* and *dppesebssiwaa* of 4.8369E + 04 and 2.64538E + 05 intergene bases with a P_{eff} of 0.183 *esebssiwaagoT*$_Q$ units (Table 6).

RARA is a 2 M 5 initial and final SEB gene at *x*-, *y*-vertical axis angulation 68.1°. *RARA* has an *uppasebssiwa*, *dppasebssiwa*, *uppmsebssiwa* and *dppmsebssiwa* of 2.0934E + 04, 1.76592E + 05, 1.8669E + 04 and 4.2109E + 04 intergene bases. *RARA* has an *uppesebssiwaa* and *dppesebssiwaa* of 1.9801E + 04 and 1.09351E + 05 intergene bases with a P_{eff} of 0.181 *esebssiwaagoT*$_Q$ units (Table 6).

NCOR2 is a 4 M 9 initial and final SEB gene at *x*-, *y*-vertical axis angulation 68.5°. *NCOR2* has an *uppasebssiwa*, *dppasebssiwa*, *uppmsebssiwa* and *dppmsebssiwa* of 1.6316E + 04, 3.4858E

+ 04, 1.52E + 04 and 1.42541E + 05 intergene bases. *NCOR2* has an *uppesebssiwaa* and *dppesebssiwaa* of 1.5758E + 04 and 8.8699E + 04 intergene bases with a P_{eff} of 0.178 *esebssiwaagoT*$_Q$ units (Table 6).

THRA is a 2 M 7 ACM final SEB gene at *x*-, *y*-vertical axis angulation 68.6°. *THRA* has an *uppasebssiwa*, *dppasebssiwa*, *uppmsebssiwa* and *dppmsebssiwa* of 2.1732E + 04, 4.7912E + 04, 9.383E + 03 and 1.27923E + 05 intergene bases. *THRA* has an *uppesebssiwaa* and *dppesebssiwaa* of 1.5557E + 04 and 8.7918E + 04 intergene bases with a P_{eff} of 0.177 *esebssiwaagoT*$_Q$ units (Table 6).

NRIP1 is a 2 M 7 ACM final SEB gene at *x*-, *y*-vertical axis angulation 69.1°. *NRIP1* has an *uppasebssiwa*, *dppasebssiwa*, *uppmsebssiwa* and *dppmsebssiwa* of 2.36743E + 05, 5.72072E + 05, 4.6198E + 04 and 1.059404E + 06 intergene bases. *NRIP1* has an *uppesebssiwaa* and *dppesebssiwaa* of 1.41470E + 05 and 8.15738E + 05 intergene bases with a P_{eff} of 0.173 *esebssiwaagoT*$_Q$ units (Table 6).

CYP1B1 is a 5 M 11 initial and final SEB gene at *x*-, *y*-vertical axis angulation 69.6°. *CYP1B1* has an *uppasebssiwa*, *dppasebssiwa*, *uppmsebssiwa* and *dppmsebssiwa* of 6.4259E + 04, 1.90422E + 05, 5.8349E + 04 and 5.36193E + 05 intergene bases. *CYP1B1* has an *uppesebssiwaa* and *dppesebssiwaa* of 6.1304E + 04 and 3.63307E + 04 intergene bases with a P_{eff} of 0.169 *esebssiwaagoT*$_Q$ units (Table 6).

ALDH3A1 is a 3 A 7 initial and final SEB gene at *x*-, *y*-vertical axis angulation 69.7°. *ALDH3A1* has an *uppasebssiwa*, *dppasebssiwa*, *uppmsebssiwa* and *dppmsebssiwa* of 7.446E + 03, 9.0420E + 04, 1.3274E + 04 and 3.2789E + 04 intergene bases. *ALDH3A1* has an *uppesebssiwaa* and *dppesebssiwaa* of 1.0360E + 04 and 6.1604E + 04 intergene bases with a P_{eff} of 0.168 *esebssiwaagoT*$_Q$ units (Table 6).

ACSM2A is a 2 A 5 initial and final SEB gene at *x*-, *y*-vertical axis angulation 70.9°. *ACSM2A* has an *uppasebssiwa*, *dppasebssiwa*, *uppmsebssiwa* and *dppmsebssiwa* of 8.452E + 03, 1.14103E + 05, 1.2592E + 04 and 1.8897E + 04 intergene bases. *ACSM2A* has an *uppesebssiwaa* and *dppesebssiwaa* of 1.0522E + 04 and 6.6500E + 04 intergene bases with a P_{eff} of 0.158 *esebssiwaagoT*$_Q$ units (Table 6).

NQO1 is a 2 A 5 initial and final SEB gene at *x*-, *y*-vertical axis angulation 72.2°. *NQO1* has an *uppasebssiwa*, *dppasebssiwa*, *uppmsebssiwa* and *dppmsebssiwa* of 8.720E + 03, 1.85367E + 05, 2.8226E + 04 and 6.5249E + 04 intergene bases. *NQO1* has an *uppesebssiwaa* and *dppesebssiwaa* of 1.8473E + 04 and 1.25308E + 05 intergene bases with a P_{eff} of 0.147 *esebssiwaagoT*$_Q$ units (Table 6).

ESR2 is a 2 A 5 initial and final SEB gene at *x*-, *y*-vertical axis angulation 73.6°. *ESR2* has an *uppasebssiwa*, *dppasebssiwa*, *uppmsebssiwa* and *dppmsebssiwa* of 1.810E + 03, 1.26875E + 05, 2.5861E + 04 and 7.6369E + 04 intergene bases. *ESR2* has an *uppesebssiwaa* and *dppesebssiwaa* of 1.3835E + 04 and 1.01622E + 05 intergene bases with a P_{eff} of 0.136 *esebssiwaagoT*$_Q$ units (Table 6).

ME1 is a 2 M 5 initial and final SEB gene at *x*-, *y*-vertical axis angulation 73.7°. *ME1* has an *uppasebssiwa*, *dppasebssiwa*, *uppmsebssiwa* and *dppmsebssiwa* of 5.2685E + 04, 1.58850E + 05, 2.6415E + 04 and 4.27755E + 05 intergene bases. *ME1* has an *uppesebssiwaa* and *dppesebssiwaa* of 3.9550E + 04 and 2.92302E + 05 intergene bases with a P_{eff} of 0.135 *esebssiwaagoT*$_Q$ units (Table 6).

CYP3A7 is a 2 M 5 initial and final SEB gene at *x*-, *y*-vertical axis angulation 76.6°. *CYP3A7* has an *uppasebssiwa*, *dppasebssiwa*, *uppmsebssiwa* and *dppmsebssiwa* of 1.9558E + 04, 5.2160E + 04, 2.4091E + 04 and 3.42328E + 05 intergene bases. *CYP3A7* has an *uppesebssiwaa* and *dppesebssiwaa* of 2.1824E + 04 and 1.97244E + 05 intergene bases with a P_{eff} of 0.111 *esebssiwaagoT*$_Q$ units (Table 6).

UGT1A7 is a 2 M 5 ACM final extended SEB gene at *x*-, *y*-vertical axis angulation 77.2°. *UGT1A7* has an *uppasebssiwa*, *dppasebssiwa*, *uppmsebssiwa* and *dppmsebssiwa* of 1.4610E + 04, 3.4472E + 04, 4.4440E + 04 and 5.20736E + 05 intergene bases. *UGT1A7* has an *uppesebssiwaa* and *dppesebssiwaa* of 2.9540E + 04 and 2.77604E + 05 intergene bases with a P_{eff} of 0.106 *esebssiwaagoT*$_Q$ units (Table 6).

DIO3 is a 2 A 5 initial and final SEB gene at *x*-, *y*-vertical axis angulation 78.4°. *DIO3* has an *uppasebssiwa*, *dppasebssiwa*, *uppmsebssiwa* and *dppmsebssiwa* of 4.463E + 03, 6.6352E + 04, 2.545E +03 and 6.385E + 03 intergene bases. *DIO3* has an *uppesebssiwaa* and *dppesebssiwaa* of 3.504E + 03 and 3.6368E + 04 intergene bases with a P_{eff} of 0.096 *esebssiwaagoT*$_Q$ units (Table 6).

ARNT is a 2 M 5 initial and final SEB gene at *x*-, *y*-vertical axis angulation 82.4°. *ARNT* has an *uppasebssiwa*, *dppasebssiwa*, *uppmsebssiwa* and *dppmsebssiwa* of 3.424E + 03, 1.23406E + 05, 5.151E + 03 and 1.2359E + 04 intergene bases. *ARNT* has an *uppesebssiwaa* and *dppesebssiwaa* of 4.287E +03 and 6.7882E + 04 intergene bases with a P_{eff} of 0.063 *esebssiwaagoT*$_Q$ units (Table 6).

TSPAN14 is a 2 A 8 ACM ACM final SEB gene at *x*-, *y*-vertical axis angulation 83.1°. *TPSAN14* has an *uppasebssiwa*, *dppasebssiwa*, *uppmsebssiwa* and *dppmsebssiwa* of 1.5608E + 04, 4.94044E + 05, 1.4376E + 04 and 3.3255E + 04 intergene bases. *TSPAN14* has an *uppesebssiwaa* and *dppesebssiwaa* of 1.4992E + 04 and 2.63650E + 05 intergene bases with a P_{eff} of 0.057 *esebssiwaagoT*$_Q$ units (Table 6).

***co*-planar polychlorinated biphenyl.** *HNF4A* is a 2 A 5 NCA ACM final SEB gene at *x*-, *y*-vertical axis angulation 38.4°. *HNF4A* has an *uppasebssiwa*, *dppasebssiwa*, *uppmsebssiwa* and *dppmsebssiwa* of 1.0705E + 04, 1.08134E + 05, 1.47071E + 05 and 2.61534E + 04 intergene bases. *HNF4A* has an *uppesebssiwaa* and *dppesebssiwaa* of 7.8888E + 04 and 1.84834E + 05 intergene bases with a P_{eff} of 0.427 *esebssiwaagoT*$_Q$ units (Table 7).

PCK1 is a 3 M 7 ACM ACM final SEB gene at *x*-, *y*-vertical axis angulation 49.5°. *PCK1* has an *uppasebssiwa*, *dppasebssiwa*, *uppmsebssiwa* and *dppmsebssiwa* of 1.04153E + 05, 2.22857E + 05, 1.2995E + 04 and 1.29275E + 05 intergene bases. *PCK1* has an *uppesebssiwaa* and *dppesebssiwaa* of 5.8574E + 04 and 1.76066E + 05 intergene bases with a P_{eff} of 0.333 *esebssiwaagoT*$_Q$ units (Table 7).

RESP18 is a 3 M 5 ACM q term final SEB gene at *x*-, *y*-vertical axis angulation 50.5°. *RESP18* has an *uppasebssiwa*, *dppasebssiwa*, *uppmsebssiwa* and *dppmsebssiwa* of 4.9633E + 04, 1.16462E + 05, 3.133E + 05 and 4.4955 + 05 intergene bases. *RESP18* has an *uppesebssiwaa* and *dppesebssiwaa* of 2.6383E + 04 and 8.0709E + 04 intergene bases with a P_{eff} of 0.327 *esebssiwaagoT*$_Q$ units (Table 7).

CYP5A is a 2 A 5 initial and final SEB gene at *x*-, *y*-vertical axis angulation 52.6°. *CYP5A* has an *uppasebssiwa*, *dppasebssiwa*, *uppmsebssiwa* and *dppmsebssiwa* of 4.1825E + 04, 3.21263E + 05, 1.14755E + 05 and 1.84810E + 05 intergene bases. *CYP5A* has an *uppesebssiwaa* and *dppesebssiwaa* of 7.8290E + 04 and 2.53036E + 05 intergene bases with a P_{eff} of 0.309 *esebssiwaagoT*$_Q$ units (Table 7).

RARG is a 2 A 5 initial and final SEB gene at *x*-, *y*-vertical axis angulation 52.7°. *RARG* has an *uppasebssiwa*, *dppasebssiwa*, *uppmsebssiwa* and *dppmsebssiwa* of 3.847E + 03, 4.4654E + 04, 2.5927E + 04 and 5.1723E + 04 intergene bases. *RARG* has an *uppesebssiwaa* and *dppesebssiwaa* of 1.4887E + 04 and 4.8189E + 04 intergene bases with a P_{eff} of 0.309 *esebssiwaagoT*$_Q$ units (Table 7).

CYCS is a 2 M 5 initial and final SEB gene at *x*-, *y*-vertical axis angulation 54.1°. *CYCS* has an *uppasebssiwa*, *dppasebssiwa*, *uppmsebssiwa* and *dppmsebssiwa* of 7.1987E + 04, 2.02726E + 05, 1.3747E + 04 and 8.5931E + 04 intergene bases. *CYCS* has an *uppesebssiwaa* and

Table 7. Effective intracellular pressure mapping of gene activation by *co*-planar polychlorinated biphenyl via the AhR-Erα/β (Arnt): Nrf-2:: Rev-Erb β, Errα: Dio3/Dio2 (Trα) pathway•.

Human gene (no. of bases, locus bases or n/a)	Gene locus (ch, strand)	Angle (°)	Episode category (final, initial SEB structure)	*uppesebssiwaa*, *dppesebssiwaa* (P_{eff}, fract)	P_{eff} range effect fract (Δ %; Δ fract)
HNF4A, hepatocyte nuclear factor 4A (79,067; n/a)	10q26.3 (+)	38.4	2 A 4 nca acm (2 A 5)	7.8888E + 04, 1.84834E + 04 (*0.427*)	(-)[&]
AHR				(*0.395*)	(+)
COX8C				(*0.381*)	(+2.5; 0.24)
CEACAM1				(*0.379*)	(+13.9; 0.68)
SLC2A4				(*0.376*)	(-)[°]
RXRA				(0.374)	(+)
PCK1, phosphophenolpyruvate carboxykinase 1 (7,042; n/a)	20q13.31 (+)	49.8	3 A 7 acm acm ext^ (3 A 7)	5.8574E + 04, 1.76066E + 05 (*0.333*)	(-)[&]
GADD45B				(*0.332*)	(+)
NFE2L2				(*0.331*)	(+0.08; 1.14)
RESP18, regulated endocrine-specific protein 18 homolog (9,377; n/a)	2q35 (-)	50.5	3 M 5 acm q term (3 M 7)	2.6383E + 04, 8.0709E + 04 (*0.327*)	(-)[&]
ALAS1				(*0.324*)	(-)[&]
CYP5A, cytochrome P450, family 5, subfamily A (49,988; n/a)	18q22.3 (-)	52.6	2 A 5 (-)	7.8290E + 04, 2.53036E + 05 [*0.309* (*0.3094*)]	(+2.2)
RARG, retinoic acid receptor gamma (22,415; n/a)	12q13.13 (-)	52.3	2 A 5 (-)	1.48887E + 04, 4.8189E + 04 [*0.309* (0.3089)]	(+)
CYCS, cytochrome C, somatic (62,499; n/a)	7p15.3 (-)	54.1	2 M 5 (-)	4.2867E + 04, 1.44328E + 04 (*0.297*)	(+0.30)
DBP				(*0.283*)	(-)
SCD				(0.282)	(-)
RXRB				(*0.282*)	(-)
PPARGC1A				*(0.279)*	(-)
FASN, fatty acid synthase (19,962; n/a)	7q25.3 (-)	56.4	2 M 5 (-)	8.785E + 03, 3.1543E +04 (*0.278*)	(-)[&]
MT1A				(*0.273*)	(+0.11; 1.57)
NOS1, nitric oxide synthase 1 (244,082; n/a)	12q24.22 (-)	58.4	2 A 7 acm (2 A 5)	1.0595E + 04, 4.0449E + 04 (*0.262*)	(+)
GADD45A, growth arrest and DNA damage inducible alpha (3,162; n/a)	1p31.3 (+)	60.4	3 M 7 ext (+)	2.4941E + 04, 1.01955E + 05 (*0.245*)	(+0.34)
NRID2, nuclear receptor subfamily 1 group D member 2 (35,359; n/a)	3p24.2 (+)	60.8	2 A 6 ext (2 A 5)	6.2412E + 04, 2.58343E + 05 (0.242)	(+)
COL1A1, collagen type I alpha 1 chain (18,360; n/a)[◇]	17q21.33 (-)	-	-	-(*0.241*)	(+0.60)
SREBF1 (26,619; n/a)				(*0.237*)	(-)[&,°]
DIO1				(*0.236*)	(-)[CM]
TIPARP				(*0.223*)	(-)
SIN3A				[*0.223* (0.2229)]	(-)
PPARG				(*0.222*)	(-)
RARB				(0.222)	(-)
CAT, catalase (33,138)	11p13 (+)	63.4	2 M 5 (-)	1.7938E + 04, 8.1622E + 04 (*0.220*)	(+0.87)
CYP1A1				(*0.216*)	(+42.9; 1.28)
COX6C, cytochrome C oxidase subunit 6C (20,815; 20,863)	8q22.2 (-)	64.5	2 A 4 acm (2 A 5)	3.3414E + 04, 1.58072E + 05 (*0.211*)	(+0.34)
ESRRG				(*0.209*)	(-,+)[§]
CYP1A2				(*0.201*)	(+0.26; 2.60)
NRF1				(*0.200*)	(-)

(*Continued*)

Table 7. (Continued)

Human gene (no. of bases, locus bases or n/a)	Gene locus (ch, strand)	Angle (°)	Episode category (final, initial SEB structure)	*uppesebssiwaa*, *dppesebssiwaa* (P_{eff}, fract)	P_{eff} range effect fract (Δ %; Δ fract)
ESRRA				(*0.196*)	(+, -)[■,○]
ARNTL				(*0.191*)	(-)
EXOC7				(*0.190*)	(+0.23; 0.22)
ESR1				[*0.184* (0.1836)]	(+)
DIO2				(*0.183*)	□ (-)[&]
RARA				(*0.181*)	(+)
NCOR2				(*0.178*)	(+)
THRA				(*0.177*)	(+)
NRIP1				(*0.173*)	(+)[*]
CYP1B1				(*0.1687*)	(+19.5; 0.81)
GSTM2, glutathione S-transferase, mu 2 (41,530; 53,476)	1p13.3 (+)	69.6	2 M 6 nca acm (2 A 5)	1.4017E + 04, 8.3148E + 04 [0.169 (*0.1686*)]	(+6.6)
ALDH3A1				(*0.168*)	(+0.19; 0.10)
ACSM2A				(*0.158*)	(-)[&]
NQO1				(*0.147*)	(+0.79; 1.22)
ESR2				(*0.136*)	(+)
ME1				(*0.135*)	(+0.15; 1.53)^
IGHA1, immunoglobulin heavy constant alpha 1 (1,546; 4,671)[◇]	14q32.33 (-)	-	-	-(*0.131*)	(-)[&]
LGAL1, galectin 1 (4,201; n/a)	22q13.1 (+)	74.2	3 A 7 (-)	6.856E + 03, 5.2584E + 04 (*0.130*)	(+0.90)
UGT1A7				(*0.106*)	(+0.53; 0.19)
DIO3				(*0.096*)	(+)
ARNT				(*0.063*)	--
TSPAN14				(*0.057*)	--

[•] % P_{eff} duration of effect increases or decreases from Table 6; Δ ratio, ratio from % change in comparison to TCDD P_{eff} duration of effect

[&] % dec in effect genes include *RESP18*, *IGHA1*, - 0.84; *FASN*, -0.72; *PCK1*, *ACSM2A* - 0.36; and *HNF4A*, *ALAS1*, *DIO2*, *SREBF1*, - 0.24 (2-fold change threshold)

[°]*SLC2A4*, SREBF1 binding response element(s) [■] *ESRRA* over-activation during EXOC7 protein expression phase

[§] *NFIA/-B*, *PCK1* required transcription factor decrease, as does antagonist *NFIX* (as cited)

^ activation of *ME1* gene with TRα/-β response element (TRE) increases only; and

[*] RIP140 (*NRIP1*) as co-activator for AhR and ERRα transcription factors Note(s): [1)] Gene loci sub-episode block structure (SEB) variations include non-contributory anisotropy (NCA), anisotropy converted to mesotropy (ACM), 0.5-factor adjusted stabilizing mesotropy or anisotropy converted to stabilizing isotropy for anisotropy or mesotropy (stIAfM, stIMfA or stIMfM), and/or extended block (ext) SEB, ^ ie *PCK1* is a 2 M 5 (-2) acm (+2) acm extended SEB gene; and [2)] gene(s) with previously reported episode and sub-episode block structure include [◇] *COL1A1* [22] and *IGHA1* [38].

https://doi.org/10.1371/journal.pone.0236446.t007

dppesebssiwaa of 4.2867E + 04 and 1.44328E + 05 intergene bases with a P_{eff} of 0.297 *esebssiwaago*T_Q units (Table 7).

FASN is a 2 M 5 initial and final SEB gene at *x*-, *y*-vertical axis angulation 56.4°. *FASN* has an *uppasebssiwa*, *dppasebssiwa*, *uppmsebssiwa* and *dppmsebssiwa* of 1.6097E + 04, 5.0211E + 04, 1.472E + 04 or 1.2875E + 04 intergene bases. *FASN* has an *uppesebssiwaa* and *dppesebssiwaa* of 8.785E + 03 and 3.1543E + 04 intergene bases with a P_{eff} of 0.278 *esebssiwaago*T_Q units (Table 7).

NOS1 is a 3 A 7 ACM final SEB gene at *x*-, *y*-vertical axis angulation 58.4°. *NOS1* has an *uppasebssiwa*, *dppasebssiwa*, *uppmsebssiwa* and *dppmsebssiwa* of 2.496E + 03, 3.6292E + 04, 1.8694E + 04 and 4.4605E + 04 intergene bases. *NOS1* has an *uppesebssiwaa* and *dppesebssiwaa*

of 1.0595E + 04 and 4.0449E + 04 intergene bases with a P_{eff} of 0.262 *esebssiwaagoT*$_Q$ units (Table 7).

GADD45A is a 3 M 7 ext final SEB gene at *x*-, *y*-vertical axis angulation 60.4°. *GADD45A* has an *uppasebssiwa*, *dppasebssiwa*, *uppmsebssiwa* and *dppmsebssiwa* of 4.3412E + 04, 8.5949E + 04, 6.470E + 03 and 1.17960E + 05 intergene bases. *GADD45A* has an *uppesebssiwaa* and *dppesebssiwaa* of 2.4941E + 04 and 1.01955E + 05 intergene bases with a P_{eff} of 0.245 *esebssiwaagoT*$_Q$ units (Table 7).

NRID2 is a 2 A 6 ext final SEB gene at *x*-, *y*-vertical axis angulation 60.8°. *NRID2* has an *uppasebssiwa*, *dppasebssiwa*, *uppmsebssiwa* and *dppmsebssiwa* of 3.6660E + 04, 3.30263E + 05. 8.8163E + 04, 1.86423E + 05 intergene bases. *NRID2* has an *uppesebssiwaa* and *dppesebssiwaa* of 6.2412E + 04 and 2.58343E + 05 intergene bases with a P_{eff} of 0.242 *esebssiwaagoT*$_Q$ units (Table 7).

CAT is a 2 M 5 initial and final SEB gene at *x*-, *y*-vertical axis angulation 63.4°. *CAT* has an *uppasebssiwa*, *dppasebssiwa*, *uppmsebssiwa* and *dppmsebssiwa* of 3.0584E + 04, 7.9950E + 04, 5.293E + 03 and 8.3295E + 04 intergene bases. *CAT* has an *uppesebssiwaa* and *dppesebssiwaa* of 1.7938E + 04 and 8.1622E + 04 intergene bases with a P_{eff} of 0.220 *esebssiwaagoT*$_Q$ units (Table 7).

COX6C is a 2 A 4 ACM final SEB gene at *x*-, *y*-vertical axis angulation 64.5°. *COX6C* has an *uppasebssiwa*, *dppasebssiwa*, *uppmsebssiwa* and *dppmsebssiwa* of 5.3278E + 04, 1.13133E + 05, 1.3550E + 04 and 2.03011E + 05 intergene bases. *COX6C* has an *uppesebssiwaa* and *dppesebssiwaa* of 3.3414E + 04 and 1.58072E + 05 intergene bases with a P_{eff} of 0.211 *esebssiwaagoT*$_Q$ units (Table 7).

GSTM2 is a 2 M 5 NCA ACM final SEB gene at *x*-, *y*-vertical axis angulation 59.6°. *GSTM2* has an *uppasebssiwa*, *dppasebssiwa*, *uppmsebssiwa* and *dppmsebssiwa* of 2.2001E + 04, 4.1822E + 04, 6.033E + 03 and 1.24474E + 05 intergene bases. *GSTM2* has an *uppesebssiwaa* and *dppesebssiwaa* of 1.4017E + 04 and 8.3148E + 04 intergene bases with a P_{eff} of 0.169 *esebssiwaagoT*$_Q$ units (Table 7).

LGALS1 is a 3 A 7 initial and final SEB gene at *x*-, *y*-vertical axis angulation 74.2°. *LGALS1* has an *uppasebssiwa*, *dppasebssiwa*, *uppmsebssiwa* and *dppmsebssiwa* of 6.039E + 03, 8.6386E + 04, 7.672E + 03 and 1.8783E + 04 intergene bases. *LGALS1* has an *uppesebssiwaa* and *dppesebssiwaa* of 6.856E + 03 and 5.2584E + 04 intergene bases with a P_{eff} of 0.130 *esebssiwaagoT*$_Q$ units (Table 7).

***ortho*-planar intracellular, o*rtho*-*co*-planar extracellular polychlorinated biphenyl.**

DCAKD is a 2 M 5 acm final SEB gene at *x*-, *y*-vertical axis angulation 72.1°. *DCAKD* has an *uppasebssiwa*, *dppasebssiwa*, *uppmsebssiwa* and *dppmsebssiwa* of 6.7286E + 04, 1.07727E + 05, 3.77E + 02 and 5.3956E + 04 intergene bases. *DCAKD* has an *uppesebssiwaa* and *dppesebssiwaa* of 3.3832E + 04 and 8.0842E + 04 intergene bases with a P_{eff} of 0.418 *esebssiwaagoT*$_Q$ units (Table 8).

PPARA is a 2 A 4 NCA final SEB gene at *x*-, *y*-vertical axis angulation 39.7°. *PPARA* has an *uppasebssiwa*, *dppasebssiwa*, *uppmsebssiwa* and *dppmsebssiwa* of 5.7120E + 04, 1.23677E + 05, 2.116E + 03 and 1.8633E + 04 intergene bases. *PPARA* has an *uppesebssiwaa* and *dppesebssiwaa* of 2.9618E + 04 and 7.1155E + 04 intergene bases with a P_{eff} of 0.416 *esebssiwaagoT*$_Q$ units (Table 8).

DDIT3 is a 3 M 5 NCA ACM final SEB gene at *x*-, *y*-vertical axis angulation 40.97°. *DDIT3* has an *uppasebssiwa*, *dppasebssiwa*, *uppmsebssiwa* and *dppmsebssiwa* of 5.2432E + 04, 1.09617E + 05, 6.288E + 03 and 3.5032E + 04 intergene bases. *DDIT3* has an *uppesebssiwaa* and *dppesebssiwaa* of 2.9360E + 04 and 7.2324E + 04 intergene bases with a P_{eff} of 0.406 *esebssiwaagoT*$_Q$ units (Table 8).

Table 8. Effective intracellular pressure mapping of gene activation by (*co*-) *ortho*-planar polychlorinated biphenyls and metabolites via the Car/PxR, Rarγ: Pparα/γ, Rxrβ (Srebf1, -LxRβ): Arnt (AhR-Erβ)/Ar:: Dio1/Dio2 (Trβ) pathway•.

Human gene (no. of bases, locus bases or n/a)	Gene locus (ch, strand)	Angle (°)	Episode category (final, initial SEB structure)	*uppesebssiwaa*, *dppesebssiwaa* (P_{eff}, fract)	P_{eff} range effect fract (% inc)
DCAKD, dephospho-CoA kinase domain containing (37,804)	17q21.31 (-)	72.1	2 M 3 acm (2 M 5)	3.3832E + 04, 8.0842E + 04 (*0.418*)	(+1.0)
PPARA, peroxisome proliferator activated receptor alpha (93,236, 237,141)	22q13.31 (+)	39.7	2 A 4 nca (2 A 5)	2.9618E + 04, 7.1155E + 04 (*0.416*)	(+)^
DDIT3, DNA damage inducible transcript 3 (5,150; n/a)	12q13.3 (-)	41	3 M 5 nca acm (3 M 7)	2.9360E + 04, 7.2324E + 04 (0.406)	(+)
AHR				(*0.395*)	(-)
TRFC, transferrin receptor 1 (54,979; 75,665)	3q29 (-)	43.25	2 M 5 (-)	2.5135E + 04, 6.4948E + 04 [0.3870 (*0.387*)]	(+)
NR1I3, nuclear receptor subfamily 1 group I member 3 (8,933; n/a)	1p23.3 (-)	43.2	3 M 5 acm (3 M 7)	4.6203E + 04, 1.19293E + 05 [0.3873 (*0.387*)]	(+)
FOXA1, forkhead box protein A1 (6,508; n/a)‡	14q21.1 (-)	43.6	3 A 5 acm (3 A 7)	5.5470E + 04, 1.44398E + 05 [*0.384* (0.3841)]	(+0.7)
RXRA				(0.374)	(+)
NRID1				(0.373)	(+)
FKBP5, FKBP proplyl isomerase 5 (154,999; 163,363)	6q21.3 (-)	48.7	2 A 7 acm (2 A 5)	2.5366E + 04, 7.4138E + 04 (*0.342*)	(+)
PCK1				(*0.333*)	(-)&
NCOA1, nuclear receptor coactivator 1 (278,789; n/a)	2p23.3 (+)	50.8	3 M 9 stIMfa nca acm (3 M 7)	4.3171E + 04, 1.33165E + 05 [*0.324* (0.3242)]	(-)
CYP2B6, cytochrome P450, family 2, subfamily B6 (27,170, 31,800)•,‡	19q13.2 (+)	50.9	2 M 5 (-)	9.056E + 03, 2.7967E + 04 [*0.324* (0.3238)]	(+7.2)
NR1I2, nuclear receptor subfamily 1 group I member 2 (38,002; n/a)	3q13.33 (+)	52.3	2 A 5 (-)	2.7625E + 04, 8.8611E + 04 (*0.312*)	(+)
RARG, retinoic acid receptor gamma (22,415; n/a)	12q13.13 (-)	52.3	2 A 5 (-)	1.48887E + 04, 4.8189E + 04 (*0.309*)	(+)
CIDEA, cell death-inducing DNA fragmentation factor, alpha subunit (23,277; n/a)	18p11.21 (+)	54.7	2 A 3 stIMfA (2 A 5)	3.5735E + 04, 1.22190E + 05 (*0.292*)	(+1.3)
THRB, thyroxine receptor beta (378,604; n/a)	3p24.2 (-)	55.2	3 A 9 (-)	6.4001E + 04, 2.22137E + 05 (*0.288*)	(+)
MIR132, microRNA 132 (101; n/a)○	17p13.3 (-)	55.6	3 A 7 (-)	8.318E + 03, 2.9199E + 04 (*0.285*)	(+)
SCD				(0.282)	(+30.3)
RXRB				(*0.282*)	(+)
CYP3A4, cytochrome P450, family 3, subfamily A4 (27,306; n/a)	7q22.1 (-)	56.1	2 M 3 acm (2 M 5)	7.567E + 03, 2.6969E + 04 (*0.281*)	(+)^
PPARGC1A				(*0.279*)	(+)
CUL2, cullin2 (118,349; 118,470)	10p11.21 (-)	56.4	2 A 3 nca acm (2 A 5)	1.13635E + 05, 4.08028E + 05 (*0.278*)	(+1.0)
DUSP1, dual specificity phosphatase 1 (3,111; n/a)	5q35.1 (-)	57.2	3 M 7 (-)	1.9317E + 04, 7.1123E + 04 (*0.272*)	(-)&
NR1H2, Nuclear Receptor Subfamily 1 Group H Member 2 (53,736; 194,843)	19q13.3 (+)	57.3	2 M 5 (-)	1.7949E + 04, 6.6382E + 04 (*0.270*)	(-)
CEACAM5, carcinoembryonic antigen related cell adhesion molecule 1 (21,849; 63,627)	19q13.2 (+)	59.5	2 M 4 stIMfA (2 M 5)	(*0.252*)	(+)
MAFG, musculo-aponeurotic fibrosarcoma G (13,292; 19,622)	17q25.3 (-)	59.6	2 M 5 (-)	1.1026E + 04, 4.3832E + 04 (*0.252*)	(+)
SCD5, stearoyl-coenzyme A desaturase 5 (169,321; n/a)	4q21.22 (-)	59.6	2 M 5 (-)	6.0123E + 04, 2.39146E + 05 (*0.251*)	(+)
SREBF1				(*0.237*)	(+)
DIO1				(*0.236*)	□CM (+)
ALAS2, 5'-aminolevulinate synthase 2 (22,010; n/a)	Xp11.21 (-)	62.55	2 A 3 p term (2 A 5)	4.0611E + 04, 1.78730E + 04 (*0.227*)	(+0.7)
MBP, myelin basic protein (154,882; 235,160)○	18q23 (-)	62.9	2 A 3 q term (2 A 5)	5.7628E + 04, 2.57020E + 05 (0.224)	(-)
TIPARP				(*0.223*)	(+)
SIN3A				[*0.223* (0.2229)]	(+)

(*Continued*)

Table 8. (Continued)

Human gene (no. of bases, locus bases or n/a)	Gene locus (ch, strand)	Angle (°)	Episode category (final, initial SEB structure)	*uppesebssiwaa*, *dppesebssiwaa* (P_{eff}, fract)	P_{eff} range effect fract (% inc)
PPARG				(*0.222*)	(+)
CYP1A1				(*0.216*)	(+)
ESRRG				(*0.209*)	(+)
NR1H3				(*0.209*)	(+)
ESRRA				(*0.196*)	(-)
ARNTL				(*0.191*)	(+)
EXOC7				(*0.190*)	(+)
ESR1				(*0.184*)	(-)
DIO2				(*0.183*)	□ (-)[&]
NCOR1, nuclear receptor corepressor 1 (189,029; n/a)	17p11.2 (-)	70.6	2 A 5 (-)	1.1215E + 04, 6.9779E + 04 (*0.161*)	(+)
CASP3, caspase 3 (21,824; n/a)	4q35.1 (-)	70.7	2 M 5 (-)	2.0709E + 04, 1.29486E + 05 (*0.160*)	(+)
CES2, carboxylesterase 2 (10,653; 40.706)	16q21 (+)	70.8	2 A 4 acm (2 A 5)	1.5814E + 04, 9.9445E + 04 (*0.159*)	(+1.3)
CYP3A5, cytochrome P450, family 3, subfamily A5 (31,838: n/a)	7q22.1 (-)	71.05	3 M 5 ncax2 acm (3 M 7)	1.0477E + 04, 6.6776E + 04 (0.157)	(+44.7)
AR, androgen receptor (186,599; n/a)	Xp12 (+)	71.1	2 A 5 (-)	3.7729E + 04, 2.41270E + 05 (*0.156*)	(+)
CYP4A11, cytochrome P450, family 4, subfamily A11 (12,326; n/a)	1p33 (-)	72.0	2 M 5 (-)	1.3322E + 04, 8.9254E + 04 (*0.149*)	(+)
GTF2IRD1, general transcription factor II I repeat domain-containing (148,816; n/a)	7q11.23 (+)	73.1	2 M 7 acm (2 M 5)	1.5928E + 04, 1.14060E + 05 (*0.140*)	(-)[&]
ESR2				[*0.136* (*0.1361*)]	(+)
PPP1R9B, protein phosphatase 1 regulatory subunit 9B (17,288; n/a)[○]	17q21.33 (-)	74.4	2 M 5 (-)	3.9081E + 04, 3.03867E + 05 (*0.129*)	(+)
FABP3, fatty acid binding protein 3 (24,436; n/a)	1p35.2 (-)	74.5	2 A 7 (2 A 5)	1.1053E + 04, 8.6640E + 04 (*0.128*)	(+)
UGT1A1				[*0.106* (0.1064)]	(+)
FABP6, fatty acid binding protein 6 (51,369; 98,133) [‡]	5q33.3 (+)	78.3	2 M 4 (2 A 5)	3.9038E + 04, 4.04726E + 05 [*0.096* (0.0965)]	(+1.0)
DIO3				[*0.096* (0.0963)]	(-)
ARNT				(*0.063*)	(+)
TSPAN14				(*0.057*)	(+2.0)

[•] % P_{eff} duration of effect increases or decreases from baseline

[&] % P_{eff} duration of effect decrease genes include *GTF2IRD1*, -14.3; *PCK1*, *DUSP1*–10.7; *DIO2*, -7.1; and *NFIA*, P_{eff} n.d. (2-fold change threshold)

[○] *MIR132*, *MBP* and *PPP1R9B* P_{eff} duration of effect from sub-acute exposure to *ortho*-PCB-95 (intracellular) or *ortho*-PCB-136 (extracellular) and substituent metabolities (-OH, Ch3-SO2-) as cited

^*CYP3A4* is a PPARA-activated gene in the pathway

[‡] 4-digit *esebssiwaagoT*$_Q$ genes include *CYP2B6*, 0.3238 (*ALAS1*, 0.3236) and *FABP6*, 0.0965 (*DIO3*, 0.0963); • *CYP2B6* and *CYP3A5* are orthologs (pred) of rodent *CYP2B2* and *CYP2B15/-12*; and *PGC1α (*PPARGC1A*) as co-activator for PPARA, SREBPF1 and ERRα transcription factors Note(s): Gene loci sub-episode block structure (SEB) variations include non-contributory anisotropy (NCA), anisotropy converted to mesotropy (ACM), 0.5-factor adjusted stabilizing mesotropy or anisotropy converted to stabilizing isotropy for anisotropy or mesotropy (stIAfM, stIMfA or stIMfM), and/or extended block (ext) SEB.

https://doi.org/10.1371/journal.pone.0236446.t008

NR1I3 is a 3 M 5 ACM final SEB gene at *x*-, *y*-vertical axis angulation 43.2°. *NR1I3* has an *uppasebssiwa*, *dppasebssiwa*, *uppmsebssiwa* and *dppmsebssiwa* of 6.3252E + 04, 1.04908E + 05, 2.9155E + 04 and 1.33970E + 05 intergene bases. *NR1I3* has an *uppesebssiwaa* and *dppesebssiwaa* of 4.6203E + 04 and 1.19293E + 05 intergene bases with a P_{eff} of 0.387 *esebssiwaagoT*$_Q$ units (Table 8).

FOXA1 is a 3 M 7 ACMx2 final SEB gene at *x*-, *y*-vertical axis angulation 43.6°. *FOXA1* has an *uppasebssiwa*, *dppasebssiwa*, *uppmsebssiwa* and *dppmsebssiwa* of 8.365E + 03, 5.8310E + 04,

1.02576E + 05 and 2.30487E + 05 intergene bases. *FOXA1* has an *uppesebssiwaa* and *dppesebssiwaa* of 5.5470E + 04 and 1.44398E + 05 intergene bases with a P_{eff} of 0.384 (0.3841) *esebssiwaagoT*$_Q$ units (Table 8).

FKBP5 is a 2 A 7 ACM final SEB gene at *x*-, *y*-vertical axis angulation 48.7°. *FKBP5* has an *uppasebssiwa*, *dppasebssiwa*, *uppmsebssiwa* and *dppmsebssiwa* of 9.472E + 03, 6.3245E + 04, 4.1261E + 04 and 8.5032E + 04 intergene bases. *FKBP5* has an *uppesebssiwaa* and *dppesebssiwaa* of 2.5366E + 04 and 7.4138E + 04 intergene bases with a P_{eff} of 0.342 *esebssiwaagoT*$_Q$ units (Table 8).

NCOA1 is a 3 M 7 stIMfA NCA ACM final SEB gene at *x*-, *y*-vertical axis angulation 50.8°. *NCOA1* has an *uppasebssiwa*, *dppasebssiwa*, *uppmsebssiwa* and *dppmsebssiwa* of 7.5277E + 04, 1.69917E + 05, 1.1065E + 04 and 9.6413E + 04 intergene bases. *NCOA1* has an *uppesebssiwaa* and *dppesebssiwaa* of 4.3171E + 04 and 1.33165E + 05 intergene bases with a P_{eff} of 0.324 *esebssiwaagoT*$_Q$ units (Table 8).

CYP2B6 is a 2 M 5 initial and final SEB gene at *x*-, *y*-vertical axis angulation 50.9°. *CYP2B6* has an *uppasebssiwa*, *dppasebssiwa*, *uppmsebssiwa* and *dppmsebssiwa* of 1.4887E + 04, 3.2241E + 04, 3.224E + 03 and 2.3693E + 04 intergene bases. *CYP2B6* has an *uppesebssiwaa* and *dppesebssiwaa* of 9.056E + 03 and 2.7967E + 04 intergene bases with a P_{eff} of 0.324 *esebssiwaagoT*$_Q$ units (Table 8).

NR1I2 is a 2 A 5 initial and final SEB gene at *x*-, *y*-vertical axis angulation 52.3°. *NR1I2* has an *uppasebssiwa*, *dppasebssiwa*, *uppmsebssiwa* and *dppmsebssiwa* of 1.0367E + 04, 1.00223E + 05, 4.4883E + 04, 7.6998E + 04 intergene bases. *NR1I2* has an *uppesebssiwaa* and *dppesebssiwaa* of 2.7625E + 04 and 8.8611E + 04 intergene bases with a P_{eff} of 0.312 *esebssiwaagoT*$_Q$ units (Table 8).

CIDEA is a 2 A 3 stIMfA final SEB gene at *x*-, *y*-vertical axis angulation 54.7°. *CIDEA* has an *uppasebssiwa*, *dppasebssiwa*, *uppmsebssiwa* and *dppmsebssiwa* of 4.9350E + 04, 2.09403E + 05, 2.1519E + 04 and 3.4977E + 04 intergene bases. *CIDEA* has an *uppesebssiwaa* and *dppesebssiwaa* of 3.5735E + 04 and 1.22190E + 05 intergene bases with a P_{eff} of 0.292 *esebssiwaagoT*$_Q$ units (Table 8).

THRB is a 3 A 9 stIMfA final SEB gene at *x*-, *y*-vertical axis angulation 55.2°. *THRB* has an *uppasebssiwa*, *dppasebssiwa*, *uppmsebssiwa* and *dppmsebssiwa* of 1.9549E + 04, 2.47380E + 05, 1.08453E + 05 and 1.96893E + 05 intergene bases. *THRB* has an *uppesebssiwaa* and *dppesebssiwaa* of 6.4001E + 04 and 2.22137E + 05 intergene bases with a P_{eff} of 0.288 *esebssiwaagoT*$_Q$ units (Table 8).

MBP is a 2 A 3 NCA ACM q term final SEB gene at *x*-, *y*-vertical axis angulation 62.9°. *MBP* has an *uppasebssiwa*, *dppasebssiwa*, *uppmsebssiwa* and *dppmsebssiwa* of 3.8325E + 04, 2.97769E + 05, 7.6708E + 04 and 2.16048E + 05 intergene bases. *MBP* has an *uppesebssiwaa* and *dppesebssiwaa* of 5.7628E + 04 and 2.57020E + 05 intergene bases with a P_{eff} of 0.224 *esebssiwaagoT*$_Q$ units (Table 8).

CYP3A4 is a 2 A 3 ACM final SEB gene at *x*-, *y*-vertical axis angulation 56.1°. *CYP3A4* has an *uppasebssiwa*, *dppasebssiwa*, *uppmsebssiwa* and *dppmsebssiwa* of 1.3755E + 04, 3.8086E + 04, 1.379E + 03 and 1.5851E + 04 intergene bases. *CYP3A4* has an *uppesebssiwaa* and *dppesebssiwaa* of 7.567E + 03 and 2.6969E + 04 intergene bases with a P_{eff} of 0.281 *esebssiwaagoT*$_Q$ units (Table 8).

NR1H2 is a 2 M 5 final SEB gene at *x*-, *y*-vertical axis angulation 57.3°. *NR1H2* has an *uppasebssiwa*, *dppasebssiwa*, *uppmsebssiwa* and *dppmsebssiwa* of 2.4733E + 04, 6.2238E + 04, 1.1164E + 04 and 7.0526E + 04 intergene bases. *NR1H2* has an *uppesebssiwaa* and *dppesebssiwaa* of 1.7949E + 04 and 6.6382E + 04 intergene bases with a P_{eff} of 0.270 *esebssiwaagoT*$_Q$ units (Table 8).

CEACAM5 is a 2 A 4 stIMfA final SEB gene at *x*-, *y*-vertical axis angulation 59.5°. *CEACAM5* has an *uppasebssiwa*, *dppasebssiwa*, *uppmsebssiwa* and *dppmsebssiwa* of 2.1447E + 04, 5.6869E + 04, 6.140E + 03 and 5.2392E + 04 intergene bases. *CEACAM5* has an *uppesebssiwaa* and *dppesebssiwaa* of 1.3793E + 04 and 5.4631E + 04 intergene bases with a P_{eff} of 0.252 *esebssiwaagoT*$_Q$ units (Table 8).

MAFG is a 2 M 5 initial and final SEB gene at *x*-, *y*-vertical axis angulation 59.6°. *MAFG* has an *uppasebssiwa*, *dppasebssiwa*, *uppmsebssiwa* and *dppmsebssiwa* of 7.819E + 03, 5.4643E + 04, 1.4233E + 04 and 3.3022E + 04 intergene bases. *MAFG* has an *uppesebssiwaa* and *dppesebssiwaa* of 1.1026E + 04 and 4.3832E + 04 intergene bases with a P_{eff} of 0.252 *esebssiwaagoT*$_Q$ units (Table 8).

SCD5 is a 2 M 5 initial and final SEB gene at *x*-, *y*-vertical axis angulation 59.6°. *SCD5* has an *uppasebssiwa*, *dppasebssiwa*, *uppmsebssiwa* and *dppmsebssiwa* of 7.7158E + 04, 1.60532E + 05, 4.3087E + 04 and 3.17760E + 05 intergene bases. *SCD5* has an *uppesebssiwaa* and *dppesebssiwaa* of 6.0123E + 04 and 2.39146E + 05 intergene bases with a P_{eff} of 0.251 *esebssiwaagoT*$_Q$ units (Table 8).

MBP is a 2 A 4 ACM q term final SEB gene at *x*-, *y*-vertical axis angulation 60.5°. *MBP* has an *uppasebssiwa*, *dppasebssiwa*, *uppmsebssiwa* and *dppmsebssiwa* of 1.9347E + 04, 1.76854E + 05, 7.6708E + 04 and 2.16048E + 05 intergene bases. *MBP* has an *uppesebssiwaa* and *dppesebssiwaa* of 4.8027E + 04 and 1.96451E + 05 intergene bases with a P_{eff} of 0.244 *esebssiwaagoT*$_Q$ units (Table 8).

CUL2 is a 2 A 3 NCA ACM final SEB gene at *x*-, *y*-vertical axis angulation 56.4°. *CUL2* has an *uppasebssiwa*, *dppasebssiwa*, *uppmsebssiwa* and *dppmsebssiwa* of 1.8848E + 04, 2.74921E + 05, 2.08721E + 05, 5.41134E + 05 intergene bases. *CUL2* has an *uppesebssiwaa* and *dppesebssiwaa* of 1.13635E + 05 and 4.08028E + 05 intergene bases with a P_{eff} of 0.278 *esebssiwaagoT*$_Q$ units (Table 8).

ALAS2 is a 2 A 3 p term final SEB gene at *x*-, *y*-vertical axis angulation 62.55°. *ALAS2* has an *uppasebssiwa*, *dppasebssiwa*, *uppmsebssiwa* and *dppmsebssiwa* of 2.0152E + 04, 2.56510E + 05, 6.1069E + 04 and 1.00950E + 05 intergene bases. *ALAS2* has an *uppesebssiwaa* and *dppesebssiwaa* of 4.0611E + 04 and 1.78730E + 05 intergene bases with a P_{eff} of 0.227 *esebssiwaagoT*$_Q$ units (Table 8).

NCOR1 is a 2 A 5 NCAx3 final SEB gene at *x*-, *y*-vertical axis angulation 70.6°. *NCOR1* has an *uppasebssiwa*, *dppasebssiwa*, *uppmsebssiwa* and *dppmsebssiwa* of 1.2911E + 04, 2.4777E + 04, 9.52E + 03 and 1.14781E + 05 intergene bases. *NCOR1* has an *uppesebssiwaa* and *dppesebssiwaa* of 1.1215E + 04 and 6.9779E + 04 intergene bases with a P_{eff} of 0.161 *esebssiwaagoT*$_Q$ units (Table 8).

CASP3 is a 2 M 5 initial and final SEB gene at *x*-, *y*-vertical axis angulation 70.7°. *CASP3* has an *uppasebssiwa*, *dppasebssiwa*, *uppmsebssiwa* and *dppmsebssiwa* of 2.2778E + 04, 4.4665E + 04, 1.8640E + 04 and 2.14308E + 05 intergene bases. *CASP3* has an *uppesebssiwaa* and *dppesebssiwaa* of 2.0709E + 04 and 1.29486E + 05 intergene bases with a P_{eff} of 0.160 *esebssiwaagoT*$_Q$ units (Table 8).

CES2 is a 2 A 4 ACM final SEB gene at *x*-, *y*-vertical axis angulation 70.8°. *CES2* has an *uppasebssiwa*, *dppasebssiwa*, *uppmsebssiwa* and *dppmsebssiwa* of 3.0860E + 04, 9.0630E + 04, 7.68E + 02 and 1.08260E + 05 intergene bases. *CES2* has an *uppesebssiwaa* and *dppesebssiwaa* of 1.5772E + 04 and 9.9445E + 04 intergene bases with a P_{eff} of 0.159 *esebssiwaagoT*$_Q$ units (Table 8).

CYP3A5 is a 3 M 5 NCAx2 ACM final SEB gene at *x*-, *y*-vertical axis angulation 71.05°. *CYP3A5* has an *uppasebssiwa*, *dppasebssiwa*, *uppmsebssiwa* and *dppmsebssiwa* of 1.3739E + 04, 3.3986E + 04, 7.215E + 03 and 9.9566E + 04 intergene bases. *CYP3A5* has an *uppesebssiwaa*

and *dppesebssiwaa* of 1.0477E + 04 and 6.6776E + 04 intergene bases with a P_{eff} of 0.157 *esebssiwaagoT*$_Q$ units (Table 8).

AR is a 2 A 5 initial and final SEB gene at *x*-, *y*-vertical axis angulation 71.1°. *AR* has an *uppasebssiwa*, *dppasebssiwa*, *uppmsebssiwa* and *dppmsebssiwa* of 1.9384E + 04, 3.80800E + 05, 5.6075E + 04 and 1.01739E + 05 intergene bases. *AR* has an *uppesebssiwaa* and *dppesebssiwaa* of 3.7729E + 04 and 2.41270E + 05 intergene bases with a P_{eff} of 0.156 *esebssiwaagoT*$_Q$ units (Table 8).

CYP4A11 is a 2 M 5 initial and final SEB gene at *x*-, *y*-vertical axis angulation 72.0°. *CYP4A11* has an *uppasebssiwa*, *dppasebssiwa*, *uppmsebssiwa* and *dppmsebssiwa* of 1.4063E + 04, 3.9722E + 04, 1.2582E + 04 and 1.38786E + 05 intergene bases. *CYP4A11* has an *uppesebssiwaa* and *dppesebssiwaa* of 1.3322E + 04 and 8.9254E + 04 intergene bases with a P_{eff} of 0.149 *esebssiwaagoT*$_Q$ units (Table 8).

GTF2IRD1 is a 2 M 7 ACM final SEB gene at *x*-, *y*-vertical axis angulation 73.1°. *GTF2IRD1* has an *uppasebssiwa*, *dppasebssiwa*, *uppmsebssiwa* and *dppmsebssiwa* of 2.9160E + 04, 5.2809E + 04, 2.697E + 03 and 1.75310E + 05 intergene bases. *GTF2IRD1* has an *uppesebssiwaa* and *dppesebssiwaa* of 1.5928E + 04 and 1.14060E + 05 intergene bases with a P_{eff} of 0.140 *esebssiwaagoT*$_Q$ units (Table 8).

PPP1R9B is a 2 M 5 initial and final SEB gene at *x*-, *y*-vertical axis angulation 74.4°. *PPP1R9B* has an *uppasebssiwa*, *dppasebssiwa*, *uppmsebssiwa* and *dppmsebssiwa* of 4.2770E + 04, 1.02872E + 05, 3.5391E + 04 and 5.04863E + 05 intergene bases. *PPP1R9B* has an *uppesebssiwaa* and *dppesebssiwaa* of 3.9081E + 04 and 3.03867E + 05 intergene bases with a P_{eff} of 0.129 *esebssiwaagoT*$_Q$ units (Table 8).

FABP3 is a 2 A 5 initial and final SEB gene at *x*-, *y*-vertical axis angulation 74.5°. *FABP3* has an *uppasebssiwa*, *dppasebssiwa*, *uppmsebssiwa* and *dppmsebssiwa* of 1.2880E + 04, 1.56459E + 05, 9.227E + 03 and 1.6822E + 04 intergene bases. *FABP3* has an *uppesebssiwaa* and *dppesebssiwaa* of 1.1053E + 04 and 8.6640E + 04 intergene bases with a P_{eff} of 0.128 *esebssiwaagoT*$_Q$ units (Table 8).

FABP6 is a 2 M 4 final SEB gene at *x*-, *y*-vertical axis angulation 78.3°. *FABP6* has an *uppasebssiwa*, *dppasebssiwa*, *uppmsebssiwa* and *dppmsebssiwa* of 5.8309E + 04, 7.63245E + 05, 1.9768E + 04 and 4.6206E + 04 intergene bases. *FABP6* has an *uppesebssiwaa* and *dppesebssiwaa* of 3.9038E + 04 and 4.04726E + 04 intergene bases with a P_{eff} of 0.096 *esebssiwaagoT*$_Q$ units (Table 8).

van der Waals diameter, structural lipophilicity and pressure regulation grade half-life parameters for small molecules with exterior structural lipophilicity

Aldosterone ($C_{21}H_{28}O_5$) has a Log *P* of 1.06, a vdWD of 0.856 nm and a Log *P*/vdWD of 1.23 nm^{-1}. Aldosterone has a calc $L_{external\ structure}/H_{polar\ group}$ ratio of 1.31, and a nl calc $L_{external\ structure}/H_{polar\ group}$ quotient of 0.478. The $t_{1/2}$ at receptor·receptor count ($t_{1/2}{\cdot}R_{count}$) for aldosterone at MR is 2.366E + 04 *min·count*, at GR is 6.610E + 03 *min·count*, and the Σ *min·count* is 3.0270E + 04 (Table 9).

Cortisol ($C_{21}H_{30}O_5$) has a Log *P* of 1.28, a vdWD of 0.861 nm and a Log *P*/vdWD of 1.49 nm^{-1}. Cortisol has a calc $L_{external\ structure}/H_{polar\ group}$ ratio of 1.36, and a nl calc $L_{external\ structure}/H_{polar\ group}$ quotient of 0.495. The $t_{1/2}$ at receptor·receptor count ($t_{1/2}{\cdot}R_{count}$) for cortisol at MR is 7.605E + 03 *min·count*, at GR is 6.610E + 03 *min·count*, and the Σ *min·count* is 1.42E + 04 (Table 9).

Dexamethasone (DEX; $C_{22}H_{29}FO_5$) has a Log *P* of 1.68, a vdWD of 0.873 nm and a Log *P*/vdWD of 1.92 nm^{-1}. Corticosterone (Cort; $C_{21}H_{30}O_4$) has a Log *P* of 2.02, a vdWD of 0.854

Table 9. Effective intracellular pressure grade of effect for molecular size-excluded steroid axis small molecule ligands at cell membrane receptors.

Small molecule[1]	Formula	Log *P*	Molecular Weight (Da)	Size (Ang^3)	vdWD (nm)	Polar SA (Ang^2)	$L_{external\ structure}/H_{polar\ group}$ (Ch_3Oh nl); *Log* P/vdWD (nm^{-1})[3]	$t_{1/2}{\cdot}R_{count}$ ($min{\cdot}count$)[2]	Σ *min·count*
Aldosterone	$C_{21}H_{28}O_5$	1.06	360	341	0.856	92	0.478 (1.23)	2.366E + 04 (MR), 6.610E + 03 (GR)	3.0270E + 04
Cortisol	$C_{21}H_{30}O_5$	1.28	362	347	0.861	95	0.495 (1.49)	7.605E + 03 (MR), 6.610E + 03 (GR)	1.4215E + 04
Dexamethasone (Dex)	$C_{22}H_{29}FO_5$	1.68	392	362	0.873	95	0.461 (1.92)	1.183E + 03 (MR), 1.32200E + 05 (GR)	1.33383E + 05
Diethylstilbestrol (DES)	$C_{18}H_{20}O_2$	5.19	268	263	0.786	40	1.31 (6.60)	1.863745E + 06 (ERα)	-
17β-estradiol	$C_{18}H_{24}O_2$	3.75	272	270	0.792	40	1.18 (4.73)	1.2E +06 (ERα)	-
Dihydroxytestosterone (Dht)	$C_{19}H_{30}O_2$	3.41	290	301	0.822	37	1.15 (4.15)	1.79812E + 05 (AR)	-
Methyltrienolone (R1881)	$C_{19}H_{24}O_2$	2.53	284	278	0.800	37	0.932 (3.16)	2.47340E + 05 (AR)	-
Insulin-like growth factor II[§]	-	-	20.1^{kDa}	-	-	-	-	1.943502E + 06 (IGFIIR)	

[§] Macromolecular standard for negative Δ C_{micro} shift at lower limit of P_{eff}

[1)] half-lives at receptor ($t_{1/2}$) for DES at ERα ($t_{1/2}$ = 663), DHT—R1881 at AR ($t_{1/2}$ = 38.3–52.6 min) and IGFII at IGRIIR/M6P ($t_{1/2}$ = 55.5) are determined by semi-exponential power regression *x*, *y*-plotting of radiolabeled hormone disassociation constants (K_D, *x*-axis) and values of $t_{1/2}$ at receptor (min, *y*-axis), $y = 3E - 05{\cdot}x^{0.6784}$, $R^2 = 0.955$ ($y = 1E\text{-}08x + b = 45.50$, $R^2 = 0.999$)

[2)] the rank order for the steroid axis hormone $t_{1/2}{\cdot}R_{count}$ (Σ *min·count*) P_{eff} regulation effect is cortisol, aldosterone, DEX/corticosterone (Cort), DHT/R1881 (positive) and E_2, DES (negative); and

[3)] the rank order of steroid axis hormone ligands for receptor subtypes ($L_{external\ structure}/H_{polar\ group}$ quotient) is 0.461–0.495 (corticosteroid), 0.932–1.15 (androgen) and 1.18–1.31 (estrogen).

https://doi.org/10.1371/journal.pone.0236446.t009

nm and a Log *P*/vdWD of 2.37 nm^{-1}. Corticosterone has a calc $L_{external\ structure}/H_{polar\ group}$ ratio of 1.72, and a nl calc $L_{external\ structure}/H_{polar\ group}$ quotient of 0.627. The $t_{1/2}$ at receptor·receptor count ($t_{1/2}{\cdot}R_{count}$) for dexamethasone at MR is 1.183E + 03 *min·count*, at GR is 1.32200E + 05 *min·count*, and the Σ *min·count* is 1.33383E + 05 (Table 9).

Diethylstilbestrol (DES; $C_{18}H_{20}O_2$) has a Log *P* of 5.19, a vdWD of 0.786 nm and a Log *P*/vdWD of 6.60 nm^{-1}. DES has a calc $L_{external\ structure}/H_{polar\ group}$ ratio of 3.59, and a nl calc $L_{external\ structure}/H_{polar\ group}$ quotient of 1.31. The $t_{1/2}$ at receptor·receptor count ($t_{1/2}{\cdot}R_{count}$) for diethylstilbestrol at ERα is 1.863745E + 06 *min·count* (Table 9).

17β-estradiol (E2; $C_{18}H_{24}O_2$) has a Log *P* of 3.75, a vdWD of 0.792 nm and a Log *P*/vdWD of 4.73 nm^{-1}. E2 has a calc $L_{external\ structure}/H_{polar\ group}$ ratio of 4.73, and a nl calc $L_{external\ structure}/H_{polar\ group}$ quotient of 1.18. The $t_{1/2}$ at receptor·receptor count ($t_{1/2}{\cdot}R_{count}$) for 17β-estradiol at ERα is 1.2E + 06 *min·count* (Table 9).

Dihydroxytestosterone (DHT; $C_{19}H_{30}O_2$) has a Log *P* of 3.41, a vdWD of 0.822 nm and a Log *P*/vdWD of 4.15 nm^{-1}. DHT has a calc $L_{external\ structure}/H_{polar\ group}$ ratio of 3.16, and a nl calc $L_{external\ structure}/H_{polar\ group}$ quotient of 1.15. The $t_{1/2}$ at receptor·receptor count ($t_{1/2}{\cdot}R_{count}$) for dihydroxytestosterone at AR is 1.79812E + 05 *min·count* (Table 9).

Methyltrienolone (R1881; $C_{19}H_{24}O_2$) has a Log *P* of 2.41, a vdWD of 0.800 nm and a Log *P*/vdWD of 3.16 nm^{-1}. R1881 has a calc $L_{external\ structure}/H_{polar\ group}$ ratio of 2.56, and a nl calc $L_{external\ structure}/H_{polar\ group}$ quotient of 0.932. The $t_{1/2}$ at receptor·receptor count ($t_{1/2}{\cdot}R_{count}$) for methyltrienolone at AR is 2.47340E + 05 *min·count* (Table 9).

Insulin-like growth factor II (20.1 kDa) $t_{1/2}$ at receptor·receptor count ($t_{1/2}{\cdot}R_{count}$) at IGRIIR/M6P is 1.943502E + 06 *min·count* (Table 9, legend).

Gene expression effective pressure mapping for small molecule hormones and bisphenol as ligands of cell membrane steroid axis receptors (in pharmacokinetic non-competition)

GCLC is a 2 A 3 ACM final SEB gene at *x*-, *y*-vertical axis angulation 32.4°. *GCLC* has an *uppasebssiwa*, *dppasebssiwa*, *uppmsebssiwa* and *dppmsebssiwa* of 2.128E + 03, 3.8969E + 04, 1.39792E + 05 and 2.58868E + 05 intergene bases. *GCLC* has an *uppesebssiwaa* and *dppesebssiwaa* of 7.0960E + 04 and 1.48918E + 05 intergene bases with a P_{eff} of 0.477 *esebssiwaagoT*$_Q$ units (Table 10).

PER1 is a 2 A 6 ACM final SEB gene at *x*-, *y*-vertical axis angulation 42.4°. *PER1* has an *uppasebssiwa*, *dppasebssiwa*, *uppmsebssiwa* and *dppmsebssiwa* of 3.3824E + 04, 7.2463E + 04, 2.173E + 03 and 1.8993E + 04 intergene bases. *PER1* has an *uppesebssiwaa* and *dppesebssiwaa* of 1.7998E + 04 and 4.5728E + 04 intergene bases with a P_{eff} of 0.394 *esebssiwaagoT*$_Q$ units (Table 10).

PMCH is a 3 M 5 ACM final SEB gene at *x*-, *y*-vertical axis angulation 43.3°. *PMCH* has an *uppasebssiwa*, *dppasebssiwa*, *uppmsebssiwa* and *dppmsebssiwa* of 6.5883E + 04, 1.27508E + 05, 1.1105E + 04 and 7.1788E + 04 intergene bases. *PMCH* has an *uppesebssiwaa* and *dppesebssiwaa* of 3.8494E + 04 and 9.9848E + 04 intergene bases with a P_{eff} of 0.386 *esebssiwaagoT*$_Q$ units (Table 10).

NR3C1 is a 2 A 3 ACM final SEB gene at *x*-, *y*-vertical axis angulation 44.5°. *NR3C1* has an *uppasebssiwa*, *dppasebssiwa*, *uppmsebssiwa* and *dppmsebssiwa* of 1.2643E + 04, 2.26184E + 05, 2.10238E + 05, 3.65899E + 05 intergene bases. *NR3C1* has an *uppesebssiwaa* and *dppesebssiwaa* of 1.11440E + 05 and 2.96042E + 05 intergene bases with a P_{eff} of 0.376 *esebssiwaagoT*$_Q$ units (Table 10).

GPER1 is a 3 A 7 initial and final SEB gene at *x*-, *y*-vertical axis angulation 44.6°. *NR3C1* has an *uppasebssiwa*, *dppasebssiwa*, *uppmsebssiwa* and *dppmsebssiwa* of 4.697E + 03, 3.4332E + 04, 5.6825E + 04 and 1.29323E + 05 intergene bases. *NR3C1* has an *uppesebssiwaa* and *dppesebssiwaa* of 3.0761E + 04 and 8.1827E + 04 intergene bases with a P_{eff} of 0.376 *esebssiwaagoT*$_Q$ units (Table 10).

INSL3 is a 3 A 7 initial and final SEB gene at *x*-, *y*-vertical axis angulation 47.9° (act). *INSL3* has an *uppasebssiwa*, *dppasebssiwa*, *uppmsebssiwa* and *dppmsebssiwa* of 6.248E + 03, 5.8905E + 04, 3.7545E + 04 and 6.6648E + 04 intergene bases (act). *INSL3* has an *uppesebssiwaa* and *dppesebssiwaa* of 2.1896E + 04 and 6.2777E + 04 intergene bases with a P_{eff} of 0.349 *esebssiwaagoT*$_Q$ units (act) (Table 10).

DLK1 is a 2 M 5 initial and final SEB gene at *x*-, *y*-vertical axis angulation 48.3°. *DLK1* has an *uppasebssiwa*, *dppasebssiwa*, *uppmsebssiwa* and *dppmsebssiwa* of 7.2336E + 04, 1.62011E + 05, 3.088E + 03 and 5.6714E + 04 intergene bases. *DLK1* has an *uppesebssiwaa* and *dppesebssiwaa* of 3.7712E + 04 and 1.69362E + 05 intergene bases with a P_{eff} of 0.345 *esebssiwaagoT*$_Q$ units (Table 10).

OLFM1 is a 2 M 5 initial and final SEB gene at *x*-, *y*-vertical axis angulation 50.5°. *OLFM1* has an *uppasebssiwa*, *dppasebssiwa*, *uppmsebssiwa* and *dppmsebssiwa* of 2.7728E + 04, 6.0118E + 04, 9.980E + 03 and 5.7711E + 04 intergene bases. *OLFM1* has an *uppesebssiwaa* and *dppesebssiwaa* of 1.8854E + 04 and 5.7711E + 04 intergene bases with a P_{eff} of 0.327 *esebssiwaagoT*$_Q$ units (Table 10).

ADAM8 is a 2 M 5 initial and final SEB gene at *x*-, *y*-vertical axis angulation 52.8°. *ADAM8* has an *uppasebssiwa*, *dppasebssiwa*, *uppmsebssiwa* and *dppmsebssiwa* of 3.0415E + 04, 6.0950E + 04, 9.529E + 03 and 6.8596E + 04 intergene bases. *ADAM8* has an *uppesebssiwaa* and *dppesebssiwaa* of 1.9972E + 04 and 6.4773E + 04 intergene bases with a P_{eff} of 0.308 *esebssiwaagoT*$_Q$ units (Table 10).

Table 10. Effective intracellular pressure mapping of gene activation by molecular size-excluded small molecule hormones via cell membrane Gr, Mr, Erα/β and AR receptor pathways as compared to bisphenol A[‡].

Human gene (no. of bases, locus bases or n/a)	Gene locus (ch, strand)	Angle (°)	Episode category (final, initial SEB structure)	*uppesebssiwaa*, *dppesebssiwaa* (P_{eff}, fract)	CM receptor ligand[Cell type (tr)] (decrease, dec)
GABPA (37,891; n/a)[◇]	21q21.3 (+)	-	-	-(*0.494*)	Dex [PC12]
GCLC, glutamate-cysteine ligase catalytic subunit (119, 630; n/a)	6p12.1 (-)	32.4	2 A 3 acm (2 A 5)	7.0960E + 04, 1.48918E + 05 (*0.477*)	Bpa[HCC]
PER1, period circadian protein homolog 1 (24,299; n/a)	17p13.1 (-)	42.4	2 A 6 acm (2 A 5)	1.7998E + 04, 4.5728E + 04 (*0.394*)	Dex[PC12]
PMCH, pro-melanin concentrating hormone (1,378; n/a)	12q23.2 (-)	43.3	3 M 5 acm (3 M 7)	3.8494E + 04, 9.9848E + 04 (*0.386*)	Dht [Bpa (dec)]
NR3C1, nuclear receptor subfamily 3 group C member 1 (157,582; n/a)	5q31.3 (-)	44.5	2 A 3 acm (2 A 5)	1.1144E + 05, 2.96042E + 05 [0.3764 (*0.376*)]	Dex (dec)
GPER1, G protein-coupled estrogen receptor 1 (11, 608; n/a)	7p22.3 (+)	44.6	3 A 7 (-)	3.0761E + 04, 8.1827E + 04 [0.3759 (*0.376*)]	Ald [Dex (dec)]
INSL3, insulin like 3 (5,063; n/a)[act]	19p13.11 (-)	47.9	3 A 7 (-)	2.1896E + 04, 6.2777E + 04 (*0.349*)[C]	Bpa
DLK1, delta like non-canonical notch ligand 1 (12,520; n/a)	14q32.31 (+)	48.3	2 M 5 (-)	3.7712E + 04, 1.69362E + 05 [*0.345*]	Bpa
FKBP5				(*0.342*)	Dex (Dex + Dht)
OLFM1, olfactomedin 1 (45,942; n/a)	9q34.3 (+)	50.5	2 M 5 (-)	1.8854E + 04, 5.7711E + 04 (*0.327*)	E_2
ADAM8, ADAM metallopeptidase domain 8 (14,468; n/a)	10q26.3 (-)	52.8	2 M 5 (-)	1.9972E + 04, 6.4773E + 04 (*0.308*)	Bpa
SIM1, single-minded homolog 1 (79,921; n/a)	6q16.3 (-)	55.0	2 A 5 (-)	3.1171E + 04, 1.02794E + 05 (*0.303*)	Bpa
CCND1, cyclin D1 (13,888; n/a)	11q13.3 (+)	55.0	2 A 5 (-)	2.5646E + 04, 8.8315E + 04 (*0.290*)	E_2 [Bpa (dec)]
RAPGEFL1, link guanine nucleotide exchange factor II (182,670; n/a)	17q21.2 (+)	55.9	2 A 5 (-)	9.904E + 03, 3.5054E + 04 (*0.283*)	E_2
CYP3A4				(*0.281*)	Dex (inc); E2 (dec)
CDKNIA, Cyclin-dependent kinase inhibitor 1A (p21, 10,880; n/a)	6p21.2 (+)	56.7	3 A 5 acm stIMfA (3 A 7)	2.3343E + 04, 8.4648E + 04 (*0.276*)	Bfap[HCC]
DUSP1				(*0.272*)	Dex
JUN				(0.267)	Bpa
FABP4, fatty acid binding protein 4 (4,845; n/a)	8q21.13 (-)	58.1	3 A 7 (-)	5.8408E + 04, 2.21498E + 05 (*0.264*)	Bpa (+ Dex)
NR3C2, nuclear receptor subfamily 3, group C, member 2 (366,517; n/a)	4q31.23 (-)	58.4	4 A 9 (-)	5.1635E + 04, 1.97691E + 05 (*0.261*)	Dex (Ald)
MEG3, maternally expressed 3 (259,450; 81,622)	14q32.31 (+)	58.9	2 A 2 acm acm ext (2 A 5)	5.5514E + 04, 2.55416E + 05 (*0.258*)	--
DFFA, DNA fragmentation factor subunit alpha (16,015; n/a)	1p36.22 (-)	58.9	2 A 5 (-)	3.7047E + 04, 1.43906E + 05 (*0.257*)	Bpa
FOS, fos proto-oncogene, AP-1 transcription factor subunit (3,461; n/a)	14q24.3 (+)	59.1	3 M 9 acm (3 M 7)	4.4895E + 04, 9.5063E + 04 (*0.256*)	Bpa
TIMM8B, translocase of inner mitochondrial membrane 8 homolog 8 (1,999; n/a)	11q23.2 (-)	60.2	3 A 8 acm acm ext (3 A 7)	3.9647E + 04, 1.60497E + 05 (*0.247*)	Bpa
GADD45A				(*0.245*)	Bfap[HCC]
CYP1A1				(*0.216*)	Bpa[HCC], Bfap[HCC]
ESRRG				(*0.209*)	Bpa
MIAT, myocardial infarction associated transcript (30,068; n/a)	22q12.1 (+)	65.2	2 M 6 acm (2 A 5)	6.444E + 03, 3.1409E + 04 (*0.205*)	Bpa
NRF1	-	-	-	[0.200 (0.2001)]	Bpa
CYP17A1, cytochrome P450 family 17 subfamily A member 1 (7,003; n/a)	10q24.32 (-)	65.8	3 A 5 nca acm (3 A 7)	2.8621E + 04, 1.43391E + 05 [*0.200* (0.1996)]	Dht

(*Continued*)

Table 10. (Continued)

Human gene (no. of bases, locus bases or n/a)	Gene locus (ch, strand)	Angle (°)	Episode category (final, initial SEB structure)	*uppesebssiwaa*, *dppesebssiwaa* (P_{eff}, fract)	CM receptor ligand$^{Cell\ type\ (tr)}$ (decrease, dec)
ESRRA				0.196	--
FOSB				[*0.194* (0.1943)]	Dex (dec)
PLEKHG4, pleckstrin homology and RhoGEF containing G4 (11,991; n/a)	16q21 (+)	66.6	2 A 8 acm acm ext (2 A 5)	9.490E + 03, 4.8961E + 04 [*0.194* (0.1938)]	Bpa
ESR1				[*0.184* (0.1836)]	E_2
FLNA, filamin A (26,115; n/a)	Xq28 (-)	67.8	2 A 5	1.1217E + 04, 6.1000E + 04 [*0.184* (0.1839)]	E_2
SLC9A1, solute carrier family 9 member A1 (68,173; n/a)	1p36.11 (-)	68.8	2 M 5 (-)	1.8447E + 04, 1.10234E + 05 (*0.167*)	Ald
AR				(*0.156*)	Dht
HMOX1				*0.153* (0.1531)	Bpa (inc, m)
TFF1, trefoil factor 1 (4,313; n/a)	21q22.3 (-)	72.2	3 M 7 (-)	2.3119E + 04, 1.57237E + 04 (*0.147*)	E_2
ESR2				[*0.136* (0.1361)]	E_2 (dec) [Bpa (s.s; inc, m) + agonist]
CYP11B2, cytochrome P450 family 11 subfamily B member 2 (7,305; 36,731)	8q24.3 (-)	76.5	2 A 5 (-)	1.6007E + 04, 1.43026E + 05 (*0.112*)	$E_2 + X^{HAC15}$ (Ald)
UGT1A1				(*0.106*)	Bpa^{HCC}
CYP11B1, cytochrome P450 family 11 subfamily B member 1 (7,498; n/a)	8q24.3 (-)	78.1	3 M 7 (-)	1.4197E + 04, 1.43639E + 05 (*0.099*)	Dex (dec)
TGIF1, TGFB induced factor homeobox 1 (194,834; 48,371)	18p11.31 (+)	80.3	2 A 5 (-)	1.9246E + zz04, 2.40600E + 05 (*0.080*)	&

BPA, intracellular ligand, ERRγ; BPAF, extracellular ligand, ERα/β; cell type, if transformed (ie PC12, HCC); Dht, dihydroxytestosterone; Ald, aldosterone; X, CM receptor inverse agonist(s)/antagonist; ^{act}, actual; s-s, sex specific

$^{\&}P_{eff}$ at duration for expression of AhR gene reporter plasmid; *SLC9A1*, NHE-1; *SLC9A1*, NHE-1;; *CYP11B1*, 11-beta-hydroxylase; *CYP11B2*, aldosterone synthase; * *FOS*, *JUN*, *ESR1* and *ESR2*, ERE containing genes

‡ AhR, CAR & GR response element-containing genes, *UGT1A1*; *CYP1A1*, Ahr (Arnt) recruitment of ER to XRE; and *GSTA1*, JUN recruitment of GR to TRE

$^{◇}$ PPARG coactivator 1 alpha (PGC1α), ERRγ/-α, SREBPF and CAR protein binding partner; and § secondary activation of genes at P_{eff} 0.106 for variable duration as applicable to both pathways (ie *UGT1A*) $^{§\ 1)}$ gene loci sub-episode block structure (SEB) variations include non-contributory anisotropy (NCA), anisotropy converted to mesotropy (ACM), 0.5-factor adjusted stabilizing mesotropy or anisotropy converted to stabilizing isotropy for anisotropy or mesotropy (stIAfM, stIMfA or stIMfM), and/or extended block (ext) SEB; and $^{2)}$ gene(s) with previously reported episode and sub-episode block structure include *INSL3* and *GABPA* [22].

https://doi.org/10.1371/journal.pone.0236446.t010

SIM1 is a 2 A 5 initial and final SEB gene at *x*-, *y*-vertical axis angulation 54.9°. *SIM1* has an *uppasebssiwa*, *dppasebssiwa*, *uppmsebssiwa* and *dppmsebssiwa* of 2.9304E + 04, 1.50699E + 05, 3.3038E + 04 and 5.4889E + 04 intergene bases. *SIM1* has an *uppesebssiwaa* and *dppesebssiwaa* of 3.1171E + 04 and 1.02794E + 05 intergene bases with a P_{eff} of 0.303 *esebssiwaagoT*$_Q$ units (Table 10).

RAPGEFL1 is a 2 A 5 initial and final SEB gene at *x*-, *y*-vertical axis angulation 55.9°. *RAPGEFL1* has an *uppasebssiwa*, *dppasebssiwa*, *uppmsebssiwa* and *dppmsebssiwa* of 5.474E + 03, 3.2272E + 04, 1.4334E + 04 and 3.7835E + 04 intergene bases. *RAPGEFL1* has an *uppesebssiwaa* and *dppesebssiwaa* of 9.904E + 03 and 3.5054E + 04 intergene bases with a P_{eff} of 0.283 *esebssiwaagoT*$_Q$ units (Table 10).

CDKNIA is a 3 A 5 ACM stIMfA extended final SEB gene at *x*-, *y*-vertical axis angulation 56.7°. *CDKN1A* has an *uppasebssiwa*, *dppasebssiwa*, *uppmsebssiwa* and *dppmsebssiwa* of 4.400E + 03, 6.4050E + 04, 4.2285E + 04 and 1.05247E + 05 intergene bases. *CDKN1A* has an *uppesebssiwaa* and *dppesebssiwaa* of 2.3343E + 04 and 8.4648E + 04 intergene bases with a P_{eff} of 0.276 *esebssiwaagoT*$_Q$ units (Table 10).

FABP4 is a 3 A 7 initial and final SEB gene at *x*-, *y*-vertical axis angulation 58.1°. *FABP4* has an *uppasebssiwa*, *dppasebssiwa*, *uppmsebssiwa* and *dppmsebssiwa* of 3.6724E + 04, 2.66777E + 05, 8.0092E + 04 and 1.76219E + 05 intergene bases. *SIM1* has an *uppesebssiwaa* and *dppesebssiwaa* of 5.8408E + 04 and 2.21498E + 05 intergene bases with a P_{eff} of 0.264 *esebssiwaagoT*$_Q$ units (Table 10).

NR3C2 is a 4 A 9 initial and final SEB gene at *x*-, *y*-vertical axis angulation 58.4°. *NR3C2* has an *uppasebssiwa*, *dppasebssiwa*, *uppmsebssiwa* and *dppmsebssiwa* of 2.4496E + 04, 1.86526E + 05, 7.8774E + 04 and 2.08855E + 05 intergene bases. *NR3C2* has an *uppesebssiwaa* and *dppesebssiwaa* of 5.1635E + 04 and 1.97691E + 05 intergene bases with a P_{eff} of 0.261 *esebssiwaagoT*$_Q$ units (Table 10).

MEG3 is a 2 A 2 ACMx2 ext final SEB gene at *x*-, *y*-vertical axis angulation 58.9°. *MEG3* has an *uppasebssiwa*, *dppasebssiwa*, *uppmsebssiwa* and *dppmsebssiwa* of 5.197E + 03, 1.77555E + 05, 1.05830E + 05 and 2.53278E + 05 intergene bases. *MEG3* has an *uppesebssiwaa* and *dppesebssiwaa* of 5.5514E + 04 and 2.15416E + 05 intergene bases with a P_{eff} of 0.258 *esebssiwaagoT*$_Q$ units (Table 10).

DFFA is a 3 A 5 initial and final SEB gene at *x*-, *y*-vertical axis angulation 58.9°. *DFFA* has an *uppasebssiwa*, *dppasebssiwa*, *uppmsebssiwa* and *dppmsebssiwa* of 1.4323E + 04, 1.44368E + 05, 5.9771E + 04 and 1.43444E + 05 intergene bases. *DFFA* has an *uppesebssiwaa* and *dppesebssiwaa* of 3.7047E + 04 and 1.43906E + 05 intergene bases with a P_{eff} of 0.257 *esebssiwaagoT*$_Q$ units (Table 10).

FOS is a 3 A 9 ACM final SEB gene at *x*-, *y*-vertical axis angulation 59.1°. *DFFA* has an *uppasebssiwa*, *dppasebssiwa*, *uppmsebssiwa* and *dppmsebssiwa* of 1.5182E + 04, 1.39901E + 05, 4.4895E + 04 and 9.5063E + 04 intergene bases. *FOS* has an *uppesebssiwaa* and *dppesebssiwaa* of 3.0039E + 04 and 1.17482 + 05 intergene bases with a P_{eff} of 0.256 *esebssiwaagoT*$_Q$ units (Table 10).

TIMM8B is a 3 A 8 ACMx2 ext final SEB gene at *x*-, *y*-vertical axis angulation 60.2°. *TIMM8B* has an *uppasebssiwa*, *dppasebssiwa*, *uppmsebssiwa* and *dppmsebssiwa* of 2.5423E + 04, 2.04260E + 05, 5.3871E + 04 and 1.16735E + 05 intergene bases. *TIMM8B* has an *uppesebssiwaa* and *dppesebssiwaa* of 3.9647E + 04 and 1.60497E + 05 intergene bases with a P_{eff} of 0.247 *esebssiwaagoT*$_Q$ units (Table 10).

MIAT is a 2 M 6 acm final SEB gene at *x*-, *y*-vertical axis angulation 65.2°. *MIAT* has an *uppasebssiwa*, *dppasebssiwa*, *uppmsebssiwa* and *dppmsebssiwa* of 1.1481E + 04, 1.9667E + 04, 1.408E + 03 and 4.3151E + 04 intergene bases. *MIAT* has an *uppesebssiwaa* and *dppesebssiwaa* of 6.444E + 03 and 3.1409E + 04 intergene bases with a P_{eff} of 0.205 *esebssiwaagoT*$_Q$ units (Table 10).

CYP17A1 is a 3 A 5 NCA ACM final SEB gene at *x*-, *y*-vertical axis angulation 65.8°. *CYP17A1* has an *uppasebssiwa*, *dppasebssiwa*, *uppmsebssiwa* and *dppmsebssiwa* of 1.4406E + 04, 1.79367E + 05, 4.2836E + 04 and 1.07414E + 05 intergene bases. *CYP17A1* has an *uppesebssiwaa* and *dppesebssiwaa* of 2.8621E + 04 and 1.43391E + 05 intergene bases with a P_{eff} of 0.200 *esebssiwaagoT*$_Q$ units (Table 10).

PLEKHG4 is a 2 A 9 ACMx2 final SEB gene at *x*-, *y*-vertical axis angulation 66.6°. *PLEKHG4* has an *uppasebssiwa*, *dppasebssiwa*, *uppmsebssiwa* and *dppmsebssiwa* of 8.609E + 03, 7.7744E + 04, 1.0374E + 04 and 2.0179E + 04 intergene bases. *PLEKHG4* has an *uppesebssiwaa* and *dppesebssiwaa* 9.490E + 03 and 4.8961E + 04 intergene bases with a P_{eff} of 0.194 *esebssiwaagoT*$_Q$ units (Table 10).

FLNA is a 2 A 5 initial and final SEB gene at *x*-, *y*-vertical axis angulation 67.8°. *FLNA* has an *uppasebssiwa*, *dppasebssiwa*, *uppmsebssiwa* and *dppmsebssiwa* of 9.480E + 03, 8.6967E + 04, 1.2954E + 04, 3.5033E + 04 intergene bases. *FLNA* has an *uppesebssiwaa* and *dppesebssiwaa* of 1.1214E + 04 and 6.1000E + 04 intergene bases with a P_{eff} of 0.184 *esebssiwaagoT*$_Q$ units (Table 10).

CEBPD is a 5 M 11 initial and final SEB gene at *x*-, *y*-vertical axis angulation 69.7°. *CEBPD* has an *uppasebssiwa*, *dppasebssiwa*, *uppmsebssiwa* and *dppmsebssiwa* of 8.8872E + 04, 1.85923E + 05, 5.5818E + 04 and 6.74877E + 05 intergene bases. *CEBPD* has an *uppesebssiwaa* and *dppesebssiwaa* of 7.2345E + 04 and 4.30400E + 05 intergene bases with a P_{eff} of 0.168 *esebssiwaagoT*$_Q$ units (Table 10).

SLC9A1 is a 2 M 5 initial and final SEB gene at *x*-, *y*-vertical axis angulation 69.8°. *SLC9A1* has an *uppasebssiwa*, *dppasebssiwa*, *uppmsebssiwa* and *dppmsebssiwa* of 2.8999E + 04, 7.1281E + 04, 7.895E + 03 and 1.49186E + 05 intergene bases. *SLC9A1* has an *uppesebssiwaa* and *dppesebssiwaa* of 1.8447E + 04 and 1.10234E + 05 intergene bases with a P_{eff} of 0.167 *esebssiwaagoT*$_Q$ units (Table 10).

TFF1 is a 3 M 7 initial and final SEB gene at *x*-, *y*-vertical axis angulation 72.2°. *TFF1* has an *uppasebssiwa*, *dppasebssiwa*, *uppmsebssiwa* and *dppmsebssiwa* of 3.0485E + 04, 7.8313E + 04, 1.5753E 04 and 2.36160E + 05 intergene bases. *TFF1* has an *uppesebssiwaa* and *dppesebssiwaa* of 2.3119E + 04 and 1.57237E + 05 intergene bases with a P_{eff} of 0.147 *esebssiwaagoT*$_Q$ units (Table 10).

GSTA1 is a 2 M 7 final SEB gene at *x*-, *y*-vertical axis angulation 72.35°. *GSTA1* has an *uppasebssiwa*, *dppasebssiwa*, *uppmsebssiwa* and *dppmsebssiwa* of 7.761E + 03, 2.6442E + 04, 7.148E + 03 and 5.1039E + 04 intergene bases. *GSTA1* has an *uppesebssiwaa* and *dppesebssiwaa* of 7.454E + 03 and 5.1039E + 04 intergene bases with a P_{eff} of 0.146 *esebssiwaagoT*$_Q$ units (Table 10).

CYP11B2 is a 2 A 5 initial and final SEB gene at *x*-, *y*-vertical axis angulation 76.5°. *CYP11B2* has an *uppasebssiwa*, *dppasebssiwa*, *uppmsebssiwa* and *dppmsebssiwa* of 2.4767E + 04, 2.73740E + 05, 7.246E + 03 and 1.2312E + 04 intergene bases. *CYP11B2* has an *uppesebssiwaa* and *dppesebssiwaa* of 1.6007E + 04 and 1.43026E + 05 intergene bases with a P_{eff} of 0.112 *esebssiwaagoT*$_Q$ units (Table 10).

CYP11B1 is a 3 M 7 initial and final SEB gene at *x*-, *y*-vertical axis angulation 78.1°. *CYP11B1* has an *uppasebssiwa*, *dppasebssiwa*, *uppmsebssiwa* and *dppmsebssiwa* of 1.8541E + 04, 4.5978E + 04, 9.853E + 03 and 2.41300E + 05 intergene bases. *CYP11B1* has an *uppesebssiwaa* and *dppesebssiwaa* of 1.4197E + 04 and 1.43639E + 05 intergene bases with a P_{eff} of 0.099 *esebssiwaagoT*$_Q$ units (Table 10).

TGIF1 is a 2 A 5 initial and final SEB gene at *x*-, *y*-vertical axis angulation 80.3°. *TGIF1* has an *uppasebssiwa*, *dppasebssiwa*, *uppmsebssiwa* and *dppmsebssiwa* of 2.2126E + 04, 4.50996E +05, 1.6366E + 04 and 3.0205E + 04 intergene bases. *TGIF1* has an *uppesebssiwaa* and *dppesebssiwaa* of 1.9246E + 03 and 2.40600E + 05 intergene bases with a P_{eff} of 0.099 *esebssiwaagoT*$_Q$ units (Table 10).

Gene expression effective pressure mapping for diethylstilbestrol (DES) as a ligand of the cell membrane ERα/β steroid axis receptor

A2M is a 2 A 5 initial and final SEB gene at *x*-, *y*-vertical axis angulation 43.1°. *A2M* has an *uppasebssiwa*, *dppasebssiwa*, *uppmsebssiwa* and *dppmsebssiwa* of 8.931E + 03, 5.9005E +04, 5.7966E + 04 and 1.32425E + 05 intergene bases. *A2M* has an *uppesebssiwaa* and *dppesebssiwaa* of 3.3448E + 04 and 8.6274E + 04 intergene bases with a P_{eff} of 0.388 *esebssiwaagoT*$_Q$ units (Table 11).

HOXA13 is a 2 M 5 initial and final SEB gene at *x*-, *y*-vertical axis angulation 48.2°. *HOXA13* has an *uppasebssiwa*, *dppasebssiwa*, *uppmsebssiwa* and *dppmsebssiwa* of 1.04360E + 05, 2.55391E + 05, 1.9369E + 04 and 1.02576E + 05 intergene bases. *HOXA13* has an *uppesebssiwaa* and *dppesebssiwaa* of 6.1864E + 04 and 1.78884E + 05 intergene bases with a P_{eff} of 0.346 *esebssiwaagoT*$_Q$ units (Table 11).

Table 11. Effective intracellular pressure mapping of directional gene activation by DES via the cell membrane ERα receptor in the mullerian axis in differentiation.

Human gene (no. of bases, locus bases or n/a)	Gene locus (ch, strand)	Angle (°)	Episode category (final, initial SEB structure)	*uppesebssiwaa*, *dppesebssiwaa* (P_{eff}, fract) [§, ‡]	P_{eff} effect pathway
A2M, alpha-2-macorglobulin (48,566; n/a)	12p13.31 (-)	43.2	2 A 5 (-)	3.3448E + 04, 8.6274E + 04 *(0.388)*	Des (ovi)
HOXA13, homeobox A13 (13,694; n/a)	17q15.3 (-)	48.2	2 M 5 (-)	6.1864E + 04, 1.78884E + 05 (*0.346*)	Des (n/c)
HOXA11, homeobox A11 (4,067; n/a)	7q15.3 (-)	49.9	2 M 8 acm (3 A 7)	6.3386E + 04, 1.90703E + 05 (*0.332*)	Des (dec, ut)
CCND1				(*0.290*)	Des (dec, ut)
HOXA10, homeobox A10 (12,827; 17,827)	7p15.3 (-)	56.62	2 M 5 (-)	2.6583E + 04, 9.6199E + 04 (*0.2763*)[§]	Des (dec, ut)
HOXA9, homeobox A9 (5,084; 17,827)	-	56.62	-	(> *0.2763*)[§]	Des (inc, ut; dec, ovi)
FOS				(*0.256*)	Des (inc, ut)
KLF4, kruppel like factor 4 (5,631; n/a)	17q21.2 (+)	66.65	3 A 7	5.3916E + 04, 2.21844E + 05 (*0.243*)	Des (ut)
TFF1				(*0.147*)	E_2 (inc)
ESR2				[*0.136* (0.1361)]	Des
WNT5A, Wnt family member 5A (39.547; n/a)	3q14.3 (-)	73.6	2 A 5 (-)	3.3867E + 04, 2.49146E + 05 [*0.1359*] [‡]	Des (inc, ut)
CYP11B1				(*0.099*)	Des

DES, diethylstilbesterol; n/c, no change; uterine; ovi, oviduct

[§ a)] same locus genes include *HOXA9* with P_{eff} towards ≥ 0.2763 (5' downstream; P_{eff} (adj) 0.27630) and *HOXA10* with P_{eff} 0.2763 (5' upstream; P_{eff} 0.27630); [b)] *HOXA9* *z*, *x*-plane alignment $P_{eff\ (adj)}$ is 0.27633 when (+) Δ P_{eff} is 0.01078 (*WNT5A*, P_{eff} 0.1359, DES; *TFF1*, P_{eff} 0.1470, E_2) and 5-digit adjustment is ($P_{eff\ HoxA10}$ · 2.9788E – 05) [‡] sequentially ∫ *esebssiwaagoT*$_Q$s to final P_{eff} for *WNT5A* gene expression are: 0.0656, 0.0895, 0.1138, 0.1430, *0.1359*, 0.1939; [&] Gene loci sub-episode block structure (SEB) variations include non-contributory anisotropy (NCA), anisotropy converted to mesotropy (ACM), 0.5-factor adjusted stabilizing mesotropy or anisotropy converted to stabilizing isotropy for anisotropy or mesotropy (stIAfM, stIMfM).

https://doi.org/10.1371/journal.pone.0236446.t011

HOXA11 is a 2 M 8 ACM final SEB gene at *x*-, *y*-vertical axis angulation 49.9°. *HOXA11* has an *uppasebssiwa*, *dppasebssiwa*, *uppmsebssiwa* and *dppmsebssiwa* of 1.14015E + 05, 2.54118E + 05, 1.2758E + 04 and 1.27288E + 05 intergene bases. *HOXA11* has an *uppesebssiwaa* and *dppesebssiwaa* of 6.3386E + 04 and 1.90703E + 05 intergene bases with a P_{eff} of 0.332 *esebssiwaagoT*$_Q$ units (Table 11).

HOXA9/HOXA10 is a 2 M 5 initial and final SEB gene at *x*-, *y*-vertical axis angulation ≥ 56.6°. *HOXA9/HOXA10* has an *uppasebssiwa*, *dppasebssiwa*, *uppmsebssiwa* and *dppmsebssiwa* of 4.34614E + 04, 9.8407E + 04, 9.552E + 03 and 9.3991E + 04 intergene bases. *HOXA9/HOXA10* has an *uppesebssiwaa* and *dppesebssiwaa* of 2.6583E + 04 and 9.6199E + 04 intergene bases with a P_{eff} of ≥ 0.2763 *esebssiwaagoT*$_Q$ units.

KLF4 is a 3 A 7 initial and final SEB gene at *x*-, *y*-vertical axis angulation 60.65°. *KLF4* has an *uppasebssiwa*, *dppasebssiwa*, *uppmsebssiwa* and *dppmsebssiwa* of 2.9538E + 04, 3.7755E + 05, 7.8294E + 04 and 1.66138E + 05 intergene bases. *KLF4* has an *uppesebssiwaa* and *dppesebssiwaa* of 5.3916E + 04 and 2.21844E + 05 intergene bases with a P_{eff} of 0.243 *esebssiwaagoT*$_Q$ units (Table 11).

WNT5A is a 2 A 5 initial and final SEB gene at *x*-, *y*-vertical axis angulation 73.6°. *WNT5A* has an *uppasebssiwa*, *dppasebssiwa*, *uppmsebssiwa* and *dppmsebssiwa* of 3.4162E + 04, 4.41140E + 05, 3.3572E + 05 and 5.7151E + 04 intergene bases. *WNT5A* has an *uppesebssiwaa* and *dppesebssiwaa* of 3.3867E + 04 and 2.49146E + 05 intergene bases with a P_{eff} of 0.1359 *esebssiwaagoT*$_Q$ units (Table 11).

van der Waals diameter, structural lipophilicity and hydrophilicity parameters for small molecules with exterior or interior structural lipophilicity

Tetradotoxin ($C_{11}H_{18}N_3{}^{1+}O_8$) has a Log *D* of -6.84, a vdWD of 0.774 nm and a Log *D*/vdWD of -8.84 nm^{-1}. 2,4-diazatetracyclotetradecane ($C_{11}H_{18}N_2O_2$) has a Log *P* of 0.847, a vdWD of 0.624 nm and a Log *P*/vdWD of 1.36 nm^{-1}. Tetradotoxin has a calc $L_{internal\ structure}/H_{polar\ group}$ ratio of 0.2323, and a nl calc $L_{internal\ structure}/H_{polar\ group}$ quotient of 0.085 (Table 12).

Saxitoxin ($C_{10}H_{19}N_7{}^{1+,1+}O_4$; 1+ SS 1+) has a Log *D* of -7.12, a vdWD of 0.764 nm and a Log *D*/vdWD of -9.32 nm^{-1}. 3,4-pyrrolo-4,5-imidazolo-6-methyl-piperazine ($C_9H_{16}N_4$) has a Log *P* of 0.13, a vdWD of 0.682 nm and a Log *P*/vdWD of 0.19 nm^{-1}. Saxitoxin has a calc $L_{internal\ structure}/H_{polar\ group}$ ratio of 0.2784, and a nl calc $L_{internal\ structure}/H_{polar\ group}$ quotient of 0.101 (Table 12).

m-xylenediamine ($C_8H_{14}N_2{}^{2+}$) has a Log *D* of -5.84, a vdWD of 0.635 nm and a Log *D*/vdWD of -9.20 nm^{-1}. 1,2-dimethylbenzene (C_8H_{10}) has a Log *P* of 3.00, a vdWD of 0.598 nm and a Log *P*/vdWD of 5.02 nm^{-1}. *m*-xylenediamine has a calc $L_{external\ structure}/H_{polar\ group}$ ratio of 0.252, and a nl calc $L_{external\ structure}/H_{polar\ group}$ quotient of 0.092 (Table 12).

Phthalate ($C_8H_4O_4{}^{2-}$) has a Log *D* of -4.70, a vdWD of 0.633 nm and a Log *D*/vdWD of -7.42 nm^{-1}. Benzene (C_8H_{10}) has a Log *P* of 1.97, a vdWD of 0.532 nm and a Log *P*/vdWD of 3.70 nm^{-1}. Phthalate has a calc $L_{external\ structure}/H_{polar\ group}$ ratio of 0.215, and a nl calc $L_{external\ structure}/H_{polar\ group}$ quotient of 0.078 (Table 12).

1,2-diaminocyclohexane ($C_6H_{16}N_2{}^{2+}$) has a Log *D* of -6.07 (-2.05), a vdWD of 0.622 nm and a Log *D*/vdWD of -9.76 (-3.34) nm^{-1}. Cyclohexane (C_6H_{12}) has a Log *P* of 2.67, a vdWD of 0.699 nm and a Log *P*/vdWD of 4.67 nm^{-1}. *m*-xylenediamine has a calc $L_{external\ structure}/H_{polar\ group}$ ratio of 0.233 (0.470), and a nl calc $L_{external\ structure}/H_{polar\ group}$ quotient of 0.085 (0.171) (Table 12).

N-acetylneuraminic acid ($C_{21}H_{30}O_4$; Neu5ac) has a Log *D* of -7.40, a vdWD of 0.790 nm and a Log *D*/vdWD of -9.37 nm^{-1}. Pentane has a Log *P* of 2.69, a vdWD of 0.561 nm and a Log *P*/vdWD of 4.97 nm^{-1}. Neu5ac has a calc $L_{external\ structure}/H_{polar\ group}$ ratio of 0.2189, and a nl calc $L_{external\ structure}/H_{polar\ group}$ quotient of 0.0796 (Table 12).

Discussion

Molecular philicity interval for facilitated transport though cell membrane channels as determined by $L_{external\ structure} \cdot H_{polar\ group}{}^{-1}$ of C_1 –C_4 alkane hydroxylate isomers

The molecular philicity interval limit for facilitated transport though cell membrane channel pores is determined in this study by *in silico* modeling of transporter threshold for mono-, di-

Table 12. Small molecules with external hydrophilicity and interior or exterior lipophilicity as ligands for cell membrane receptors or channels.

Small molecule	Formula	Log *P* (*D*)	Molecular Weight (Da)	Size (Ang^3)	vdWD (nm)	Polar SA (Ang^2)	Log *D*/vdWD (nm^{-1})	$L_{external\ (or\ internal)\ structure}/H_{polar\ group}$ (Ch_3oh nl)
Tetradotoxin	$C_{11}H_{18}N_3{}^1{}^+O_8$	-4.59 (-6.84)	319	252	0.774	188	-8.84	0.085
2,4-diazatetracyclotetradecane	$C_8H_{12}O_2$	0.847	140	132	0.847	18	1.36	$-L_{internal}$
m-xylenediamine	$C_8H_{14}N_2{}^{2+}$	0.22 (-5.84)	136	139	0.635	52	-9.20	0.092
1,2-dimethylbenzene	C_8H_{10}	3.00	106	116	0.598	-	5.02	$-L_{external}$

[1)] *m*-xylenediamine (1+ IS 1+; 2+ at pH 7.4, '97%, pKa 8.82, 9.52) has exterior structural lipophilicity in the $L_{external\ structure} \cdot H_{polar\ group}{}^{-1}$ in the range of interaction with CM receptor motifs (1,2-diaminocyclohexane, 1+ IS 1+ at pH 7.4, ~50%; Log *D* -6.07/-2.05, vdWD: 0.622 nm; -9.76, -3.34 nm^{-1}; $L_{external\ structure} \cdot H_{polar\ group}{}^{-1}$: 0.085/0.171), 0.078 (phthalate, 2-; Log *P* -4.70, vdWD: 0.633 nm; -7.42 nm^{-1})– 0.092 (*m*-xylenediamine)

[2)] saxitoxin (STX) has interior structural lipophilicity in the range for interactions with CM channel wall domains (superior), 0.085 ≥ 0.101 (saxitoxin, 1+ SS 1+, 2+ at pH 7.4, pka 7.98, 9.32; $L_{internal\ structure} \cdot H_{polar\ group}{}^{-1}$, 0.101); and

[3)] N-acetyl-neuraminic acid (Neu5Ac; 0.790 nm, -9.37 nm^{-1}) has a $L_{internal\ structure} \cdot H_{polar\ group}{}^{-1}$ of 0.080 *Isophile ether adjustment applied to both $L_{external/intervening\ structure}$ and $H_{polar\ group}$ for determination of molecular structure lipophilicity-to-polar group hydrophilicity ratio quotient.

https://doi.org/10.1371/journal.pone.0236446.t012

and poly-hydroxylate transport through the high affinity aquaporin-9 (hAQP-9) transport channel, which has a low-micromolar (uM) transport constant (*K*m) as determined in oocyte plasmid transfectants [19,20]. Since hAQP-3 and hAQP-9 have the lowest reflection coefficients (σ, a.u.) to the flux of 1,3-propanediol and 2,3-glycer-1-ol as the polarity-specific transport substrates, in this study the lipophilicity per molecular polarity is determined for C_1 –C_4 hydroxylates ($L_{external\ structure} \cdot H_{polar\ group}^{-1}$). Based on study findings, 2,3-glycer-1-ol has an external structure lipophilicity Log *P*/vdWD of 3.71 nm^{-1} with an unadjusted Log $P_{alkane} \cdot vdWD_{alkane}^{-1}$/Log $P_{OH} \cdot vdWD_{OH}^{-1}$ of 0.428 (0.545 nm; -3.38 nm^{-1}) in reference to methan-1-ol ($L \cdot H^{-1}$, 2.75 (1.00); 1.275 nm^{-1}), while S-(+)-1,2-propanediol has a $L_{external\ structure} \cdot H_{polar\ group}^{-1}$ of 1.047, which is a competitive inhibitor for polarity-specific transport of glycerol through hAQP-9 [19]. Furthermore, based on study findings, hydroxylates, 1,3-propanediol with a $L \cdot H^{-1}$ of 1.113 (vdWD: 0.527 nm), 1,2-butanediol with a $L \cdot H^{-1}$ of 1.207 (vdWD: 0.562 nm) will be non-specific passive transport substrates for glyceroaquaporin-9, as compared to 1,2-ethanediol with a $L \cdot H^{-1}$ of 0.535 (vdWD: 0.486 nm), more hydrophilic channel substrates, mannitol ($L \cdot H^{-1}$, 0.304; vdWD: 0.672 nm, -5.55 nm^{-1}) and lactate ($L \cdot H^{-1}$, 0.272, -1; vdWD: 0.526 nm, -7.04 nm^{-1}), of which the latter demonstrates increased flux in its un-ionized form ($L \cdot H^{-1}$, 0.328, -0.893 nm^{-1}) with maintained polarity-specificity for the channel. Therefore, based on the study findings, a $L_{external\ structure} \cdot H_{polar\ group}^{-1}$ of $\geq$ 1.07 is the molecular structure lipophilicity limit for non-specific carrier-mediated transmembrane diffusion through polarity-selective transport channels of the cell membrane (Table 1, Fig 1).

Pressure regulated gene activation by C_2 –C_4 halogenates, C_9 –C_{12} alcohols and unsubstituted biphenyl with asphyxiant properties

The part-molecular structural $L_{external\ structure} \cdot H_{polar\ group}^{-1}$ of C_2 –C_4 halogenates and halogenate ethers (-O-) with vdWD in the 0.554–0.610 nm range was studied as a determinant of the potency of the halogenate-mediated effect on gene activation, as vdWD is shown to be an independent predictive determinant of end-tidal minimum alveolar concentration (MAC; vol %) based on trichloromethane ($CHCl_3$; 0.505 nm), halothane ($C_2HBrClF_3$; 0.554 nm), isoflurane and enflurane ($C_3H_2ClF_5O$, 0.588 nm), and sevoflurane ($C_4H_3F_7O$; 0.610 nm) as standards 0.73 (R^2 = 0.73) compared to respective molecular weights (da) (R^2 = 0.29; Table 2). Further, based on the study findings, 1,1,1-trifluoro-2-chloroethane ($C_2H_2ClF_3$; 3.48 nm^{-1}), 1-chloro-1,2,2-trifluoroethane ($C_2H_2ClF_3$; 2.99 nm^{-1}) and 1,1,1-trifluoro-2-fluoroethane ($C_2H_2F_4$; 2.70 nm^{-1}) are the primary determinant moieties of overall structural $L_{external\ structure} \cdot H_{polar\ group}^{-1}$ for Isoflurane ($L \cdot H^{-1}$: 4.09), Enflurane ($L \cdot H^{-1}$: 3.72) and Desflurane ($L \cdot H^{-1}$: 3.50); 1,1,1,3,3,3-hexaflouropropane ($C_3H_2F_6$; 3.85 nm^{-1}) and fluoromethane ($CH_{2\text{-}3}F$; 0.939 nm^{-1}) are co-determinant moieties of overall structural $L \cdot H^{-1}$ for Sevoflurane (3.83), which bell curve (☐) rank orders anesthetic potency of part-structure halogenates inclusive of Desflurane that deviates from the Meyer-Overton rule due to lower part-structural structural $L_{external\ structure} \cdot H_{polar\ group}^{-1}$, as do the aliphatic alcohols due to a lower Log *P*/carbon; particularly C_2 –C_8 carbon length within a lower Log *P*/vdWD range [23] that deviate less than their non-polar alkane counterparts [24], in comparison to Halothane with more lipophilic substitution ($C_2HBrClF_3$; 3.82 nm^{-1}, $L \cdot H^{-1}$: n/a) and uM K_d affinity for cytochrome P450 catalysis under atmospheric pressure *in vitro* [25].

Studies on gene activation upon exposure to C_2 –C_4 halogenates have shown the differential expression of characteristic genes in response to Sevoflurane, Isoflurane and Halothane or to a combination (COMB) of non-inhalation (ie pentobarbital, midazolam) or chloral hydrate (CH) alone in a spectrum of cells (hippocampal neuron, type II alveolar cell, hepatocyte, T-lymphocyte). In these studies it is shown that cellular *FOSB* expression (P_{eff}, 0.194) decreases with *in vivo* COMB or CH exposure while expression remains unchanged with Isoflurane exposure (4 vol %, 1 min)

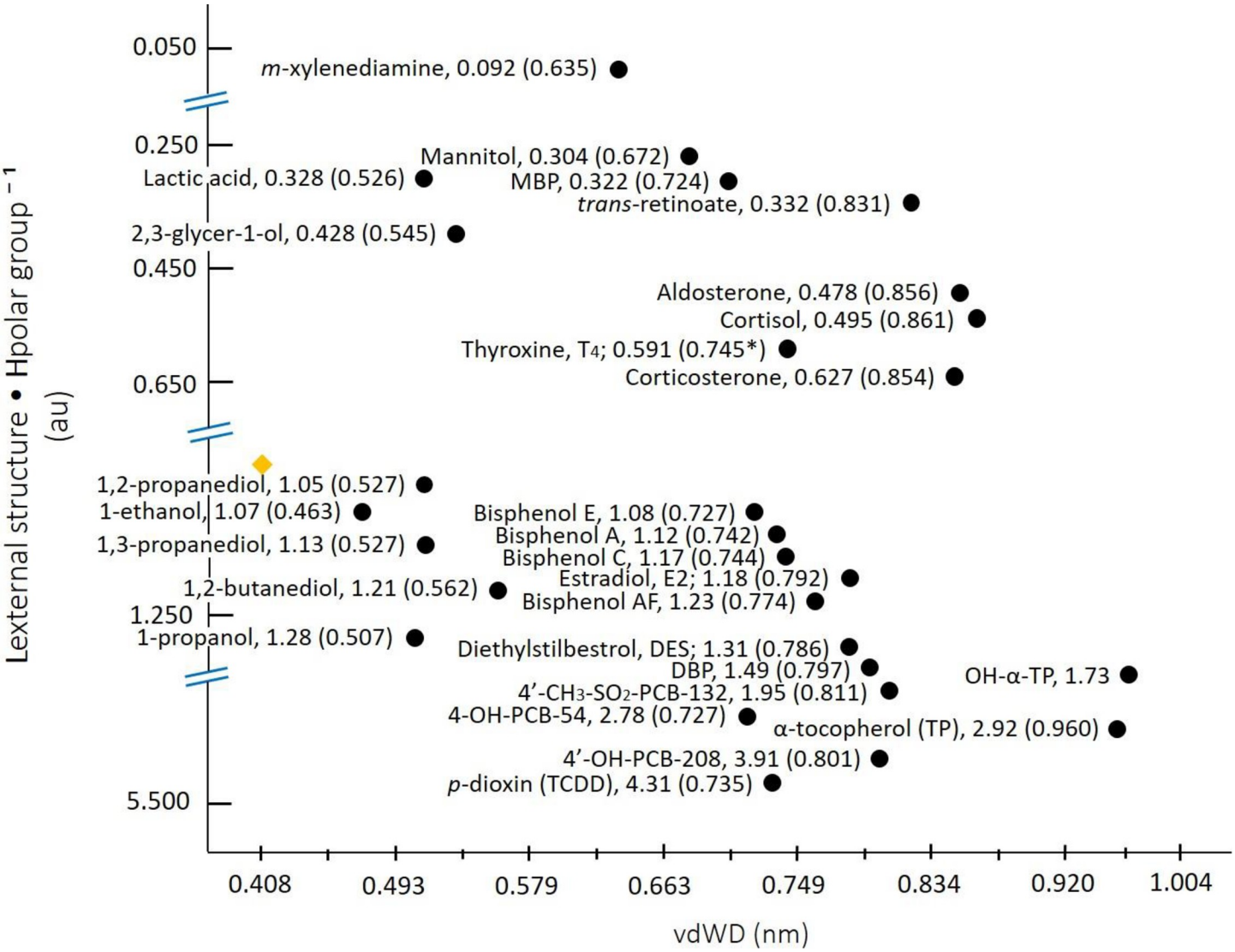

Fig 1. Molecular structural lipophilicity per polar group hydrophilicity intervals for acyclic and cyclic small molecule hormone receptor axis endogenous ligands and inverse agonists. The $L_{external} \cdot H_{polar\ group}^{-1}$ interval for non-selective carrier-mediated diffusion through polarity-specific transport channels is ≤ 1.07, which includes alkanols (1-propanol, 1.28; 1,2-butanediol, 1.21; 1,3-propanediol, 1.13; 1-ethanol, 1.07; vdWD, 0.463–0.562 nm) in addition to bisphenols [BPA—BPE, 1.08–1.12, intracellular (ERRγ/ERRα), vdWD 0.727–0.742 nm; BPC, intracellular–BPAF, extracellular 1.17–1.23, vdWD 0.744–0.774 nm (ERα/ERβ, GPER)], and diethylstilbestrol (DES; 1.31, vdWD 0.786 nm) as toxicants within the $L_{external} \cdot H_{polar\ group}^{-1}$ interval 1.08–1.31, and PCB metabolites 4-OH-PCB-54, 2.78 (vdWD 0.727 nm), 4'-OH-PCB-208, 3.91 (0.801 nm) and 4'-CH_3-SO_2-PCB-132, 1.95 (0.811 nm), and *p*-dioxin (TCDD), 4.31 (0.735 nm) as toxicants within the $L_{external} \cdot H_{polar\ group}^{-1}$ interval 1.95–4.31 (OH-PCB-3, $L \cdot H^{-1} = 2.13$; not shown). The $L_{external} \cdot H_{polar\ group}^{-1}$ interval for endogenous small molecule hormone ligands for the CM MR receptor is within the interval 0.478 (Aldosterone) and 0.495 (Cortisol), and for the CM GR receptor is around 0.627 (Corticosterone). The $L_{external} \cdot H_{polar\ group}^{-1}$ for complete OH-Iodothyroxine (T_4) zwitterion adjusted for intervening ether is 0.591, while the $L_{external} \cdot H_{polar\ group}^{-1}$ for (4'-hydroxy-3',5'-diiodophenoxy)-1-ethyl-3,5-diiodophenyl (non-zwitterion part-T_4) is 3.24. The $L_{external} \cdot H_{polar\ group}^{-1}$ interval for the broad selectivity CM hydroxylate channel polarity-specific substrates is between 0.328–0.428 (vdWD range 0.526–0.672 nm). Saxitoxin (STX) with internal structural lipophilicity has a $L_{external} \cdot H_{polar\ group}^{-1}$ of 0.101 (not shown), as compared to *m*-xylenediamine with external structural lipophilicity and a $L_{external} \cdot H_{polar\ group}^{-1}$ of 0.098. The $L_{ext} \cdot H^{-1}$ interval ranges for substrate binding affinity to CYP450 monooxygenases, UDP-glucouronosyl-/sulfo-transferases, and ester hydrolases is 1.91–4.31 (*p*-dioxin, OH-*p*-2,3,7-TriCDD), 1.73–2.69 (OH-α-tocopherol, *UGT1A_*; OH-PCB-3, *SULT1A_*) and 0.322–1.49 (mono-butylphthalate, MBP; dibutylphthalate, DBP), respectively. The $L_{ext} \cdot H^{-1}$ interval (min) for glucouronidation is 0.419 (glucouronate-2,3,7-TriCDD)– 0.459 (glucouronate-α-tocopherol). $^{\diamond}$ Methanol reference standard, 1 * Thyroxine, vdWD is adjusted for *x*, *y* plane-dimensional aspect (0.745 nm).

https://doi.org/10.1371/journal.pone.0236446.g001

[26]; *HMOX1* expression (P_{eff}, 0.153) increases with *in vivo* Sevoflurane or Isoflurane exposure (2–4 vol %) [27]; *SFTPC* expression (P_{eff}, 0.257) increases with *in vitro* Halothane exposure (1–4 vol %) or with *in vivo* Pentobarbital analog exposure, and decreases with *in vivo* Halothane exposure

(1%, 4 hr) [28]; and that *CASP3* (P_{eff}, 0.160) expression can increase *in vitro* during exposure to high concentrations of Sevoflurane and Isoflurane (5–8 vol %, 24 hr) [29]. These discordances between gene expression *in vitro* and *in vivo* may be reconciled by maintained concentration exposure *in vivo* in the presence of system tissue macro-compliance (- $P_{eff\ intracellular}$). Based on the effective intracellular pressure mapping findings of the study, there is contraction-expansion decrease in cell P_{eff} beginning from > 0.344 *esebssiwaagoT*$_Q$ units, between a P_{eff} 0.344 (*CYP2E1*) and P_{eff} 0.160 (*CASP3*) - 0.153 (*HMOX1*) *esebssiwaagoT*$_Q$ units. The P_{eff} 0.153–160 range appears to be the convergent peri-nadir for the *in vivo* inhalational anesthesia regulatory effect at equipotency and pro-apoptotic as *CREB1* (P_{eff} 0.154) is transcriptionally active, one that involves intermediate P_{eff} stages at 0.331 (*NFE2L2*) for expression of *HMOX1* (HO-1), and in addition to cell compliance maintenance at 0.267 (*JUN*, *TFB2M*) for the respective genes (**Table 3**).

Molecular size-exclusion limit for facilitated transport though cell membrane channels as determined by differential P_{eff} mapping of higher-substituted biphenyls

The molecular size-exclusion limit for facilitated transport though cell membrane channel pores is determined by study of the differential P_{eff} response to higher-substituted polychlorinated biphenyls, 3,4,4',5,5'-*co*-planar PCB-126 (0.749 nm) and *co*-, *ortho*-planar 2',3,4,4',5',6-PCB-153 (0.758 nm). During applied exposure to 3'-OH-3,4,4',5,5'-*co*-planar PCB-126 *in silico* as a representative *co*-planar PCB at a chiral carbon *x*, *y*, *z*-plane van der Waals diameter of 0.752 nm, the lower limit of P_{eff} decreases to the *x*, *z*-plane alignment pressure for *DIO3* (P_{eff}, 0.096) during which the upper limit of P_{eff} decreases to 0.379 (*CEACAM1*[a] [22]) and 0.331 (*NFE2L2*, NRF-2 [22]) *esebssiwaagoT*$_Q$ units during which contraction occurs; whereas, during applied exposure to PCB-153, the lower limit of P_{eff} decreases to 0.057 (*TSPAN12*) with contraction to P_{eff} 0.159 (*CES2*). Thus, there are distinct alterations in cell micro-compliance in response to TCDD and *co*-planar PCB (ie 5-OH-PCB-126; 2-OH-3,3',4, 4'-PCB-77) in comparison to applied *co*-, *ortho*-planar PCB (ie 5-OH-PCB-153; 4-OH-PCB-54), which implies a lower affinity Dio-2 enzyme non-exothermy inactivation pathway for the former (*co*-planar; 3'-OH-PCB-126, vdWD: 0.752 nm) relative to the higher affinity Dio-1/-3 enzyme inactivation pathway in case of the latter (*co*-, *ortho*-planar; PCB-153, vdWD: 0.758).

C_6 –C_{13} carbon length straight alcohols of increasing *n*-alkyl chain length and molecular weight (Da) have been shown to exert concentration dependent inhibitory effects on the P450 cytochrome monooxygenase activity (aminopyrine demethylase) *in vitro*, with disassociation constants (K_i) ranging between 1.3 mM (C_6, hexanol) and 2.66 mM (C_{13}, tridecanol) with uM inhibition by dodecanol (C_{12}; 35 uM) [30, 31], indicative of a cutoff of enzyme activity at a chain length of between 12- and 13-C (vdWD: 0.744–0.762 nm) at the cell membrane channel pore vdWD, in which case C_2-ethanol (mM) is non-exothermic (-ΔT; ˚C) as compared to C_{16}-hexadecan-1-ol ($C_{16}H_{34}O$, cetyl; uM) with inhibitory effect at a CM receptor [32]. Therefore, the decrease in cell P_{eff} (0.153–0.160) due to $C_{2\text{-}4}$ halogenate-mediated inner mitochondrial membrane (IMM) micro-compliance alteration is attributable to resultant ATP deficit, and synergistic with the affinity perturbation of CM by larger poly-substituted alcohols (ie $C_{16}H_{34}O_4$ isomers) [33], which are convergent mechanisms of decreased cell micro-compliance (-Δ C_{micro}) initially, prior to protein adduct effects on C_{micro}. These findings support the study determinations of cell membrane channel pore size of > 0.752 and < 0.758 nm based on a 3-D ellipsoid model (substituted biphenyl), and within the molecular diameter size range 0.744 and 0.762 nm based on a 2-D elliptical model (acyclic alcohol) (**Tables 2,4 and 5**).

Cell micro-compliance increase due to 2,3,7,8-tetrachlorodibenzo-*p*-dioxin exposure results in activation of the AhR-Erβ (Arnt): Nrf-2:: Pparδ, Errγ (LxRα): Dio3/Dio2 (Trα) pathway with limited response

There is an increase or decrease in the P_{eff} duration at the transcriptionally active zero (0)-degree *x*, *z*-transcription plane of genes as compared to a set of genes at baseline expression, for example as result of subacute *in vivo* exposure to TCDD, PCB-126 and PCB-153 in a rodent model (p.o.) [34, 35]. Based on the differential gene expression P_{eff} mapping of these genes as standards, it is determined that there is an increase in cell micro-compliance (Δ) that results in the activation of the AhR pathway by TCDD, as *p*-dioxin can be considered an unaspected size molecular standard with a non-chiral carbon 2-D spherical vdWD at 0.735 nanometers, as it has been shown to localize intracellularly [36]. The AhR-*p*-dioxin-(Arnt)-Erβ limb of the pathway is transcriptional active between a P_{eff} interval of between 0.381–0.379 and 0.106 (*UGT1A7*), as *IGHM* (P_{eff} 0.088) [37, 38] or other gene at equivalent P_{eff} decreases in expression with minimal contraction response. There is increased duration of activation (+Δ%) at P_{eff} cell pressures of 0.381 (*COX8C*; *Cox8h* ortholog, +10.2), 0.379 (*CEACAM1*; *Ceacam10* ortholog, +20.3), 0.373 (*NR1D1*, Rev-Erbα +0.16), 0.331 (Nrf-2, *NFE2L2*, +0.07), 0.283 (*DBP*, +0.3), 0.282 (*SCD*; *Scd2* ortholog, +0.16), 0.273 (*MT1A*, +0.07), 0.224 (*FABP5*, +0.07), 0.216 (*CYP1A1*, +33.5), 0.201 (*CYP1A2*, +0.10), 0.190 (*EXOC7*; *Exoc3* ortholog, +1.05), 0.169 (*CYP1B1*, +24.3), 0.168 (*ALDH3A1*, +1.9), 0.147 (*NQO1*, +0.65), 0.135 (*ME1*, +0.10) and 0.106 (*UGT1A7*, +2.8), in which additional genes with increases place at P_{eff} pressures of 0.376 (*SLC2A4*, Glut-4), 0.374 (*RXRA*), 0.332 (*GADD45B*), 0.282 (*RXRB*), 0.223 (*TIPARP*), 0.223 (*SIN3A*), 0.222 (*RARB*), 0.209 (*NR1H3*, *ESRRG*), 0.191 (*ARNTL*, aka Bmal1), 0.178 (*NCOR2*), 0.177 (*THRA*), 0.173 (*NRIP1*), 0.136 (*ESR2*) and 0.096 (*DIO3*); and during which there is decreased duration of activation (-Δ %) at P_{eff} cell pressures of 0.348 (*DAO*, -4.1), 0,324 (*ALAS1*, - 0.54), 0.183 (*DIO2*, -0.54), 0.158 (*ASCM2A*, -7.0) and 0.111 (*CYP3A7*, -37.6), in which additional genes with decreases place at P_{eff} pressures of 0.200 (*NRF1*), 0.196 (*ESRRA*), 0.184 (*ESR1*) and 0.179 (*RARA*) (Table 6, Fig 2 [top bracket]).

Based on the differential increases in P_{eff} pressure duration and interactions of characterized pathways, there is overactivation of the i) AhR (P_{eff} 0.395) [TCDD] ERβ—RIP140 and intracellular ligand (E_1, E_2 or E_3)-tuned overactivation of both *CYP1A1* and *CYP1B1* with the former being dependent on Erβ recruitment by AhR to XRE than the latter [39] for maximal nano-stability of transcription complex at *z*, *x*-plane alignment P_{eff}. and its maximal activation, while the latter being sensitive to ERα/β-mediated transcription repression during recruitment to ERE and obligatory presence of common co-adapter RIP140 for ER and ERR, and the former via high affinity interaction. There is ii) Nrf-2 (P_{eff} 0.331) overactivation of *MT1A* [3], with overexpression of *MT1A* attributable to a decrease in % duration at P_{eff} 0.200 (*NRF1*) and NRF1 underexpression with resultant overactivation of both *HMOX1* (P_{eff} 0.153) and *NQO1* (P_{eff} 0.147) in the presence of transcription factor Nrf-2 and a potential Maf as an enhancer as co-adaptor. Furthermore, there is overexpression of proximal and distal *UGT1A_* locus genes (5') *UGT1A7* and *UGT1A6* (3'), with a concomitant decrease in expression of *UGT1A1* [34, 40], which are AhR and Nrf-2 transcription factor-responsive genes at P_{eff} 0.106, while *UGT1A1* is transcriptionally active during the presence of CAR (PXR). There is iii) an increase in the P_{eff} duration of transcriptional activation between P_{eff} interval 0.216 to 0.236, in which PPARγ and TIPARP are activated, and *ESR1* gene transcriptional repressor SIN3A [41] are overexpressed, while *ESR2* remains activated at P_{eff} 0.136, as does *RAPGEFL1* (Link-GEFII; P_{eff} 0.283). There is likely a minimal increase in *FABP5* expression (P_{eff} 0.224) [34] during Δ C_{micro} duration at P_{eff} due to the presence of *RARB* gene activation (P_{eff} 0.222) along with binding partner for 9-*cis*-retinoic acid-RXRα (P_{eff} 0.374) and transcriptional repression of

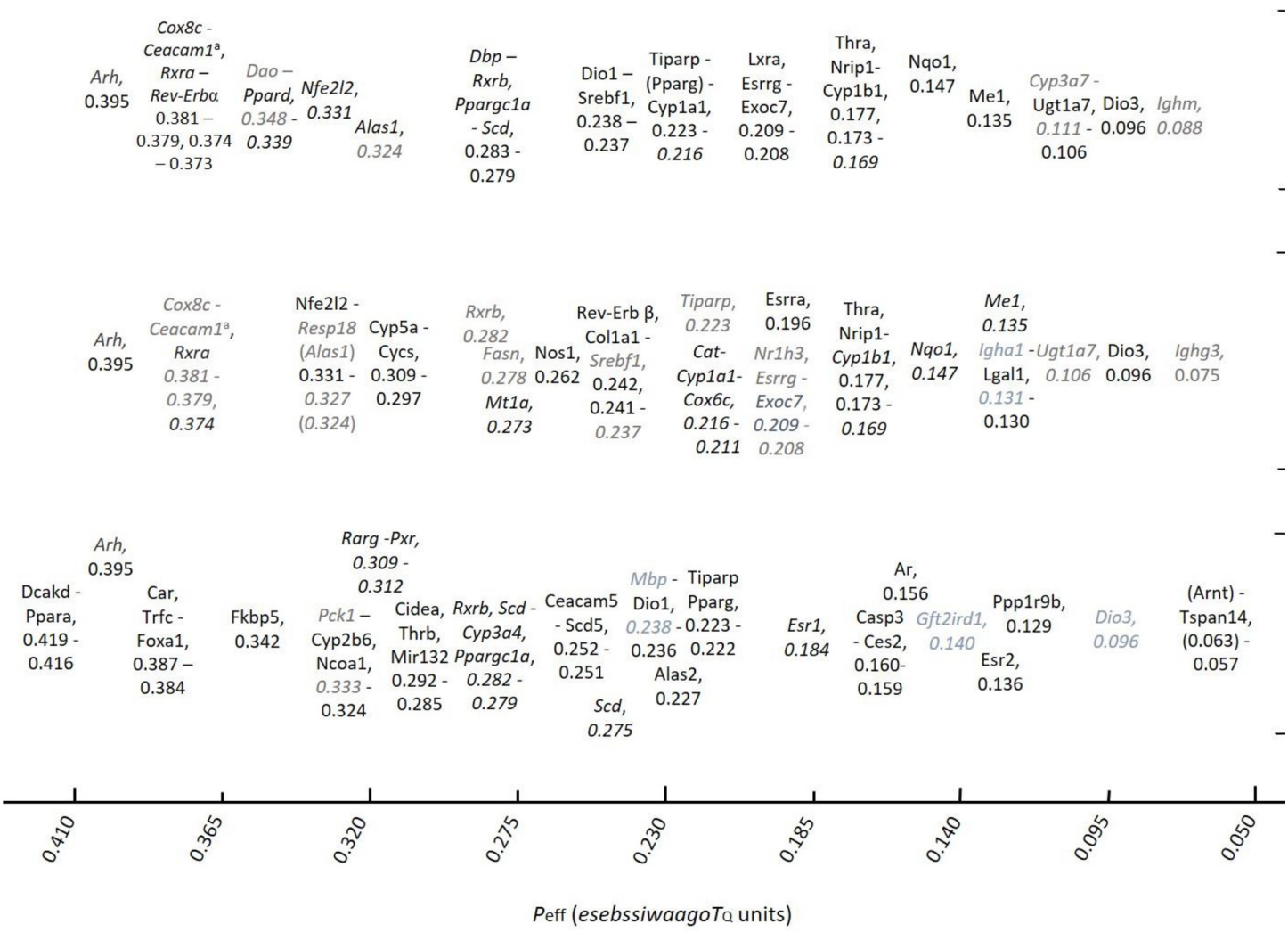

Fig 2. Alterations in cell micro-compliance due to sub-acute exposure to polychlorinated biphenyl high affinity metabolites with specificity for intracellular or extracellular deiodinases. Lower limit of the lower tier P_{eff} for transcriptional activation is increased to 0.106 (*Ugt1a7*) during a C_{micro} contraction response with a decrease in P_{eff} C_{micro} to $< 0.106 > 0.088$ (*Ighm*) *esebssiwaagoT*$_Q$ units during the expansion response; and the lower limit of the upper tier P_{eff} is increased to between ~0.395 (*AhR*) to 0.381 (*Cox8c*) - 0.379 (*Ceacam1*[a]) with an interval increase in P_{eff} C_{micro} in juxtaposition to ≤ 0.416 (*Pparα*) ≥ 0.395 (*AhR*) *esebssiwaagoT*$_Q$ units. The upper tier apparent interval P_{eff} C_{micro} contraction response is between a P_{eff} of 0.348 (*Dao1*) - 0.331 (*Nfe2l2*) and 0.379 *esebssiwaagoT*$_Q$ units. The C_{micro} contraction-expansion response range is 0.225–0.275 (min BoR; *Cox8c*, *Nfe2l2*; *Ugt1a7*) to 0.243–0.293 (max BoR; *Cox8c*, *Nfe2l2*; *Ighm*) [*p*-dioxin (TCDD), upper bracket, no. 1]. In the AhR-Erβ (Arnt), Pparδ, Errγ (LxRα): Dio3/Dio2 (Trα) pathway, the minimum expansion response phase of the positive P_{eff} contraction-expansion is a result of transient Errα decrease in activation-mediated de-repression of Dio2. Lower limit of the lower tier P_{eff} for transcriptional activation is increased to 0.130 (*Lgal1*) during a C_{micro} contraction response with a decrease in P_{eff} C_{micro} to $< 0.088 \geq 0.080$ (*Tgif1*) -0.075 (*Ighg3*) *esebssiwaagoT*$_Q$ units during the expansion response; and the lower limit of the upper tier P_{eff} is increased to between > 0.395 (*AhR*) and 0.387–0.381 (*Cox8c*) with an interval increase in P_{eff} C_{micro} in juxtaposition to < 0.416 (*Pparα*) $>$ 0.395 (*AhR*) *esebssiwaagoT*$_Q$ units. The upper tier apparent interval P_{eff} C_{micro} contraction response is between a P_{eff} of > 0.327 (*Resp18*) - 0.331 (*Nfe2l2*) and 0.381 *esebssiwaagoT*$_Q$ units. The C_{micro} contraction-expansion response range is 0.201–0.251 (min BoR; *Nfe2l2*, *Cox8c* - *Lgal1*) to 0.2585–0.3085 [max BoR; *Cox8c*, *Nfe2l2*; *Ighm*, *Tspan12* (avg)]. The range of delta (Δ) micro-compliance (Δ C_{micro}) for the bracket no. 2 (*co*-planar PCB-126) and no. 1 (TCDD, std) comparison is between 0.024 (0.89) [Δ, ratio contraction] and 0.0155 (1.05) [Δ, ratio expansion; a.u.]. In the AhR-Erα (Arnt): Nrf-2:: Rev-Erbβ, (+,-) Errα: Dio3/Dio2 (Trα) pathway, the expansion response phase of the positive P_{eff} contraction-expansion is a result of Trα-mediated overactivation of Dio3. Lower limit of the lower tier P_{eff} for transcriptional activation is increased to 0.159 (*Ces2*) during a C_{micro} contraction response with a decrease in P_{eff} C_{micro} to between $< 0.080 \geq 0.063$–0.057 (*Tspan14*) *esebssiwaagoT*$_Q$ units during the expansion response, and the lower limit of the upper tier P_{eff} is increased to between 0.387 (*Nr1h3*, CAR; *Trfc*) and 0.384 (*FoxA1*) with an interval increase in P_{eff} C_{micro} in juxtaposition to between 0.427 (*Hnf4a*) and 0.418 (*Pparα*)– 0.416 (*Dcakd*) *esebssiwaagoT*$_Q$ units. The upper tier apparent interval P_{eff} C_{micro} contraction response is between a P_{eff} of 0.324 (*Cyp2b6*, *Ncoa1*) and 0.312 (*Nr1I2*) *esebssiwaagoT*$_Q$ units. The C_{micro} contraction-expansion response range is 0.165 [min BoR; *Cyp2b6*, *Ces2*] to 0.346 [max BoR; *Dcakd*, *Nr1h3* (avg); *Tspan12*]. The range of delta (Δ) micro-compliance (C_{micro}) for the bracket no. 3 (ie PCB-95, -153) and no. 1 (TCDD, std) comparison is between 0.060 (0.73) [Δ, ratio contraction] and 0.053 (1.18) [Δ, ratio expansion; a.u.]. In the Car (Pxr), Rarγ: Pparα/γ, Rxrβ (Srebf1 -Lxrβ): Arnt (AhR-Er)/ Ar:: Dio1/Dio2 (Trβ) pathway, in which the expansion response phase of the positive P_{eff} contraction-expansion is a result of Trβ-mediated overactivation of Dio1 and transcriptional repression of Dio2 at P_{eff} (*esebssiwaagoT*$_Q$ units). plain text, increase in duration at P_{eff} in reference to baseline; text in italics, increase in duration at P_{eff} in reference to *p*-dioxin; and grey text in italics, decrease in duration at P_{eff} in reference to baseline Legend text: maximum bounds of range (max BoR); minimum bounds of range (min BoR).

https://doi.org/10.1371/journal.pone.0236446.g002

RARA at P_{eff} 0.181 by ERRγ, which is transcriptional co-adaptor complex regulator for *PPARD* (P_{eff} 0.339) [42] that is expressed, in addition to at half-site TRE response elements of deiodinase genes with co-recruited TRα/β. Furthermore, an increased duration of Rev-Erbα at P_{eff} (P_{eff} 0.373; +0.16) results in the overactivation of thyroid responsive target genes at half-site RRE response elements (AGGTCA) by overexpression of *ARNTL*, prior to auto-repression [43], which is an additional gene enhancer of *DBP* gene activation (P_{eff} 0.283) in combination with TRα (RXRα/β) that increases 9x-overfold in expression [34]. And, there will be iv) the basal transcriptional activation of *PPARGC1A* (PGC1α; P_{eff} 0.279) as co-activator adaptor of SREBF1 (P_{eff} 0.237), in addition to ERRγ (P_{eff} 0.209), is within the P_{eff} interval for *SCD* gene overexpression (P_{eff} 0.282) [44] during the transcriptional overactivation of LXRα (P_{eff} 0.209). Thus, a transcriptional duration at P_{eff} increase of +0.16% for *SCD* is commensurate with minimal increased duration at P_{eff} % for PGC1α and LXRα; and analogous to Nrf-2 (P_{eff} 0.331, +0.07)-mediated target gene activation upon P_{eff} *z*, *x*-plane alignment, in which case a common co-activator such as Maf-g (P_{eff} 0.251) will be involved for activation of *ALDH3A1* (P_{eff} 0.168, +1.9) as another non-canonical pathway gene (Table 6).

In addition to direct overactivation of the AhR (Arnt): Nrf-2 pathway by *p*-dioxin (TCDD), the other indirect pathways involved include the (+,-) Errγ and Dio2 (TRα), in addition to *PPARG* gene auto-repression due to the overexpression of SMRT (*NCOR2*; P_{eff} 0.178) interaction that results in a non-increase, during which TRα (*THRA*, P_{eff} 0.177) transcription will also increase due to the presence of PCB-displaced free T_4 ligand. The (±, -) Errγ pathway will result in re-activation of gene *Arntl* (P_{eff} 0.191) as there is an overactivation of std gene Rev-Erbα at P_{eff}, in which ARNTL will be overexpressed and enhance the transcription of GLUT-4 as does SREBF1, prior to Rev-Erbα autorepression [45] This is further supported by the experimental data that *Arntl* gene mRNA levels increase in $Rev\beta^{-/shRev\beta}$ knockdown cells, in which *NR1D1* (Rev-Erbα, P_{eff} 0.373) levels decrease with *NR1D2* (Rev-Erb β, P_{eff} 0.242) knockdown [46]. During TCDD mediated co-activation of the (±, -) Errγ pathway, there is inactivation of *ARNTL* (P_{eff} 0.191) and cytochrome C (*CYCS*, P_{eff} 0.297), which are both ERRα target genes [47].

Based on study findings, h*EXOC7* (P_{eff} 0.190) is overactivated, in which case rodent *Exoc3* may be a remnant exocyst in humans (P_{eff} u.d.), as Exoc7 is a plasma membrane post-golgi vesicular docking complex protein such as Exoc4 [48]. *EXOC7* is the *Exoc3* gene homolog is supported by the finding that it is required for Glut-4 channel expression (*SLC2A4*, P_{eff} 0.376) and exocytosis [49], however PPARγ gene transcription is not affected at P_{eff} 0.222 upon mutant *Exoc7* induction, which is a dioxin response element (DRE) responsive gene. There is an increase in duration at P_{eff} to +1.05 around the *Arntl* gene expression of P_{eff} at 0.191, based on which it is determined that there can be a decrease in P_{eff} via cell membrane (CM) exocytosis, and it is proposed to be the reason for the *z*, *x*-plane horizontal alignment of genes *ESR1* (P_{eff} 0.184) and *DIO2* (P_{eff} 0.183) for repressor interaction within the P_{eff} 0.183–0.186 interval in the TCDD pathway (Table 6). There is re-expression activation of *ARNTL* in this pathway at P_{eff} 0.191, which is proposed to be due to coupling of exocytosis transcription (P_{eff} 0.184) and endocytosis transcription (P_{eff} 0.191). The (±,-) Errγ pathway will be active during an increase in duration at upward contraction shift lower P_{eff} interval at 0.208–0.209 matched with an upper interval in-between 0.381 (*COX8C*) - 0.376 (*SLC2A4*) units.

Antagonism of the intracellular T_4/rT_3-Dio2 enzyme pathway by thyroxine (T_4) structural mimicry is proposed to be the umbrella mechanism for the decrease in delta (Δ)-C_{micro} from the maximum expression range of this pathway (0.361, max; 0.79), which is the C_{micro} range of the expansion response of the Arnt (AhR) pathway. The C_{micro} contraction in response to *p*-dioxin to within the $<$ 0.183 to 0.169 P_{eff} units range in addition results in the transcriptional activation of *THRA* (TRα, P_{eff} 0.177) and will its target genes via intracellularly-accumulated

T_3 agonism [49, 50], as the transcription of both std genes *ME1* (P_{eff} 0.135) and *DBP* (P_{eff} 0.283). Furthermore, since *NRIP1* is *z*, *x*-plane aligned at P_{eff} 0.173, RIP140 can function either as a higher-binding affinity partner for (AhR) ERα/β (P_{eff} 0.136, 0.184) [51], or as a lesser binding affinity co-adapter for ERRα/γ (P_{eff} 0.196/0.209) in comparison to related receptor affinity for PGC1α (P_{eff} 0.279) [52], which is via its dual ligand binding domains for estrogen receptor and related receptors. Therefore, *p*-dioxin (TCDD) exposure results in gene activation of AhR (Arnt)-ERβ, Nrf-2, Rev-Erbα, Errγ, LxRα and T_4/rT_3-Trα limbs in which there is an increase in retinoic X receptor α expression (*RXRA*, P_{eff} 0.374) with a decrease in cell micro-compliance (C_{micro}) due to high affinity intracellular Dio2 enzyme antagonism when at lesser than 10^{-12} affinity for the aryl hydrocarbon receptor (AhR) associated with CYP450 metabolism of *p*-dioxin.

Cell micro-compliance increase due to *co*-planar polychlorinated biphenyl exposure results in activation of the AhR-Erα/β (Arnt): Nrf-2:: Rev-Erbβ, Errα: Dio3/Dio2 (Trα) pathway with contraction-expansion response

The AhR-*co*-planar PCB-(Arnt)-ERα limb of the pathway is transcriptional active between duration of increase at P_{eff} of greater than (>) 0.381–0.379 to < 0.096 (*DIO3*) > 0.057 (*TSPAN14*) inclusive of expansion response, with contraction increases in P_{eff} at 0.331 (*NFE2L2*) and 0.130 (*LGAL1*) of the positive C_{micro} response. There is increased duration of activation (+Δ% or ratio) at P_{eff} cell pressures of 0.331 (*NFE2L2*, 1.14), 0.309 (*CYP5A*, +2.2), 0.297 (*CYCS*, +0.30), 0.273 (*MT1A*, 1.57), 0.241 (*COL1A1*, +0.60), 0.245 (*GADD45A*, +0.34), 0.220 (*CAT*, +0.87), 0.216 (*CYP1A1*, 1.28), 0.211 (*COX6C*, +0.34), 0.201 (*CYP1A2*, 2.60), 0.1686 (*GSTM2*, +6.6), 0.147 (*NQO1*, 1.22), 0.135 (*ME1*, 1.53) and 0.130 (*LGAL1*, +0.90), in which additional genes with increases place at P_{eff} pressures of 0.262 (*NOS1*), 0.242 (*NRID2*, Rev-Erb β), 0.196 (*ESRRA*), 0.184 (*ESR1*) and 0.096 (*DIO3*); and during which there is decreased duration of activation (-Δ %) at P_{eff} cell pressures of 0.427 (*HNF4A*, - 0.24), 0.384 (*CEACAM1*, 0.68–0.69), 0.381 (*COX8C*, 0.24–0.25), 0.331 (*PCK1*, - 0.36), 0.327 (*RESP18*, - 0.84), 0.324 (*ALAS1*, -0.24), 0.278 (*FASN*, -0.72), 0.190 (*EXOC7*; *Exoc3* ortholog, 0.22), 0.1687 (*CYP1B1*, 0.81), 0.168 (*ALDH3A1*, 0.10), 0.237 (*SREBF1*, - 0.24), 0.183 (*DIO2*, -0.24), 0.131 (*IGHA1*, -0.84) and 0.106 (*UGT1A7*, 0.19), in which additional genes with decreases place at P_{eff} pressures of 0.376 (*SLC2A4*), 0.374 (*RXRA*), 0.279 (*PPARGC1A*), 0.223–0.222 (*TIPARP*, *SIN3A*, *PPARG*), 0.200 (*NRF1*), 0.191 (*ARNTL*) and 0.136 (*ESR2*) (**Table 7**., **Fig 2** [middle bracket]).

The difference between the AhR-*co*-planar PCB and AhR-TCDD pathway P_{eff} regulation limb includes a P_{eff} contraction shift to within the 0.135 (*ME1*) to 0.147 (*NQO1*) *esebssiwaagoT*$_Q$ units interval with micro-expansion in-between a P_{eff} interval of 0.147 and 0.136 (*ESR2*), and similarly contraction within the 0.211 (*COX6C*) to 0.220 (*CAT*) P_{eff} gene expression interval, which results in an increase in the transcription of *CYP1A1* (P_{eff} 0.216) during increased overall ER expression (ERα) at P_{eff} due to decreased *SIN3A* activation at P_{eff}, thus increased ERα recruitment to ERE for decreased nano-stability at promoter, and relative *CYP1B1* gene de-activation during activation of *CYP1A1* at P_{eff} with *AHR* (P_{eff} 0.395) bound-xenobiotic response elements (**Table 7**). The decrease in expression of std gene *DBP* (P_{eff} 0.283) [34], is consistent with increased CRY1 at the *DBP* promoter E-box motif (CANNTG) [47], and an increase in lower affinity Rev-Erbβ (P_{eff} 0.242) at RRE response elements with limited availability of co-adapter BMAL1 (*ARNTL1*, P_{eff} 0.191), which is ERRα activated only on reporter assay [47] in the 0.191–0.196 P_{eff} interval during a concomitant increase in the activation of *ME1* at P_{eff} 0.135 (1.53x) [34, 53], as both *Dbp* and *Me1* are T_3 liganded-TRα (RXRα) TRE-response pathway regulated genes [49]. The intracellularly accumulated T_3-TRα/β pathway is the higher affinity pathway (K_d, 10^{-10}) [54] than the T_4/rT_3-extracellular (Dio-1/-3) or

-intracellular (Dio-2) deiodinase enzyme pathways (K_d, 10^{-7} to 10^{-9}) [55]. Therefore, the probability exists that chiral configuration halogenated molecules (ie PCBs) with 1- to 2-orders lower affinity *co*-planar affinity for AhR could be higher affinity substrates for deiodinases as antagonists as proposed.

There are also P_{eff} contraction shifts in activation to in-between 0.297 (*CYCS*) and 0.309 (*CYP5A*) and to in-between 0.262 (*NOS1*) [56] and 0.273 (*MT1A*) from deactivation within the 0.278–0.282 P_{eff} interval by which activation of *FASN* decreases (-0.72, std) decreases in which P_{eff} interval genes *PPARGC1A* and *RXRB* transcribe. The increase in activation of *CYCS* (P_{eff} 0.297) [57], as well as *COX6C* (P_{eff} 0.211) as a NRF1-responsive gene [58], is attributable to the transient overexpression of ERRα (P_{eff} 0.196) and target gene *CYCS* (P_{eff} 0.297) due to lesser duration *EXOC7* gene activation (P_{eff} 0.208, 0.22x) and decrease in C_{micro} as compared to during sub-acute TCDD exposure; whereas, increases in activation of *MT1A* and *GSTM2* can be attributed to an increase in in duration at P_{eff} for *NFE2L2* and a common Maf co-activator during the decrease in P_{eff} at 0.200 and *NRF1* inactivation. A P_{eff} contraction-expansion shift to P_{eff} at 0.130 results in *LGAL1* activation in response to *co*-planar PCB-126 metabolite exposure, a half-site TRE and ERE containing gene [59], as an example of gene that is activated at a preferred intracellular pressure *uppesebssiwaa*, *dppesebssiwaa* point increase in duration at P_{eff} to 0.130 during C_{micro} expansion within the $P_{eff} > 0.131$ (*IGHA1*) ≤ 0.135 interval (*ME1*), and during a contraction within the $P_{eff} \geq 0.262$ (*NOS1*) < 0.278 interval (*FASN*); there is a ~2.5-fold increase in *LGAL1* expression by qRT-PCR in response to applied IL-1β [60] at the upper bounds of the expansion interval, which is thus delineable as being at P_{eff} 0.130, during which the increase in activation at its P_{eff} setpoint results in an increase in pJUN (P_{eff} 0.267)-, pFOS (P_{eff} 0.256)-bound ½ site TRE response elements; whereas, the decrease in the same (*LGAL1*) in response to the combination of IL-1β and dexamethasone (Dex) is attributable to an upward shift of the P_{eff} contraction interval with expansion, when de-phosphorylation of AKT and ERK1/2 occurs ($+\Delta C_{micro}$) during decreased cell compliance. Furthermore, the extracellular Dex-induced repression of *LGALS1* activation via intracellularly-liganded GR (Dex/Cort)/MR (Cortisol) (P_{eff} 0.261) recruited to dephosphorylated JUN at *LGALS1* promoter TRE response elements, within which interval Dex-mediated contraction P_{eff} responsive *DUSP1* activation will occur at P_{eff} 0.272 during recruitment to GREs (GR). Therefore, co-planar PCB exposure (ie PCB-126) exposure results in gene activation of AhR-(Arnt), Nrf-2, Rev-Erbβ, (±,-) Errα and T_4/rT_3-Trα limbs, in which retinoic acid X receptor (*RXRA*) remains transcribable (P_{eff} 0.374) while *RXRB* gene transcription decreases (P_{eff} 0.282) with a ΔC_{micro} contraction response due to high affinity PCB metabolite antagonism of cell surface Dio3 enzymatic deiodoexothermy, which is a TRα activated gene [61], in addition to intracellular Dio2 (P_{eff} 0.183, -0.24%) antagonism by CM channel substrates (-PCB-OH, -S (= O)-Ch3) with its repression at minimum during de-activation of *ESRRA* (P_{eff} 0.183) [62], in competition with AhR at equivalent or lower concentration in a binding affinity dependent manner.

The pathway overactivation following *co*-planar-PCB-126 metabolite exposure represents the hepatocyte cell population subset at-risk for neotransformation, which are at a differential P_{eff} basal over contraction-expansion response within the lower limit P_{eff} interval range of ≥ 0.080 (*Tgif1*) ≤ 0.088 (*Ighm*) units. The basal transcription P_{eff} setpoint(s) preference for differential gene expression for the *co*-planar-PCB-126 metabolite exposed cell population is determined in case of interposed genes, *ESR1* (P_{eff} 0.184) as an example of one that is determined to be decreased in duration at P_{eff}, in comparison to *ESR2* (P_{eff} 0.136) as an example of one that is determined to be increased in duration at P_{eff} based on reporter assay P_{eff} expression correlation, as there is a requirement of estradiol (E_{1-3}) for activation of a non-integrated ERβ reporter plasmid ($+E_2$) [63], which requires endogenously transcribed *ESR2* in its native locus position that expresses at P_{eff} 0.136, whereas a ERα reporter plasmid can be expressed in

control conditions (-E_2). This finding implies that a P_{eff} 0.184 is one basal transcription P_{eff} set-point within an interval of the same in a viro-immortalized well-differentiated cell type (ie HepG2) [64] with an above baseline contraction lower bounds for differentiated cells, which are (GPER+)/ERα+/Erβ- and AR- cell types that are at risk for a switch to GPER+/ERα+/Erβ + status [65].

Cell micro-compliance increase due to *co*-, *ortho*-/*ortho*-planar polychlorinated biphenyl exposure results in activation of the Car (PxR, Rarγ): Pparα, Rxrβ (Srebf1, -Lxrβ): Arnt (AhR-Erβ)/Ar:: Dio1/Dio2 (Trβ) pathway with contraction-expansion response

In comparison to the *p*-dioxin and *co*-planar PCB pathways, the extracellular *co*-, *ortho*-planar PCB pathway is transcriptional active between duration of increase at P_{eff} of 0.387 (*NR1I3*, CAR) to 0.096 (*FABP6*, *DIO3*) with maximal apparent expansion increases intermittently to 0.418 (*DCAKD*) from 0.387 and from 0.106 to 0.057 (*TSPAN14*) during delta (Δ) expansion of 0.053 P_{eff} C_{micro} units (ratio, 1.18) as compared to the same for cellular response to applied *p*-dioxin (TCDD) modeled *in silico*, wherein the contraction response limb results in maximum transcriptional gene activation at P_{eff} point 0.324 (*CYP2B6*, *NCOA1*) in addition to between 0.157 – 0.159 (*CYP3A5*, *CES2*) e*sebssiwaago*T_Q units, delta-contraction of 0.060 P_{eff} C_{micro} units (ratio, 0.73). There is increased duration of differential activation (+Δ%) at P_{eff} of 0.384 (*FOXA1*, +0.7), 0.331 (*DCAKD*, +1.0), 0.3238 (*CYP2B6*, *Cyp2b2* ortholog; +30.3), 0.292 (*CIDEA*, +1.3), 0.285 (*MIR132*), 0.278 (*CUL2*, +1.0), 0.282 (*SCD*, +7.2), 0.227 (*ALAS2*, +0.7), 0.159 (*CES2*, +1.3), 0.157 (*CYP3A5*, *CYP2B15/-12* ortholog; +44.7), 0.096 (*FABP6*, +1.0) and 0.057 (*TSPAN14*, +2.0), in which additional genes with increases place at P_{eff} pressures of 0.416 (*PPARA*), 0.406 (*DDIT3*, *alias* CHOP), 0.387 (*TFRC*), 0.387 [*NR1I3*, CAR], 0.374 (*RXRA*), 0.373 (*NR1D1*) 0.342 (*FKBP5*), 0.312 (*NR1I2*, PxR), 0.309 (*RARG*), 0.288 (*THRB*), 0.282 (*RXRB*), 0.252 (*CEACAM5*), 0.252 (*MAFG*), 0.251 (*SCD5*), 0.237 (*SREBF1*), 0.236 (*DIO1*), 0.223 (*TIPARP*), 0.222 (*PPARG*), 0.161 (*NCOR1*), 0.160 (*CASP3*), 0.156 (*AR*), 0.136 (*ESR2*), 0.149 (*CYP4A11*), 0.129 (*PPP1R9B*), 0.128 (*FABP3*), 0.106 (*UGT1A1*) and 0.063 (*ARNT*). There is decreased duration of differential activation (-Δ%) at P_{eff} of 0.333 (*PCK1*), 0.272 (*DUSP1*), 0.224 (*MBP*), 0.183 (*DIO2*) and 0.140 (*GTF2IRD1*), in which additional genes with decreases place at P_{eff} of 0.395 (*AHR*), 0.324 (*NCOA1*), 0.281 (*CYP3A4*), 0.270 (*NR1H2*, LxRβ), 0.184 (*ESR1*) and 0.096 (*DIO3*) (**Table 8**, **Fig 2** [bottom bracket]).

Based on study findings, the common mechanism pathway for extracellular *co*-, *ortho*-planar PCBs and higher affinity-substituted PCB metabolites (-OH, -MeSO4; ie 4'-OH-2,2',3,4',5,5',6-PCB-172 (0.781 nm; 9.92 nm^{-1}), and applicable to cell membrane (CM)-permeable *co*-, *ortho*-PCBs (ie 4'-OH-PCB-95; 0.752 nm, 8.43 nm^{-1}) also, is the constitutive androstane receptor (*NR1I3*, P_{eff} 0.387) regulatory pathway as duration at P_{eff} increases at target genes *CYP2B6* (P_{eff} 0.324) [66], *CYP3A4* (P_{eff} 0.281) [66], *CES2* (P_{eff} 0.159) and *UGT1A1* (P_{eff} 0.106) [46], during pregame X receptor (PxR) recruitment (*NR1I2*, P_{eff} 0.312) to phenobarbital responsive elements (PBREM; ie *CYP2B6*) and/or CAR recruitment to PXRE response elements (ie *CYP3A4*). The expression of PPARα (P_{eff} 0.416) results in the transcriptional activation of target genes at various durations at P_{eff} and *x*, *z*-plane aligned for transcription, which include *CIDEA* (P_{eff} 0.292) [67, 68], *CYP4A11* (P_{eff} 0.149) [69], *FABP3* (P_{eff} 0.128) and *FABP6* (P_{eff} 0.096; +1.0) [70], including *SREBF1* (P_{eff} 0.236) with a predicted increase in the transcription factor gene *RXRB* (P_{eff} 0.282), which can be a recruited co-adapter, in addition to the presence of *RXRA* (P_{eff} 0.222) [71]. And, the activation of *SREBF1* at P_{eff} 0.237 will result in the transcriptional activation of target genes *SCD* (P_{eff} 0.282; +30.3) and *SCD5* (P_{eff} 0.251), for which the increase in duration at P_{eff} will be attributable to a decrease in LXRβ (P_{eff} 0.270),

during over-basal transcription at P_{eff} 0.209 (ERRγ, LXRα) and 0.222 (PPARγ), which is with interaction between LXRα or CAR and SRC-1; the pathway limbs are thus mutually antagonistic on known pathway gene expression, murine *CYP2B10* (h*Cyp2b6*) and *CYP3A11*, which are induced by CAR pathway agonist, 1,4-Bis[2-(3,5-Dichloropyridyloxy)] benzene (TCPOBOP) with activity at nM concentration *in vivo* [72]; while, the underexpression of LXRβ is transcriptionally synergistic. Furthermore, there is secondary lesser involvement of the common AhR-Arnt pathway [73] can be expected as per study determination, and limited by transcription of the *AHR* gene with a decrease in duration for P_{eff} at 0.395 during the expansion response phase with an increase in intracellular P_{eff} at 0.063 that favors transcription of the *ARNT* gene and the presence of Arnt as the obligate transcription factor for activation of *CYP1A1* [74], which will be in addition to CAR enhanced gene activity at proximal *cis*-ER8 motif PBREM binding elements with recruited pregnane X receptor [75]. Thus, CAR/PXR pathway limb become primary, as compared to the AhR driven by Arnt, during sub-acute *ortho*-planar PCB exposure, for which the preferred co-adapter is PGC1α (*PPARGC1A*, P_{eff} 0.279) [76], as it is for SREBF1 during decreased ERRγ/α in response to Δ C_{micro} (E/C, 1.18/0.73). Furthermore, gene *NCOR1* is overexpressed at P_{eff} 0.161 in this pathway based on study findings, which thus is the other co-regulator of *co*-, *ortho*-planar pathway-activated limbs and will serve as the adaptor for ligand-dependent TRβ-mediated gene transcription (ie *Dio1*, *Thrb*) as compared to *NCOR2* (P_{eff} 0.178; *Dio3*, *Thra*), and consistent with the intracellular presence or absence of liganded TRα/β (rT_3, T_3) [77], which appears to result in lesser suppression of PPARγ and target genes as compared in the applied TCDD model *in silico*.

Rodent *Cyp2b15/-12* shows high expression in normal un-differentiated cells of skin origin (keratinocytes, sebaceocytes) [78], and skin microsomal CYP *Cyp2b2* shows antibody reactivity [79]; thus, based on *esebssiwaagoT*$_Q$ determinations of keratinocyte marker CYPs 2B6 (P_{eff} 0.324), 2E1 (P_{eff} 0.344) and 3A5 (P_{eff} 0.157) [80], respective human orthologs of r*Cyp2b2* and r*Cyp2b15/-12* can be *CYP2B6* (P_{eff} +7.2) and *CYP3A5* (P_{eff} +44.7), as only these two place at the respective predicted (pred) constitutive intracellular pressures for overexpression in the P_{eff} interval at which *NCOA1* (SRC-1) is with interaction while *CYP2B6* is overactivated, and in the P_{eff} interval of 0.157–0.159 within which *CES2* increases in duration at P_{eff} with *CYP3A5*, which is an alternatively activated CAR/PXR pathway gene with EMSA supershift indicative of CAR dimerization possibly at full site PBREM [81], while *CYP3A4* is PxR (SRC-1) activatable during presence of FOXO1 [82]. Thus, since *CYP2B6* as the only B series hCYP, and *CYP3A5*, are both constitutively overexpressed in normal human keratinocytes, as are genes h*SCD* and h*SCD5* in murine epidermis-dermal junction at a common post-natal day [43], while *CYP3A4* is dexamethasone (Dex)-inducible [81–83] in contrast to std marker gene *DUSP1* (P_{eff} 0.272), which is deactivated at P_{eff} in response to Dex [60]; therefore, this finding is consistent with partial trans-differentiation to alternative lineage in a *co*-, *ortho*-/*ortho*-planar PCB-treated hepatocyte (**Table 8**), and will be applicable to other differentiated cell types.

The overactivation pathway following *co*-, *ortho*-planar PCB metabolite exposure results in delta (Δ) C_{micro} activation of gene locus within the 0.384 to 0.387 P_{eff} interval, which include *FOXA1* at P_{eff} 0.384, *PMCH* at P_{eff} 0.386 in addition to *NR1I3* (CAR) at P_{eff} 0.387, in relation to a Δ C_{micro}-mediated increase in activation duration at P_{eff} for transcription of *SREBF1* at P_{eff} 0.236 and *PPARG* at P_{eff} 0.222 and target genes (ie *FABP3*, P_{eff} 0.128) based on study determination, during which there can be tuned de-activation of genes such as *PCK1* (Pepck; P_{eff} 0.333) in the basal presence of Creb binding protein (CBP) with decreases in NF-IB, NF-1X [84] and/or Errγ. Additionally, there is a Δ C_{micro} activation relationship between gene activation at P_{eff} 0.236 and P_{eff} 0.156 (*AR*), and furthermore, at P_{eff} 0.223–0.222, at which there is relative activation of *TIPARP*, a AhR/Arnt-*p*-dioxin responsive but a Dht (AR) activatable gene at P_{eff} [85], during which there is relative de-activation of *PPARG* (P_{eff} 0.222) as a result of

SREBF1 recruitment by AR/Kruppel-like factor (KLF) [86] to the subset of Δ C_{micro} activatable AR/KLF pathway target genes including *FKBP5* at P_{eff} 0.342, a GRE element-containing gene with a significantly-enriched distal intronic ARE (AR) [87], which is a low affinity binding sequence for co-adapter SRC-1 (*NCOA1*, P_{eff} 0.324). Therefore, since *NCOA1* is transcriptionally repressed during increased duration at P_{eff} 0.324, NCoR1 will be the binding partner for T_3-TRβ (*THRB*, P_{eff} 0.288) for transcriptional activation of *DIO1* at P_{eff} 0.236 during Δ C_{micro} contraction phase, that results in the expansion phase during exposure to *ortho*-planar PCBs (ie PCB-95, -136, -153). This mechanistic correlation is in agreement with *DIO1* being transcriptionally active at *in vivo* at P_{eff} during the availability of T_3, TRβ [88] and co-adaptors SRC-1 [9], or NCOR1 and NCOR2 for ligand independent activation of *TRH* and *TSH* genes [89], for high affinity TRE (AF-2) sequence-bound transcription in $NCOA1^{-/-}/THRB^{E457A/E457A}$ and T_3-TRβ ligand-dependent *TSH* gene repression [9], which is in lieu of activation by TRα variant isoforms (*THRA*, P_{eff} 0.177) [90], as it is the lower affinity TRE-binding partner for *DIO1* (P_{eff} 0.236). Furthermore, apoptotic trans-differentiation occurs with P_{eff} interval matches of 0.285 (*MIR132*) - 0.292 (*CIDEA*) **[34; 67, 68**] and 0.155 (*CREB1*) - 0.160 (*CASP3*) [91], in addition to decreased transcription around 0.241 (*COL1A1*) [22] and 0.224 (*MBP*) P_{eff} intervals for induction of focal adhesion kinase, and with an increased risk for neurotoxicity [92, 93] during transcriptional activation of myelin basic protein gene repressor *DDIT3* (P_{eff} 0.406) in this pathway [94]. The findings of this study by further delineation of specific pathways are thus consistent with trans-differentiation to a sex steroid receptor expression pattern of ectodermal origin cells, sebaceocytes of the dermis epidermis junction [95,96], in which there is Δ C_{micro} co-activation of *ESR2* at P_{eff} 0.136, in addition to *AR* at P_{eff} 0.156, with a decrease in *ESR1* gene expression (P_{eff} 0.184) during transcriptional repression by Sin3A (P_{eff} 0.223) with interaction.

Spectrum of *p*-dioxin, *co*-planar and *co*-, *ortho*-/*ortho*-planar polychlorinated biphenyl metabolite exposure-related cell micro-compliance contraction-expansion response

Exposure to *co*-, *ortho*-OH-PCB-107 (intracellular), -PCB-136 and -PCB-146, or *co*-, *ortho*-planar PCBs OH-PCB-172 and -PCB-187 (extracellular), respectively, has been assessed in dual cohort studies of maternal exposure and infant response, in which it is shown that there is graded homuncular toxicity of the developmental eLMN-to-UMN neuroaxis in association with thyroid axis/deiodinase type 3 enzyme (Dio3) dysfunction [97], and in which a decrease in serum TSH level has been shown to be a sensitive indicator of exposure to biphenyl [98], as it has for exposure to penta-/hexa-substituted brominated diphenyl ethers such as BDE-100 and BDE-153 (vdWD: 0.775–0.793 nm) with available-3, 3' positions for hydroxylation bioactivation [99]. Based on this proposed mechanism as per study determination, the increase in T3/rT3 ratio, elevation in serum thyroxine-T4 and -T3 [97] is due to *co*-, *ortho*-planar PCB metabolite inhibition of the high affinity, high V_{max} deiodinase activity-exothermy of CM Dio3 (contraction phase) [55] during a decrease in intracellular TRα concentration ([]) and *DIO3* gene de-activation at P_{eff} with a resultant decrease in T4 to rT3 conversion in contraction phase, and an increase in intracellular T_3 liganded-TRβ [] in *DIO1* gene transcription at P_{eff} at higher serum T4 [] in expansion phase (transient hyperthyroidism), and T_3 liganded-TRα/β [] *TSH* gene inactivation. Furthermore, the finding of increased blubber tissue levels of both TRα and TRβ can be considered [100], if pan-exposure is considered with mutual-inclusivity of pathways involved (*p*-dioxin, *co*-planar PCB and *ortho*-planar PCB); and since there is decreased duration at P_{eff} for *ALAS1* (P_{eff} 0.324) in the *p*-dioxin pathway, and increased duration at P_{eff} for *ALAS2* (P_{eff} 0.227) in the *co*-, *ortho*-planar PCB pathway, for example due to

2',2',3,3',4,4'-PCB-128 (Arochlor 1260, vdWD: 0.758 nm) exposure [101], *Alas1*, *Alas2* mRNA levels could be indicators for exposure assessment.

Loss of neuronal extension has been determined in response to intracellular *co*-, *ortho*-planar 4-OH-2',3,3',4',5'-PCB-106 (vdWD: 0.752 nm) and extracellular 4-OH-2,3,3',4',5,5'-PCB-162 (vdWD: 0.767 nm) at high affinity binding concentration (10^{-11} to 10^{-12} M) [102] relative to the binding affinity of hydroxylated PCBs (K_D, 33–90 nM) for thyroid hormone receptor beta (TRβ) [103]. This favors an affinity concentration gradient between serum transthyretin (pre-albumin) and sulfated (Ch_3-SO4) PCBs (K_D, 20 nM) [104] for high affinity CM deiodinase exothermy antagonism (Do-1,2,3), in potential spatial association of, to a CM or RER receptor such as the ryanodine (RyR1/R2) with low binding affinity for *ortho*-polychlorinated biphenyls (ie PCB-95 and 4-OH-PCB-30), which is suggestive of an interrelationship between $\Delta\, C_{micro}$ contraction-expansion response and opening of the RyR-associated Mg^{2+} deactivated Ca^{2+} channel. In further support of the contraction-expansion mechanism as determined is a decrease in osteoblast cell width observed in the murine double D1/D2KO gene transgenic efficiency model, in which male mutants have been determined to have decreased appendicular bone volume with resultant increased stiffness and development of brittle bone disease [105], and agrees morphologically with the study determination of enhanced cellular contraction during deiodinase antagonism, however with an expansion response in WT cells. Additionally, sexually dimorphic axial and appendicular skeletal morphometric responses have been observed in offspring in response to dam PCB-180 exposure (7–10 d, acute, p.o.), in which 0.1 mm decreases in buccolingual molar spacing are noted in female pups, while the opposite trend is noted in male pups [106], which as per study determination is attributable to an estradiol (E_2)-opposed contraction response with resultant expansion at minima [E_2 expansion (e) + *co*-, *ortho*-planar PCB contraction-expansion (c/e)], and dihydroxytestosterone (Dht)-agonism contraction response with resultant expansion at maxima [Dht c/e + *co*-, *ortho*-planar PCB c/e], and 0.1 increased separation of molars in male pups.

It has been determined in a pituitary GH3 luciferase reporter cell model that a TRE reporter plasmid is activated only secondarily after CYP450 monooxygenase activation (*CYP1A1*), and presumably due to the formation of PCB hydroxylate metabolites [107]. Since in this study, it is shown that there is a minimal 0.5x-over fold increase in LUC activity over control due to applied PCB 6 mix with *co*-, *ortho*-planar PCBs (PCB-138, -153) as opposed to a 2.5x-over fold increase during T_3 application that the activation, this further supports the study mechanism of *z*, *x*-plane aligned TRE sequence-containing genes being activated by intracellular thyroxine-T_3 displaced from endogenous Dio1 enzyme due to OH-/Ch3(S)O_2-PCB in competition, and in the would be presence of TRβ. Furthermore, since the $\Delta\, C_{micro}$ contraction-expansion interface for the *co*-, *ortho*-planar PCB pathway is within the 0.140 (*Gft2ird1*) - 0.149 (*Cyp4a11*) P_{eff} interval, there is an inactivation of gene *TFF1* (pS2, P_{eff} 0.147) with applied *co*-, *ortho*-planar PCB-104 [108]. Thus, when paraquat, a weakly intracellularly-localizing endocytic agent with 1+ IS/SS 1+ ionicity at the lower limit of cationicity [109], results in a (+) $P_{eff}\,\Delta\, C_{micro}$ contraction-expansion response when it is applied in a PCB model (*co*-, or *ortho*-) [110], it potentiates a convergent oxidative stress pathway with gene re-activation.

P_{eff} grade of effect on delta-cell micro-compliance for regulation of gene transcription

Corticosteroids, sex steroids and the subset of inverse agonist ligands can be studied by overall structural *log* partition coefficient (P) · $vdWD^{-1}$ ratio (nm^{-1}), based on which probable steroid axis ligand-to-receptor interaction can be determined as mineralocorticoid/glucocorticoid (Ald, 1.23 –Dex, 1.92 nm^{-1}), estrogen/estrogen-related receptor (E_2, 4.73 –Des, 6.60 nm^{-1}), and

androgen (R1881, 3.16—Dht, 4.15 nm^{-1}), within which intracellular and extracellular bisphenols (Bpa -e, 0.727–0.744 nm; Bfap, 0.774 nm) classify as xenoestrogens based on overall structural partitioning parameters (Bpa, 5.14 –Bpaf, 6.17 nm^{-1}). The grade of P_{eff} duration for effect is then determined for the extracellular subset of small molecule hormone nuclear receptor ligands (Ch_4O nl $L_{external\ structure}/H_{polar\ group}$: 0.461, Dex– 1.31, Des) with molecular diameters within the 0.774 nm (Bpaf)– 0.873 nm (Dex) vdWD range with a minimum of di-polar hydroxylation hydrophilicity (- 2.10 nm^{-1}), which is on the basis of small molecule hormone and inverse agonist potential for disassociation over range of exposure concentration (K_d) and binding affinity over time ($t_{1/2}$) [111–115] as plotted independent variables for semi-exponential power-regression extrapolation of half-life at receptor of unknowns (R^2 = 0.955), and applied whole cell receptor density based on magnetic bead-enhanced amphometric detection or radioligand competition assay studies (B*max*; *n*) [115,116] for multiplicative *in silico* modeling of pressure regulatory grade of effect for gene expression in a mono-compliant cell type. The half-lives at receptor ($t_{1/2}$) for diethylstilbestrol (Des) at ERα is 663 min, and that for dihydrotestosterone (Dht) and methyltrienolone (R1881) at AR are within the 38–53 minutes (min) interval, as the K_d approximates 0.9–1.0 nM (see ref 118). The strata order for ligand · receptor grade of duration at P_{eff}, from positive with contraction-expansion response-to-negative, is 1.4215E + 04 [Cort · MR (GR)], 3.0270E + 04 [Ald · MR (GR)], 1.33383E + 05 [Dex ~ Corticosterone · GR (MR)], 1.79812E + 05 (Dht · AR), 2.47340E + 05 (R1881 · AR), 1.2E +06 (E_2 · ERα), 1.863745E + 06 (DES · ERα) adjusted for whole cell receptor count (Σ *min·count*), from positive to negative (Table 9).

Bisphenol AF with an inhibitory constant (IC_{50}) of 19 and 53 nM, as compared to 17β-estradiol (E_2) with an IC_{50} of 0.88 and 2.17 nM (ERα, Erβ), will be an inverse agonist in pharmacokinetic non-competition at trough E_2 levels, and result in a positive (+) Δ C_{micro} bisphenol AF effect at CM ERα/β with upward shift in the contraction-expansion and in non-activation of the *ESR2* gene (P_{eff} 0.136), however with maintained *ESR1* gene transcription at around P_{eff} 0.184 as is at a Δ C_{micro} P_{eff} 0.290 (see ref 128), as in LUC ERE reporter plasmid transfected Hela cells with pcDNA3.1 integrated *ESR1* and *ESR2* genes [117]. Thus, based on study determinations, the gene expression pattern for small molecule hormone receptor interaction between the 2.6 x 10^5 to 2.1 x 10^6 *min·count* range results in a negative Δ C_{micro} response and an initial downward shift in the contraction with unilateral expansion as compared to positive Δ C_{micro} response with contraction and bidirectional expansion, and irrespective of the specific steriod axis receptor class (ER, AR). Furthermore, it appears that an initial negative (-) Δ C_{micro} response within the 1.86 x 10^6 to 1.94 x 10^6 (IGF-II · IGF-IIR) *min·count* range is coupled to a positive Δ C_{micro} response, as Dht or R1881 · CM AR (1.79E + 05–2.45E + 05, + P_{eff}) results in the transcription of pro-proliferative genes [118,119], that is proposed to be by an initial (-) P_{eff} X then an (+) P_{eff} Y intermediate step coupled to resultant transcriptional activation of *MKI67* (P_{eff} 0.329) [Part I, not cited; **38**] (Table 9); thus, expression of a focal adhesion or endocytic component may be involved, which would apply to calvarial osteoblasts that overexpress the IGF-IIR/M6P receptor [120], and similarly to transformed cells with P_{eff} shift to IGF1R expression [121], and could result in altered cell phenotype such as mononucleated: multinucleated [5], or lineage commitment such as glial: non-glial during the pre: post exposure period without interaction [122].

Several further studies point in the direction of paradoxical responses to dexamethasone (Dex) treatment, as example of a biologic mimic that produces a parabolic peak grade of positive P_{eff} response and corticosterone surrogate, in which case observed divergent gene expression responses upon applied Dex are in dissimilar cell types [123], due to dose response and variant GR receptor affinity [124], or during the tuned activation of Dex responsive genes with GRE sequence sites in proximity to the TSS [125]. The magnitude of differential gene

expression response in cultured primary astrocyte and neurons to Dex stimulation is consistent with respective increases in duration at P_{eff} contraction-expansion phase gene expression in a less and more compliant cell type to the same agent (ie *PER1*, *FKBP5*; 5.3x) [123], in which case it appears that the difference in magnitude of differential gene expression achieved in-between cell types is unlikely attributable to ligand · receptor *min·count*, as astrocyte GR mRNA is 3x-overfold neuronal in which case only an apparent difference in $t_{1/2}$ at receptor exists; whereas, the same in the high affinity variant porcGR ($ala_{610}val$) transgenic model, in which an under-expression of *GCLC* (P_{eff} 0.477) and *PCK1* (P_{eff} 0.333), and overexpression of *FKBP5* (P_{eff} 0.342) follows a saturable dose-escalation differential gene expression pattern [124], and is attributable to an upward contraction-expansion shift in P_{eff} response with maintained range of ligand · receptor affinity. Moreover, the finding that there is repression of genes with Dex responsive intergenic sequences 10e4 to 10e5 kb of the transcription start site (TSS) [125], is consistent with ΔC_{micro} *z*, *x*-plane alignment of the majority of Dex responsive genes at P_{eff} for gene transcription, as 70% of GR (Dex/Cort)-responsive genes are unbound by GR, while the tuned transcriptional activation of genes with half-site GRE: half-TRE sequences within around 10e3 of the TSS within intronic promoter regions.

P_{eff} at duration intervals for endogenous steriod axis ligands

Based on study determinations, the grade of P_{eff} at duration results in positive P_{eff} contraction with negative P_{eff} expansion responses for endogenous ligands at cell membrane (CM) receptors that results in P_{eff} regulated maximal transcription of *NR3C2* (MR; P_{eff} 0.261) during the presence of either Cort · GR or Ald · MR at the promoter site P2 with basal transcription of the non-integrated plasmid being at 3x-fold [126, 127], of *NR3C1* (GR; P_{eff} 0.376) during the minimum presence of Cort · GR with ½ GRE site co-activators over 35 bases at a P site (ie -4559–4525) [128], and of constitutive transcriptional activation of *AR* (P_{eff} 0.376) by Dht (or Dhea) with binding partner SREBF1 or KLF [ie *PMCH*, P_{eff} 0.376; 85]. Furthermore, exogenous intracellularly-localizing ligands directly at nuclear receptors ERRγ and ERRα (Bpa), also result in increased P_{eff} intervals from the respective peri-nadir, for example to between < 0.146 (*GSTA1*; ERRγ/α · Bpa) > 0.135 (*ME1*) as compared to $P_{eff} \geq 0.168$ (*CEBPD*) in response to Dex/Cort (GR) and $P_{eff} \geq 0.156$ (*AR*) in response to Dht (AR), which results in the partial activation of *TIPARP* (P_{eff} 0.261) and *FKBP5* (P_{eff} 0.342) *in lieu* of overactivation by AhR and Dex/Corticosterone, respectively. In comparison, there is a decrease in the P_{eff} contraction interval to in-between 0.290 (*CCND1*) and 0.147 (*TTF1*) *esebssiwaago*T_Q units, these being nuclear ERα · $E_{1,\ 2\ or\ 3}$ transcriptionally-tuned genes during duration at P_{eff} with GR (JUN) recruitment to half-site GRE during ΔC_{micro} *FOXA1* (P_{eff} 0.384) co-activation within which P_{eff} at 0.290 (*CCND1*) remains transcribable at ΔC_{micro} (E_2; E_2 + Dex) [117, 129], and associated with a concomitant negative P_{eff} expansion ΔC_{micro} response with a decrease in P_{eff} interval to between P_{eff} 0.147 (*Tff1*) and 0.111 (*Cyp3a7*) (Table 10, Fig 3).

In the A549 lung carcinoma/HepG2 HCC cell model for AhR gene reporter plasmid expression [64], applied TGFβ1 results in activation of *z*, *x*-plane transcription-ready plasmid upon endogenous *TGIF1* transcription at P_{eff} 0.080 as the SMAD co-adapter is required for RNA polymerase transcription, however without the need for applied TGFβ1 in A549 cells that demonstrate a bidirectional negative expansion ΔC_{micro} response P_{eff} of 0.080 as compared the nadir for HepG2 cells, which would between P_{eff} 0.130 (*LGAL1*) and 0.106 (*UGT1A1*). The *in vitro* application of aldosterone (Ald) to SkBr3 mammary carcinoma and tumor-associated endothelial cells results in the transcriptional overactivation of *GPER1* (GPR30; P_{eff} 0.376) and *SLC9A1* (NHE-1, P_{eff} 0.167) [130], and will result in an increase in GR expression concomitantly (*NR3C1*, P_{eff} 0.376) (Table 10), with an increase in pEGFR/ERK1,2

levels as part of the negative C_{micro} expansion response phase, as will occur with application of a combination of E_2 and inverse agonist(s) [131] with a resultant equivalent increase in intracellular pressure to P_{eff} 0.112 at which *CYP11B2* (Ald Synthase) transcription increases at P_{eff} during Δ C_{micro} contraction; whereas, the *in vivo* application of Dex (~Corticosterone) to normal adrenocortical cells results in a 0.5x-fold decrease in *CYP11B1* (11-β-hydroxylase; P_{eff} 0.099) decrease at duration at P_{eff} while an increase with ACTH [132], while *GABPA* (P_{eff} 0.494) and *TSPAN14* (P_{eff} 0.057) increase in duration at P_{eff} during maintained sensitivity to Dex at CM GR in human B-cell ALL in a viro-transformed cell type [133], which reaffirms P_{eff} 0.057 as the maximum lower limit of the contraction-negative P_{eff} C_{micro} expansion response to positive P_{eff} regulation away from P_{eff} 0.088 (*Ighm*) [37], 0.088 (*Ighm*) and 0.075 (*Ighg3*) [134]. Since the maximum P_{eff} C_{micro} contraction-expansion response to Dex is at the lower limit of cell expansion P_{eff} and equivalent to the Δ C_{micro} response applied *co*-, *ortho*-planar PCB-153, this implies GRE and TRE site-tuned parallel pathway involvement (ie CAR, AR), as there is known GR · half-site GRE enhancement of *THRB* gene transcription [135] with the potential for JUN (FOS) recruitment of GR to half-site TRE [89] and regulation of *DIO1* (P_{eff} 0.236) gene transcription at P_{eff}.

Bisphenol A grade of P_{eff} at duration effect on gene transcription as a high affinity agonist for the Estrogen-Related Receptor (ERR)-PGC1α and NcoR1, NcoR2-TR pathway overactivation with contraction-expansion response

The biological effects of high affinity bisphenols with the potential for health effect at biological concentration exposure doses in comparison to non-specific concentration-dependent effects [136, 137], in the absence or presence of an extracellular high affinity ER inverse agonist with potentially-extended $t_{1/2}$ at receptor due to substituted external structure (ie ICI 182,780; $C_{32}H_{47}F_5O_3S$), for determination of ER ligand gene expression effects solely attributable to GPR30 receptor inverse agonism [138], as its mid-affinity nuclear/RER receptor intracellular pathway effect. It has been further determined that there exists the potential for sexually dimorphic-imprinted polymorphism for a subset of certain genes sensitive to residual BPA dose effect, for example in progeny of exposed murine dams and/or mates (ie F_0 –F_2) in a ~20 μg/kg per day subacute consumption study model [139].

Based on determination of gene expression Δ C_{micro} P_{eff} of bisphenol A-induced genes, it appears that low dose biologic exposure results in BPA mediated high affinity binding of ERRγ to PGC1α (P_{eff} 0.279), in parallel to binding of NcoR1/NcoR2 (TRα/β), with repression of *THRA*/*THRB* gene transcription but with an increase in TSH gene transcription at nM (10^{-9}) [140,141]. The putative recruitment to ERREs of highly-enriched target genes [49] such as *TIMM8B* at P_{eff} 0.247 is proposed, which is within Δ C_{micro} P_{eff} interval of convergence with bisphenol AF (BPAF) effects at CM ERα/β receptors and overactivation of apoptotic pathway gene *GADD45A* at P_{eff} 0.245. The transcriptional activation of the direct pathway limb, during which there is shown to be a dimorphic response on mRNA levels of *ESRRG* (P_{eff} 0.209) [142]. As per this mechanism, there is underactivation of BPA responsive genes begins at nM concentration and includes adiponectin (*ADIPOQ*) [143], which could would be due to deficit in PGC1α, as a binding partner for SREBF1 or PPARγ transcriptional activators at P_{eff}, and decreased NcoR1 and NcoR2 co-adapter activity at *PPARG* (P_{eff} 0.222) due to BPA-enhanced recruitment to TRβ-integrin β3 [141].

There is an increase in duration at P_{eff} for activation of genes within P_{eff} interval at 0.153 (*HMOX1*), 0.194–0.196 (*PLEKHG4* [139]; *ESRRA*, *FOSB*), 0.256 to 0.258 (*MEG3* [140], *FOS* [138]; *DFFA*), 0.264 to 0.267 (*FABP4*, aP2 [144]; *JUN*), and 0.345 to 0.349 (*DLK1*, Pref-1;

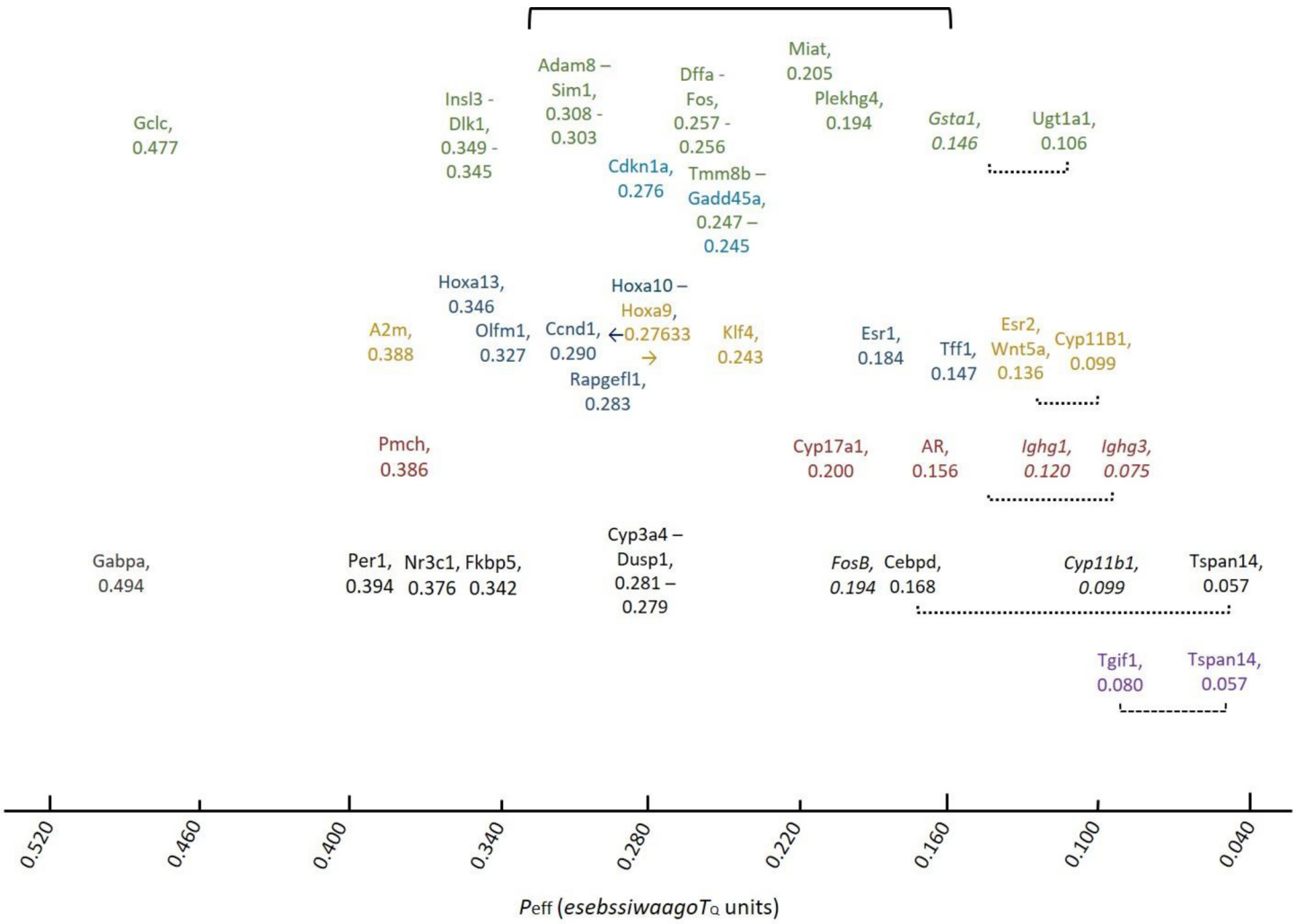

Fig 3. Directional alterations in cell micro-compliance by small molecule hormone ligands of steroid axis receptors and exposure-related bisphenol A and DES as high affinity inverse agonists. CORT/DEX pathway increases in duration at P_{eff} include at 0.394 (*Per1*; PC12 cell, A549 lung ca), 0.342 (*Fkbp5*; astrocyte, neuron), P_{eff} 0.281 (*Cyp3a4*)– 0.279 (*Dusp1*; PC12 cell, A549), P_{eff} 0.168 (*Cebpd*, A549 cell) and P_{eff} 0.057 (*Tspan14*, B-cell ALL) with decreases in P_{eff} duration at 0.376 (*Nr3c1*, GR; A549 lung ca), P_{eff} 0.194 (*FosB*, PV neuron) and P_{eff} 0.099 (*Cyp11b1*; adrenal cortex, nl). The CORT/DEX pathway Δ C_{micro} contraction-expansion response increase in the lower P_{eff} interval is 0.111 from the maximum expansion interval (punctate bracket). DHT pathway increases in duration at P_{eff} include at 0.386 (*Pmch*; neuroendocrine, hypothal), P_{eff} 0.200 (*Cyp17a1*, 17,20-lysase; Leydig) and 0.156 (*Ar*, PC cell) with decreases in P_{eff} duration at 0.120 (*Ighg1*; B-cell, nl) and P_{eff} 0.075 (*Ighg3*). The DHT pathway Δ C_{micro} contraction-expansion response increase in the lower P_{eff} interval is 0.067 from the maximum expansion interval (punctate bracket). BPA pathway increases in duration at P_{eff} include at 0.349 (*Insl3*, Leydig cell)– 0.345 (*Dlk1*, pre-adipocyte stromal cell), P_{eff} 0.308 (*Adam8*)– 0.303 (*Sim1*, whole brain), $P_{eff} \leq 0.258$ (*Meg3*)– *0.256* (*Fos*, spermatocyte), P_{eff} 0.205 (*Miat*) and P_{eff} 0.194 (*Plekhg4*) with a decrease in duration at P_{eff} at 0.146 (*Gsta1*). BPAF pathway increases in duration at P_{eff} include at 0.276 (*Cdkn1a*) and 0.245 (*Gadd45a*). The pathway C_{micro} contraction-expansion response increase in the lower P_{eff} interval is ≥ 0.040 from the maximum expansion interval (punctate bracket) for bisphenol A (BPA, intracellular) and bisphenol AF (BPAF, extracellular). DES pathway increases in duration at P_{eff} include at 0388 (*A2m*), 0.27633 (*Hoxa9*, uterine), 0.243 (*Klf4*) and 0.136 (*Wnt5a*, *Esr2*) with decreases in duration at P_{eff} 0.27630 (*Hoxa10*, uterine) and P_{eff} 0.332 (*Hoxa11*). The DES pathway upwards shift in C_{micro} contraction is to P_{eff} 0.1359–0.1361 (*Wnt5a*, *Esr2*) with response expansion to ~0.099 (*Cyp11b1*) [(+) upward shift Δ C_{micro} contraction with maxima expansion pathway] In comparison, Estradiol (E_2) pathway increases in duration at P_{eff} include at 0.290 (*Ccnd1*; MCF-7 cell), P_{eff} 0.147 (*Tff1*, pS2; MCF), with decreases in P_{eff} duration at 0.136 (*Esr2*, skeletocyte). The E_2 pathway results in downward shift C_{micro} contraction is a P_{eff} 0.14703 (*Tff1*) and a P_{eff} setpoint lower with minimal expansion [(-) downward shift Δ C_{micro} contraction with minima expansion pathway]. black text, dexamethasone (Dex)/corticosterone common GR receptor pathway; magenta brown text, dihydroxytestosterone (Dht) AR receptor pathway; blue text, estradiol (E_2) ER receptor pathway; green text, intracellular bisphenol inverse agonist pathway; teal text, extracellular bisphenol pathway; gold text, diethylstilbesterol (DES) ER receptor pathway; italics text, decreases in P_{eff} duration at activation or increases in repression duration at P_{eff} (2^{ndary}); solid black bracket, max contraction interval during increase in duration at P_{eff} (*co*-, *ortho*-planar PCB std); dotted brackets, lower P_{eff} expansion intervals; dashed brackets, lower limit range of P_{eff} expansion interval.

https://doi.org/10.1371/journal.pone.0236446.g003

INSL3 [136]), in addition to a decrease in duration at P_{eff} for deactivation of AR pathway genes, *PMCH* (P_{eff} 0.386) [139] and *CYP17A1* (steriod lysase, P_{eff} 0.200), which is rate-limiting,

as part of the indirect limb(s) of the high affinity BPA pathway, within which there is less of an increase in pCREB [145] during a delayed duration P_{eff} expansion as compared to with applied estradiol E_2 and minimal expansion (Table 10, Fig 3). The concurrent limbs of pathway for low-dose applied BPA for sub-acute duration exposure ($\geq$ 1–2 d) at octimolar concentration (10^{-8} M) include the *NRF1* de-activation/*NFE2L2* activation (*GCLC*, P_{eff} 0.477; *UGT1A1*, P_{eff} 0.106) with possible Jun (Fos)/AP-1 at half-site TRE repression of *GSTA1* (P_{eff} 0.146) as an additionally involved indirect limb of the intracellular pathway based on study determination, during which *HMOX1* (P_{eff} 0.153) is un-repressed and transcriptionally active at P_{eff} 5 to 25 μg/kg per day in a 1-month cummulative exposure to BPA male rodent model [146], while *GADD45B* (P_{eff} 0.332) is transcriptionally active at $\leq$ 5 μg/kg per day, which is agreement with secondary activation of the Nrf2 (Nrf1) limb at the 20 μg/kg per day subacute BPA exposure dose. Since *UGT1A1* is overexpressed at $P_{eff} \geq 0.10640$ at the positive pole in the *UGT1A7* (*UGT1A1-UGT1A6*) readthrough locus, this implies that the CAR/PXR minus LXRβ pathway is involved (hybrid co-pathway).

BFAP exposure and extracellular ligand · CM ERα/β pathway activation, also results in co-activation of common Nrf2 (Nrf1) limb pathway genes at P_{eff}, which include *CYP1A1* (P_{eff} 0.216) and *UTG1A1* (P_{eff} 0.106), while distinct genes activated at P_{eff} include *CDKNIA* (P_{eff} 0.276) and *GADD45A* (P_{eff} 0.245) [138], which are involved in cell cycle cessation and p53-mediated apoptosis, and activatable at a minimum concentration of 10^{-8} to 10^{-9} M concentration [117, 138]. Thus, the secondarily-activated AhR/Nrf2 (*NFE2L2*) limb co-dominates during saturation of the ERRγ (α) pathway-associated limbs, since there exists a contraction-expansion response with apparent upper and lower limits at P_{eff} 0.477 (*GCLC*) and 0.106 (*UGT1A1*) similar to the delta (Δ)-C_{micro} due to subacute *p*-dioxin/ exposure (13 wk). In further comparison, higher dose, lower affinity binding partner recruitment effect [PPARγ · BPA (PGC1α)] occurs at 70 μg/kg per day of subacute exposure [147,148]. Therefore, the overall effect of BPA on otherwise normal cells appears to be overactivation of ERR (PGC1α) and concurrent pathway limbs [Nrf2 (Nrf1)/AP-1] with resultant dysregulation of both stem cell progenitor (*DLK1*) and differentiated cell gene expression (*INSL3*; *CYP17A1*) in addition to apoptosis stage (*DFFA*), thus results in pre-mature cell fate determination and depleted stem cell population. Furthermore, since overactivation of the Nrf2 (Nrf1)/AP-1 limb results in BPA exposed cells, which are transiently apoptotic, there exists the potential for cell cycle progression to proliferation in neotransformed (SkBr3, GPER+/ERβ+) [149,150] and associated cells subject to 30-min short-term duration BPA exposure with ERRγ, GPR30 pathway activation in a high affinity, low affinity inverse agonist *in vitro* model [151]. The differences between the C_{micro} contraction-expansion responses of normal epithelial cells, and mammary carcinoma cells such as T47D (GPER+/ERα+/Erβ+) and SkBr3, to BPA are attributable to high affinity binding of endogenous estradiol (E_2) to ERα and GPR30 (K_d, 10^{-10}) [11, 112] delta (Δ)-C_{micro} downward shift in P_{eff} with resultant activation of additional anisotropic genes (*EGR1* P_{eff} 0.199; *CCN2*, CTGF P_{eff} 0.166 [22]) [150], inclusive of gene transcription at Δ C_{micro} P_{eff} 0.184, at which variant *ESR1* and *FLNA* co-express with potential for polymorphism [93, 152]. Therefore, it appears that the intermittent negative Δ C_{micro} response (E_2 expansion) in neotransformed cell types results in an intermediate (+) Δ C_{micro} step within the $P_{eff} > 0.235$ (*EMD* [22]) and < 0.256 interval that results in oscillatory progression into the G1/S cell cycle phase.

Diethylstilbestrol as a small molecule receptor ligand at cell membrane receptor due to positive contraction shift-expansion delta-micro cell compliance

Diethylstilbestrol is known to be toxic to reproductive axis cells along continuum of developmental teratogen to carcinogen over age based on subsequent follow-up of a prospective

cohort [153]. With local intraperitoneal (i.p.) exposure of dams for example, ERα-dependent homeobox cluster A (*HOXA_*) gene expression is dysregulated in the developing mullerian system [154], with resultant differential expression of single locus readthrough genes, reverse strand (-) *HoxA9* and *HoxA10* genes ($P_{eff} \geq 0.2763$) in uterine tissue cells, during which there is a decrease in *HoxA10* transcription, and an increase in *HoxA9* ($P_{eff\ (5\text{-digit adj})}$ 0.27633) with a decrease in oviductal expression of the same. Therefore, based on this study's findings, it appears that multiple promoter locus genes can be transcribed during (+) $\Delta\ C_{micro}$, and in a (+) to (-) P_{eff} gradient direction (5' to 3'), particularly at less sensitive C_{micro} intracellular pressure intervals inclusive of at around P_{eff} 0.267 (*Jun*) and 0.256 (*Fos*) (**Table 11**, **Fig 3**). Furthermore, during study of high dose cummulative p.o. DES effects on WT ERα$^{+/-}$ transgenic mice pups [155], similar uterine effects are noted for *HoxA10* and *HoxA11* (P_{eff} 0.332) in addition to differential expression of *Wnt5a* (P_{eff} 0.1359) as compared to autoregulatory genes *Wnt4* and *Wnt7a* in response [156]. Based on this study's findings on std marker gene expression cell micro-compliance P_{eff} considered together, DES exposure results in contraction shift to P_{eff} 0.136 due to a coupled-positive P_{eff} response (ie focal adhesion) due to the grade of DES at CM receptor interaction (1.863745E + 06 *min·count*) with a range of 0.388 (*A2M* [157])– 0.136 (*WNT5A*, *ESR2*), and contraction response expansion proposed to be to ~0.099 *esebssiwaago*T_Q units (*CYP11B1*), which is within the interval range for transformed cell types (Tcdd, *co*-planar PCB). In comparison, applied E_2 results in downward shift contraction to a P_{eff} of 0.147 (*TFF1*) and setpoint lower with minimal expansion, during an intra-locus shift in gene transcription from positive P_{eff} pole (*Hoxa10*) to negative (*Hoxa9*, P_{eff} 0.27633). There appears to be directional P_{eff}-mediated gene transcription due to the proximal intra-oviductal pressure potential, which appears to result from relatively increased in intracellular P_{eff} (decreased $\Delta\ C_{micro}$) compared to the distal ambient atmospheric pressure potential required for *HoxA13* gene expression (P_{eff} 0.346). Furthermore, P_{eff} at 0.256 (*FOS*) is an in-sensitive intracellular pressure, since transcription increases in case of both Bpa and Des exposures, while re-expression of stem cell required factor *Klf4* at P_{eff} 0.243, and *Wnt5A* or *Esr2* that are expressed at P_{eff} 0.136 could be considered markers for an increased early developmental risk of neotransformation, or temporally for delayed clear cell carcinoma risk in aged cells with acquired mutations over time.

Molecular philicity interval grades of increase for bioelimination of small molecule lipophiles as compared to grade of molecular philicity for molecular exclusion at the cell surface glycocalyx

CYP1A1 CYP450 monooxygenase hydroxylation of *p*-dioxin ($L_{ext.}\ H^{-1}$: 4.31) followed by UGT1A6/7 transferase glucuronidation of 8-OH-2,3,7-TriCDD ($L_{ext.}\ H^{-1}$: 1.91) to 2,3,7-TriCDD glucouronate ($L_{ext.}\ H^{-1}$: 0.419) in-between the philicity per polar group interval of 0.328 ($L_{ext.}\ H^{-1}$ Lactic acid) and 0.428 ($L_{ext.}\ H^{-1}$ 2,3-glycer-1-o1) results in hepatobiliary bioelimination [158], as an example of the primary mode of bioactivation metabolism and bioelimination clearance of polyhalogenates (PDBE, PCDD) in addition to PCBs, *co*-planar and *co*-, *ortho*-planar. This is in comparison to bioabsorption metabolism of smaller, less hydrophilic vdWD phthalates $\leq$ 0.81 nm [21] by esterase hydrolysis, which includes mono-*n*-butylphthalate (BP, 1-; vdWD: 0.724 nm; $L_{ext} \cdot H^{-1}$: 0.322) that are permeable across epidermis interepithelial junctional complexes [159], as opposed to di-*n*-butyl phthalate (DBP, vdWD: 0.797 nm; $L_{ext} \cdot H^{-1}$: 1.49) at the cusp for mono-/part-neutral small molecule permeation in absence of endocytosis-enhanced junctional permeability (ie GI barrier); whereas, the non-absorption of phthalate (2-, $L_{ext} \cdot H^{-1}$: 0.078; vdWD: 0.633 nm) upon skin esterase BP conversion is due to the hydrophilicity barrier to transepithelium absorption [21]. Furthermore, above the $L_{ext} \cdot H^{-1}$: interval ranges for binding affinity to CYP450 (1.91–4.31), glucoronosyltransferase (UGT,

1.73–2.69) and esterase (0.322–1.49) is the hydrophilicity binding affinity interval for binding affinity to *N*-acetyl-neuraminic acid (Neu5Ac; 0.790 nm, -9.37 nm^{-1}; $L_{int} \cdot H^{-1}$: 0.080) based on study determination (Fig 1), the upper limit of which is at a $L_{int} \cdot H^{-1}$ of 0.101 (saxitoxin ester amide; vdWD: 0.764 nm) with a lower limit of $L_{ext} \cdot H^{-1}$ around 0.092 (*m*-xylenediamine). Therefore, exogenous small molecule hydrophiles that stratify as such, stand to be toxins or toxicants with extended duration bioactivity due to a cell surface glycocalyx hydrophilicity barrier to clearance, with 1,2-diaminocyclohexane (vdWD: 0.622 nm; $L_{ext} \cdot H^{-1}$: 0.085, 0.171) being an example of an older epoxy part-resin known to cause type I hypersensitivity in painters [38, 160], which is could be an endocytic agent at a cell membrane (CM) receptor by caveolar mechanisms within the $L_{external} \cdot H^{-1}$: 0.085–0.171 interval, and during co-exposure to aliphatics. Based on findings, *m*-xylenediamine ($L_{ext} \cdot H_{polar\ group}^{-1}$: 0.092) · CM receptor aliphatic solvent co-exposure APC pathway activation in previously primed B-cells (IgE^+) will result in a type I contact hypersensitivity response [38] due to a synergistic ΔC_{micro} contraction-expansion response. Saxitoxin ester amide (STX) and tetradotoxin (TTX; $L_{int} \cdot H^{-1}$: 0.085–0.101) are puffer fish gland toxins that demonstrate nM affinity for sodium (Na^+) channel subunit V (Na_V) (unlabeled STX K_d = 2.1 nM) as channel blockers [161,162], application of which dissipates membrane potential, and the negative (-) ΔC_{micro} results in a pan-depression in gene transcription at an apparent P_{eff} with the lowest probability for a decrease in duration at P_{eff} for mitochondrial genes, *TFB2M* (P_{eff} 0.267; *JUN*) and *COX6C* (P_{eff} 0.211) [163], which is suggestive of additional compensatory molecular weight-maintained micro-compliance, and supported by the recent finding of limited gene overaction in *AHR* gene silenced cells [164].

α-tocopherol transfer protein (αTTP) binds reserved ligands α-tocopherol (tocotrienol; $L_{ext} \cdot H^{-1}$, 2.92; vdWD: 0.960) and 13'-hydroxy-α-tocopherol ($L_{ext} \cdot H^{-1}$, 1.73) for extended serum/half-life [165], and is a gene that can be transcriptionally-activated by LXRα/β [166] during overexpression of *SCD* (P_{eff} 0.282), while α-tocopherol as a ligand agonist of PxR [167] results in the overactivation of genes, *CYP3A4* (m*Cyp3a11*, P_{eff} 0.281) and *CYP3A5* (P_{eff} 0.157) in the proposed minus LXRβ/PPARα pathway, in addition to CAR pathway genes with co-recruitment (ie *CYP2B6*, P_{eff} 0.324). *co*-planar PCB exposure (ie OH-PCB-77, -126) results in significant over-fold expression of α-tocopherol responsive genes such as *CAT* (P_{eff} 0.220), and SOD to a lesser extent [168,169], during the concurrent activation of ERRα pathway (- P_{eff}) and biometabolism / bioactivation pathway genes (+ P_{eff}), which is indirectly indicative of α-tocopherol overutilization deficit during oxidative stress-mediated pathway activation as it has been shown to be in γ-TMT poor plants, and could be due to decreased αTTP protein levels. Since hepatobiliary neotransformation can result from applied *p*-dioxin (0.225, $\Delta C_{contraction}$; 0.293, $\Delta C_{expansion}$) > *co*-planar PCB (0.201, $\Delta C_{contraction}$; 0.3085, $\Delta C_{expansion}$), as compared to with *co*-, *ortho*-/*ortho*-planar PCB (0.165, $\Delta C_{contraction}$; 0.346, $\Delta C_{expansion}$) exposure, maintained α-tocopherol levels would be protective, as two in series $L_{ext} \cdot H^{-1}$ intervals are required to ready toxicants for glucounidation elimination ($L_{ext} \cdot H^{-1}$, 0.419–0.459). Furthermore, since cell coupled nucleus mechanics can be also be studied *in vitro*, by direct tension generation measurements (N/m; AFM), study of nuclear protein displacement (MSD) or chromatin condensation parameters (EED) [170], the application effects of such toxicants (ie PCB, bisphenol) on intracellular effective pressure are to be further confirmed in pluripotent stem cell populations in bioengineered systems [171], as the findings herein apply to differentiated cells that activate either of the three primary detoxification pathways in response, and de- or re-differentiate.

Conclusions

In silico modeling of molecular philicity by part structure reveals that a $L_{external\ structure} \cdot H_{polar\ group}^{-1}$ of ≥ 1.07 is the molecular structure lipophilicity limit for non-specific carrier-

mediated transmembrane diffusion through CM polarity-selective transport channels for small molecules with a vdWD < 0.758 (3-D ellipsoid, chiral) - 0.762 nm (2-D elliptical), the subset of halogenated vapors that initially perturb the inner MM categorize, for which vdWD is predictive of the required MAC for anesthetic potency. It also reveals that the $L \cdot H_{polar\ group}^{-1}$ interval range for the cell surface glycocalyx hydrophilicity barrier is between 0.101 (Saxitoxin, Stx; $L_{internal\ structure} \cdot H_{polar\ group}^{-1}$) and 0.092 (*m*-xylenediamine, $L_{external\ structure} \cdot H_{polar\ group}$). *In silico* modeling of ΔP_{eff} cell micro-compliance (C_{micro},) alterations in response to applied small molecule hormone ligands, biphenyls and bisphenols reveals that differential gene expression is a result of various grades of contraction-expansion response.

Subcellular or cell membrane Cyp-associated perturbation by non-endogenous molecules within a $L_{external\ structure} \cdot H_{polar\ group}^{-1}$ interval of 1.91–4.31 results in various grades of preferential transcriptional activation of either: i) the AhR (Erβ)/Nrf2 limb in addition to the Pparδ, ERRγ (LxRα), Dio3/Dio2 and TRα limbs with *p*-dioxin/metabolite (TCDD; OH-TCDD), in which increased duration at P_{eff} includes for *Ceacam1*, *Rarβ*, *Scd*, *Exoc7*, *Nrip1*, *Ncor2* and *Slc2a4*; ii) the AhR (Erα/β)/Nrf2 limb in addition to the Rev-Erbβ, ERRα, Dio3 and TRα limbs with OH-*co*-planar PCB as the toxicant in which increased duration at P_{eff} includes for *Ceacam1*, *Rarγ*, *Nrip1* and *Exoc7* with a ΔC_{micro} contraction of 0.89/ΔC_{micro} expansion of 1.05 as compared to *p*-dioxin; or iii) the Car/PxR limb in addition to the Rarγ, Pparα/γ (Srebf1, -LXRβ), Arnt (AhR-Erβ)/Ar, Dio1, Trβ limbs with OH-*co*-, *ortho*-planar PCB in which increased duration at P_{eff} includes for *Cyp2B6*, *Cyp3a5*, *Pgc1α*, *Ncor1*, *Ceacam5*, *Mafg* and *Scd5* with a ΔC_{micro} contraction of 0.73/ΔC_{micro} expansion of 1.18 consistent with trans-differentiation as compared to *p*-dioxin. Therefore, based on study determination of PCB exposure pathway limbs, the mechanism for toxicantity is via alterations in cell micro-compliance via *p*-dioxin/PCB metabolite Dio enzyme exothermy-antagonism (Δ contraction) coupled with T_4/rT_3-TRα or TRβ agonism and *Dio3/Dio2* or *Dio1* gene transcription (Δ expansion), which implies the intervals of altered cell compliance that result in increased risk for neotransformation (Tcdd, *co*-planar PCB; Des), or trans-differentiation (*co*-, *ortho*-planar PCB).

Bisphenol A, as small molecule ligand within a $L_{external\ struct} \cdot H_{polar\ group}^{-1}$ of 1.08–1.12 (BPA, BPE), results in direct transcriptional activation of the ERRγ-[intracellular bisphenol]-PGC1α pathway (*Timm8b*) with an expansion phase ΔC_{micro} of 0.040 (*Dffa*) and indirect activation of a DEX responsive hybrid AhR/Nrf-2, Car/Pxr co-limb pathway during a decrease in duration at P_{eff} at *Nrf1* gene transcription and consistent with cell de-differentiation. Since the Dht · AR ΔC_{micro} expansion phase is 0.067 with a grade of duration at P_{eff} (*min·count*) of 1.8–$2.53x10^5$ (Dht/R1881), sexually dimorphic differences result in gene transcription duration at P_{eff} with co-exposure (Dht, Bpa) due to an additive (+) ΔC_{micro} contraction-expansion phase, as compared to a coupled (+) ΔC_{micro} P_{eff} increase to 0.136 (*Wnt5a*, *Esr2*) with applied DES ($1.86x10^6$) as compared to estradiol E_2.

Based on study determinations of PCB and bisphenol actions in the biological system modeled *in silico* as mutually exclusive inverse ligands of endogenous small molecule hormone receptors or enzymes, the mechanism for toxicantity is via alterations in cell micro-compliance via *p*-dioxin, *co*-planar or *co*-, *ortho*-planar PCB metabolite liganded deiodinase enzyme exothermy-antagonism/liganded TRα or TRβ agonism. Furthermore, ΔC_{micro} *z*, *x*-plane alignment of genes with respect to intergene distance tropy results in differential gene activation, in which case non-aligned genes are inactive unless bound by a repressor at P_{eff} interaction. ΔC_{micro} results in *z*, *x*-plane alignment of genes with respect to intergene distance tropy and in differential gene activation, in which case non-aligned genes are inactive as are repressor-bound genes at P_{eff}. Study findings will be applicable to the field as it offers perspective on the basis for pressure regulated gene transcription by alterations in cell micro-compliance with maintenance of the effective pressure potential.

Author Contributions

Conceptualization: Hemant Sarin.

Data curation: Hemant Sarin.

Formal analysis: Hemant Sarin.

Funding acquisition: Hemant Sarin.

Investigation: Hemant Sarin.

Methodology: Hemant Sarin.

Supervision: Hemant Sarin.

Validation: Hemant Sarin.

Writing – original draft: Hemant Sarin.

Writing – review & editing: Hemant Sarin.

References

1. Beischlag T.V., Morales J.L., Hollingshead B.D., Perdew G.H. The Aryl Hydrocarbon Receptor Complex and the Control of Gene Expression. Crit Rev in Eukar Gene Expr, 2008; 18 (3): 207–50.
2. Miao W., Hu L., Scrivens P.J., Batist G. Transcriptional Regulation of NF-E2 p45-related Factor (NRF2) Expression by the Aryl Hydrocarbon Receptor-Xenobiotic Response Element Signaling Pathway: Direct Cross-talk between Phase I and II Drug-Metabolizing Enzymes. J Biol Chem, 2005; 280 (21), 20340–8. https://doi.org/10.1074/jbc.M412081200 PMID: 15790560
3. Ohtsuji M., Katsuoka F., Kobayashi A., Aburatani H., Hayes J.D., Yamamoto M. Nrf1 and Nrf2 Play Distinct Roles in Activation of Antioxidant Response Element-dependent Genes. J Biol Chem. 2008; 283 (48), 33554–62. https://doi.org/10.1074/jbc.M804597200 PMID: 18826952
4. Zhai Y., Wada T., Zhang B., Khadem S., Ren S., Kuruba R., et al. A functional cross-talk between liver X receptor-α and constitutive androstane receptor links lipogenesis and xenobiotic responses. Mol Pharm, 2010; 78 (4), 666–674.
5. Sarin H. Horizontal alignment of 5′ -> 3′ intergene distance segment tropy with respect to the gene as the conserved basis for DNA transcription. Future Sci OA, 2016; 3 (1), FSO160. https://doi.org/10.4155/fsoa-2016-0070 PMID: 28344824
6. Madak-Erdogan Z., Katzenellenbogen B.S. Aryl Hydrocarbon Receptor Modulation of Estrogen Receptor α-Mediated Gene Regulation by a Multimeric Chromatin Complex Involving the Two Receptors and the Coregulator RIP140. Toxicol Sci, 2011; 125 (2), 401–11. https://doi.org/10.1093/toxsci/kfr300 PMID: 22071320
7. Ahmed S., Valen E., Sandelin A. and Matthews J. Dioxin increases the interaction between aryl hydrocarbon receptor and estrogen receptor alpha at human promoters. Toxicol Sci, 2009; 111 (2), 254–266. https://doi.org/10.1093/toxsci/kfp144 PMID: 19574409
8. Klinge C.M. Estrogen receptor interaction with estrogen response elements. Nucl Acids Res, 2001; 29 (14), 2905–2919. https://doi.org/10.1093/nar/29.14.2905 PMID: 11452016
9. Alonso M., Goodwin C., Liao X., Ortiga-Carvalho T., Machado D.S., Wondisford F.E., et al. In vivo interaction of steroid receptor coactivator (SRC)-1 and the activation function-2 domain of the thyroid hormone receptor (TR) beta in TRbeta E457A knock-in and SRC-1 knockout mice. Endocrinol, 2009; 150 (8), 3927–34.
10. Okada H., Tokunaga T., Liu X., Takayanagi S., Matsushima A., Shimohigashi Y. Direct evidence revealing structural elements essential for the high binding ability of bisphenol A to human estrogen-related receptor-γ. Environ Health Perspect, 2008; 116 (1), 32–38. https://doi.org/10.1289/ehp.10587 PMID: 18197296
11. Prossnitz E.R., Arterburn J.B., and Larry A. Sklar, L.A. GPR30: a G protein-coupled receptor for estrogen. Mol Cell Endocrinol, 2007; 265– 266, 138–142.
12. Vandenberg LN, Chahoud I, Heindel JJ, Padmanabhan V, Paumgartten FJR, Schoenfelder G. Urinary, Circulating, and Tissue Biomonitoring Studies Indicate Widespread Exposure to Bisphenol A. Environ Health Perspect, 2010; 18 (8), 1055–70.

13. Berg MV, Birnbaum L, Bosveld AT, Brunström B, Cook P, Feeley M, et al. Toxic equivalency factors (TEFs) for PCBs, PCDDs, PCDFs for humans and wildlife. Environ Health Perspect, 1998; 106 (12), 775–92. https://doi.org/10.1289/ehp.98106775 PMID: 9831538

14. Kafafi SA, Afeefy HY, Ali AH, Said HK, Kafafi AG. Binding of polychlorinated biphenyls to the aryl hydrocarbon receptor. Environ Health Perspect, 1993; 101(5), 422–8. https://doi.org/10.1289/ehp.93101422 PMID: 8119253

15. Chu S, Covaci A, Jacobs W, Haraguchi K, Schepens P. Distribution of methyl sulfone metabolites of polychlorinated biphenyls and *p,p*-DDE in human tissues. Environ Health Perspect, 2003; 111(9), 1222–24. https://doi.org/10.1289/ehp.6141 PMID: 12842777

16. Sandala G.M., Sonne-Hansen C., Dietz R., Muir D.C., Valters K., Bennett E.R., et al. Letcher Hydroxylated and methyl sulfone PCB metabolites in adipose and whole blood of polar bear (Ursus maritimus) from East Greenland. Sci Total Environ, 2004; 331(1–3), 125–41. https://doi.org/10.1016/j.scitotenv.2003.03.001 PMID: 15325145

17. Yilmaz B., Sandal S., Chen C.H., Carpenter D.O. Effects of PCB 52 and PCB 77 on cell viability, [Ca(2+)](i) levels and membrane fluidity in mouse thymocytes. Toxicol, 2006; 217 (2–3), 184–93.

18. Agre P., Preston G.M., Smith B.L., Jung J.S., Raina S., Moon C., et al. Aquaporin CHIP: the archetypal molecular water channel. Am J Physiol—Renal Physiol, 1993; 265 (4 Pt 2), F463–476.

19. Ohgusu Y., Ohta K. Y., Ishii M., Katano T., Urano K., Watanabe J., et al: Functional characterization of human aquaporin 9 as a facilitative glycerol carrier. Drug Metab Pharmacokinet, 2008; 23 (4), 279–284. https://doi.org/10.2133/dmpk.23.279 PMID: 18762715

20. Tsukaguchi H., Shayakul C., Berger U. V., Mackenzie B., Devidas S., Guggino W. B., et al: Molecular Characterization of a Broad Selectivity Neutral Solute Channel. J Cell Biol, 1998; 273 (38), 24737–43.

21. Sarin H. Permeation thresholds for hydrophilic small biomolecules across microvascular and epithelial barriers are predictable on the basis of conserved biophysical properties. In Silico Pharmacol, 2015; 3 (5).

22. Sarin H. Anglemetry of neural axis cell differentiation genes by structural pressurotopy of DNA loop strand segment tropy in reference to tissue macro-compliance. Trans Med Comm, 2019; 4(19).

23. Fang Z., Ionescu P., Chortkoff B.S., Kandel L., Sonner J., Laster M.J., et al. Anesthetic potencies of *n*-alkanols: results of additivity and solubility studies suggest a mechanism of action similar to that for conventional inhaled anesthetics. Anesth Analg, 1997; 84(5), 1042–8. https://doi.org/10.1097/00000539-199705000-00017 PMID: 9141929

24. Rabovsky J., Judy D. J., Pailes W.H. *In vitro* effects of straight-chain alkanes (n-hexane through n-dodecane) on rat liver and lung cytochrome P-450. J Toxicol Environ Health, 1986; 18 (3), 409–421. https://doi.org/10.1080/15287398609530881 PMID: 3486981

25. Spracklin D. K., Hankins D. C., Fisher J. M., Thummel K. E., Kharasch E.D. Cytochrome P450 2E1 is the principal catalyst of human oxidative halothane metabolism *in vitro*. J Pharmacol Exp Ther, 1997; 281 (1), 400–411. PMID: 9103523

26. Staib-Lasarzik I., Kriege O., Timaru-Kast R., Pieter D., Werner C., Engelhard K., et al. Anesthesia for Euthanasia Influences mRNA Expression in Healthy Mice and after Traumatic Brain Injury. J of Neurotrauma, 2014; 31, 1664–1671.

27. Hoetzel A., Geiger S., Loop T., Welle A., Schmidt R., Humar M., et al. Differential Effects of Volatile Anesthetics on Hepatic Heme Oxygenase–1 Expression in the Rat. Anesthesiology, 2002; 97, 1318–21. https://doi.org/10.1097/00000542-200211000-00043 PMID: 12411824

28. Paugam-Burtz C., Molliex S., Lardeux B., Corinne Rolland T.A., Aubier M., Desmonts J-M. M.D, et al. Differential Effects of Halothane and Thiopental on Surfactant Protein C Messenger RNA In Vivo and In Vitro in Rats. Anesthesiology, 2000; 93, 805–10. https://doi.org/10.1097/00000542-200009000-00030 PMID: 10969314

29. Loop T., Dovi-Akue D., Frick M., Roessiein M., Egger L., Humar M., et al. Volatile anesthetics induce caspase-dependent, mitochondria-mediated apoptosis in human T lymphocytes in vitro. Anesthesiology, 2005; 102, 1147–57. https://doi.org/10.1097/00000542-200506000-00014 PMID: 15915027

30. LaBella F. S., Chen Q. M., Stein D., Queen G. The site of general anaesthesia and cytochrome P450 oxygenases: similarities defined by straight chain and cyclic alcohols. Br J Pharmacol, 1997; 120 (6), 1158–1164. https://doi.org/10.1038/sj.bjp.0701006 PMID: 9134230

31. Nakahiro M., Arakawa O., Nishimura T., Narahashi T. Potentiation of GABA-induced Cl- current by a series of n-alcohols disappears at a cutoff point of a longer-chain n-alcohol in rat dorsal root ganglion neurons. Neurosci Lett, 1996; 205 (2), 127–30. https://doi.org/10.1016/0304-3940(96)12397-1 PMID: 8907333

32. Machta B. B., Gray E., Nouri M., McCarthy N. L. C., Gray E. M., Miller A. L., et al. Conditions that stabilize membrane domains also antagonize n-alcohol anesthesia. Biophys J, 2016; 111 (3), 537–545. https://doi.org/10.1016/j.bpj.2016.06.039 PMID: 27508437

33. Mohr J. T., Gribble G. W., Lin S. S., Eckenhoff R. G., Cantor R.S. Anesthetic potency of two novel synthetic polyhydric alkanols longer than the n-alkanol cutoff: evidence for a bilayer-mediated mechanism of anesthesia? J Med Chem, 2005: 48 (12), 4172–4176. https://doi.org/10.1021/jm049459k PMID: 15943489

34. Ovando B. J., Ellison C. A., Vezina C. M., Olson J.R. Toxicogenomic analysis of exposure to TCDD, PCB126 and PCB153: identification of genomic biomarkers of exposure to AhR ligands. BMC Genomics, 2010; 11 (1), 583

35. Watson J.D., Prokopec S.D., Smith A.B., Okey A.B., Pohjanvirta R., Boutros P.C. TCDD dysregulation of 13 AHR-target genes in rat liver. Toxicology and Applied Pharmacology, 2014; 274(3), 445–54. https://doi.org/10.1016/j.taap.2013.12.004 PMID: 24355419

36. Hankinson O. The Aryl Hydrocarbon Receptor Complex. Annual Review of Pharmacology and Toxicology, 1995; 35 (1), 307–40.

37. North C.M., Kim B-S., Snyder N., Crawford R.B., Holsapple M.P., Kaminski N.E. TCDD-mediated suppression of the in vitro anti-sheep erythrocyte IgM antibody forming cell response is reversed by interferon-gamma. Toxicol Sci, 2009; 107 (1), 85–92. https://doi.org/10.1093/toxsci/kfn223 PMID: 18948302

38. Sarin H. B-cell antibody class switchings are pressuromodulated events: Part II, gene recombination. Trans Med Comms, 2018: 3 (1).

39. Beischlag T. V., Perdew G.H. ER alpha-AHR-ARNT protein-protein interactions mediate estradiol-dependent transrepression of dioxin-inducible gene transcription. J Biol Chem, 2005; 280 (22), 21607–11. https://doi.org/10.1074/jbc.C500090200 PMID: 15837795

40. Sugatani J. Function, genetic polymorphism, and transcriptional regulation of human UDP-glucuronosyltransferase (UGT) 1A1. Drug Metab Pharmacokinet, 2013; 28 (2), 83–92. https://doi.org/10.2133/dmpk.dmpk-12-rv-096 PMID: 23089802

41. Ellison-Zelski S.J., Solodin N.M., Alarid E.T. Repression of ESR1 through actions of estrogen receptor alpha and Sin3A at the proximal promoter. Mol Cell Biol, 2009; 29(18).

42. Levi L., Wang Z., Doud M. K., Hazen S. L., Noy N. Saturated fatty acids regulate retinoic acid signalling and suppress tumorigenesis by targeting fatty acid-binding protein 5. Nat Commun, 2015; 6, 8794. https://doi.org/10.1038/ncomms9794 PMID: 26592976

43. Harding H.P., Lazar M.A. The orphan receptor Rev-ErbA alpha activates transcription via a novel response element. Mol Cell Biol, 1993; 13 (5), 3113–3121. https://doi.org/10.1128/mcb.13.5.3113 PMID: 8474464

44. Miyazaki M., Dobrzyn A., Elias P.M., Ntambi J.M. Stearoyl-CoA desaturase-2 gene expression is required for lipid synthesis during early skin and liver development. Proc Natl Acad Sci USA, 2005; 102 (35), 12501–506. https://doi.org/10.1073/pnas.0503132102 PMID: 16118274

45. Stratmann M., Stadler F., Tamanini F., van der Horst G.T., Ripperger J.A. Flexible phase adjustment of circadian albumin D site-binding protein (DBP) gene expression by cryptochrome1. Genes Dev, 2010; 24 (12), 1317–28. https://doi.org/10.1101/gad.578810 PMID: 20551177

46. Bugge A., Feng D., Everett L.J., Briggs E.R., Mullican S.E. Wang F., et al. Rev-Erbα and Rev-erbβ coordinately protect the circadian clock and normal metabolic function. Genes Dev, 2012; 26, 657–67. https://doi.org/10.1101/gad.186858.112 PMID: 22474260

47. Dufour C. R., Wilson B. J., Huss J. M., Kelly D. P., Alaynick W. A., Downes M., et al. Genome-wide Orchestration of Cardiac Functions by the Orphan Nuclear Receptors ERRα and γ. Cell Metab, 2007; 5 (5), 345–356. https://doi.org/10.1016/j.cmet.2007.03.007 PMID: 17488637

48. Barkefors I., Fuchs P.F., Heldin J., Bergstro T., Forsberg-Nilsson K., Kreuger J. Exocyst complex component 3-like2 (EXOC3L2) associates with the Exocyst Complex and Mediates Directional Migration of Endothelial Cells. J Biol Chem, 2011; 286 (27), 24189–199. https://doi.org/10.1074/jbc.M110.212209 PMID: 21566143

49. Amano I., Miyazaki W., Iwasaki T., Shimokawa N., Koibuchi N. The effect of hydroxylated polychlorinated biphenyl (OH-PCB) on thyroid hormone receptor (TR)-mediated transcription through native-thyroid hormone response element (TRE). Ind Health, 2010; 48(1), 115–8. https://doi.org/10.2486/indhealth.48.115 PMID: 20160415

50. Chatonnet F., Guyot R., Picou F., Bondesson M., Flamant F. Genome-Wide Search Reveals the Existence of a Limited Number of Thyroid Hormone Receptor Alpha Target Genes in Cerebellar Neurons. Plos One, 2012; 7 (3), e30703.

51. Castet A, Herledan A, Bonnet S, Jalaguier Sp, Vanacker J-M, Cavaillès V. Receptor-Interacting Protein 140 Differentially Regulates Estrogen Receptor-Related Receptor Transactivation Depending on Target Genes. Mol Endocrinol. 2006; 20 (5), 1035–47. https://doi.org/10.1210/me.2005-0227 PMID: 16439465

52. Huss J. M., Kopp R. P., Kelly D. P. Peroxisome proliferator-activated receptor coactivator-1alpha (PGC-1alpha) coactivates the cardiac-enriched nuclear receptors estrogen-related receptor-alpha and -gamma. Identification of novel leucine-rich interaction motif within PGC-1alpha. J Biol Chem, 2002; 277(43), 40265–74. https://doi.org/10.1074/jbc.M206324200 PMID: 12181319

53. Petty K.J., Desvergne B., Mitsuhashi T., Nikodem V.M. Identification of a thyroid hormone response element in the malic enzyme gene. J Biol Chem, 1990; 265(13), 7395–400. PMID: 2332433

54. Spindler B. J., MacLeod K. M., Ring J., Baxter J. D. Thyroid hormone receptors. Binding characteristics and lack of hormonal dependency for nuclear localization. J Biol Chem, 1975; 250 (43), 4113–9.

55. Bianco A.C., Kim B.W. Deiodinases: implications of the local control of thyroid hormone action. J Clin Invest, 2006; 116(10), 2571–79. https://doi.org/10.1172/JCI29812 PMID: 17016550

56. Aluru N., Karchner S.I., and Glazer L., Early Life Exposure to Low Levels of AHR Agonist PCB126 (3,3',4,4',5-Pentachlorobiphenyl) Reprograms Gene Expression in Adult Brain. Toxicol Sci, 2017; 160 (2), 386–397. https://doi.org/10.1093/toxsci/kfx192 PMID: 28973690

57. Wang S., Crisman L., Miller J., Datta I., Gulbranson D.R., Tian Y., et al. Inducible Exoc7/Exo70 knockout reveals a critical role of the exocyst in insulin in insulin-regulated GLUT4 exocytosis. J Biol Chem, 2019; 294(52), 19988–19996. https://doi.org/10.1074/jbc.RA119.010821 PMID: 31740584

58. Wong-Riley M.T.T. Bigenomic regulation of cytochrome c oxidase in neurons and the tight coupling between neuronal activity and energy metabolism. Adv Exp Med Biol, 2012; 748, 283–304. https://doi.org/10.1007/978-1-4614-3573-0_12 PMID: 22729863

59. Salvatore P., Contursi C., Benvenuto G., Bruni C. B., Chiariotti L. Characterization and functional dissection of the galectin-1 gene promoter. FEBS Lett, 1995; 373(2), 159–63. https://doi.org/10.1016/0014-5793(95)01032-a PMID: 7589457

60. Hirose I., Kanda A., Noda K., Ishida S. Glucocorticoid receptor inhibits Muller glial galectin-1 expression via DUSP1-dependent and -independent deactivation of AP-1 signalling. J Cell Mol Med, 2019; 23(10), 6785–96. https://doi.org/10.1111/jcmm.14559 PMID: 31328390

61. Barca-Mayo O., Liao X-H, Alonso M., Di Cosmo C., Hernandez A., Refetoff S. et al. Thyroid hormone receptor α and regulation of type 3 deiodinase. Mol Endocrinol, 2011; 25(4), 575–583. https://doi.org/10.1210/me.2010-0213 PMID: 21292823

62. Villena JA, Hock MB, Chang WY, Barcas JE, Giguere V, Kralli A. Orphan nuclear receptor estrogen-related receptor alpha is essential for adaptive thermogenesis. Proc Natl Acad Sci USA, 2007; 104(4), 1418–23. https://doi.org/10.1073/pnas.0607696104 PMID: 17229846

63. Lin Y., Velmurugan B. K., Yeh Y., Tu C. C., Ho T., Lai T. Y., et al. Activation of estrogen receptors with E2 downregulates peroxisome proliferator-activated receptor γ in hepatocellular carcinoma. Oncology Reports, 2013; 30 (6), 3027–3031. https://doi.org/10.3892/or.2013.2793 PMID: 24126791

64. Wolff S., Harper P.A., Wong J.M., Mostert V., Wang Y., Abel J. Cell-specific regulation of human aryl hydrocarbon receptor expression by transforming growth factor-beta(1). Mol Pharmacol, 2001; 59(4), 718–24.

65. Shen M., Shi H. Estradiol and Estrogen Receptor Agonists Oppose Oncogenic Actions of Leptin in HepG2 Cells. PLoS One, 2016; 11(3), e0151455. https://doi.org/10.1371/journal.pone.0151455 PMID: 26982332

66. Faucette S.R. Sueyoshi T., Smith C.M., Negishi M., Lecluyse E.L., Wang H. Differential regulation of hepatic CYP2B6 and CYP3A4 genes by constitutive androstane receptor but not pregnane X receptor. J Pharmacol Exp Ther, 2006; 317 (3), 1200–9. https://doi.org/10.1124/jpet.105.098160 PMID: 16513849

67. Viswakarma N., Yu S., Naik S., Kashireddy P., Matsumoto K., Sarkar J., et al. Transcriptional regulation of Cidea, mitochondrial cell death-inducing DNA fragmentation factor alpha-like effector A, in mouse liver by peroxisome proliferator-activated receptor alpha and gamma. J Biol Chem, 2007; 282 (25), 18613–24. https://doi.org/10.1074/jbc.M701983200 PMID: 17462989

68. Cherkaoui-Malki M., Meyer K., Cao W.Q., Latruffe N., Yeldandi A.V., Rao M.S., et al. Identification of novel peroxisome proliferator-activated receptor alpha (PPARalpha) target genes in mouse liver using cDNA microarray analysis. Gene Expr, 2001; 9 (6), 291–304. https://doi.org/10.3727/000000001783992533 PMID: 11764000

69. Savas U., Machemer D.E., Hsu M.H., Gaynor P., Lasker J.M., Tukey R.H., et al. Opposing roles of peroxisome proliferator-activated receptor alpha and growth hormone in the regulation of CYP4A11 expression in a transgenic mouse model. J Biol Chem, 2009; 284 (24), 16541–52. https://doi.org/10.1074/jbc.M902074200 PMID: 19366684

70. Smathers R.L., Petersen D.R. The human fatty acid-binding protein family: Evolutionary divergences and functions. Human Genomics, 2011; 5 (3), 170–91. https://doi.org/10.1186/1479-7364-5-3-170 PMID: 21504868

71. Fernandez-Alvarez A., Alvarez M-S., Gonzalez R., Cucarella C., Muntane J., Casado M. Human SREBP1c expression in liver is directly regulated by peroxisome proliferator-activated receptor α (PPARα). J of Biol Chem, 2011; 286 (24), 21466–477.

72. Lo R., Matthews J. High-Resolution Genome-wide Mapping of AHR and ARNT Binding Sites by ChIP-Seq. Toxicol Sci, 2012; 130 (2), 349–361. https://doi.org/10.1093/toxsci/kfs253 PMID: 22903824

73. Patel R.D., Hollingshead B.D., Omiecinski C.J., Perdew G.H. Aryl-hydrocarbon receptor activation regulates constitutive androstane receptor levels in murine and human liver. Hepatology, 2007; 46 (1), 209–18. https://doi.org/10.1002/hep.21671 PMID: 17596880

74. Tomita S., Sinal C.J., Yim S.H., Gonzalez F.J. Conditional disruption of the aryl hydrocarbon receptor nuclear translocator (Arnt) gene leads to loss of target gene induction by the aryl hydrocarbon receptor and hypoxia-inducible factor 1alpha. Mol Endocrinol, 2000: 14(10), 1674–81. https://doi.org/10.1210/mend.14.10.0533 PMID: 11043581

75. Yoshinari K., Yoda N., Toriyabe T., Yamazoe Y. Constitutive androstane receptor transcriptionally activates human CYP1A1 and CYP1A2 genes through a common regulatory element in the 5'-flanking region. Biochem Pharmacol, 2010; 79 (2), 261–9. https://doi.org/10.1016/j.bcp.2009.08.008 PMID: 19682433

76. Shiraki T., Sakai N., Kanaya E., Jingami H. Activation of orphan nuclear constitutive androstane receptor requires subnuclear targeting by peroxisome proliferator-activated receptor gamma coactivator-1 alpha. A possible link between xenobiotic response and nutritional state. J Biol Chem, 2003; 278 (13), 11344–50. https://doi.org/10.1074/jbc.M212859200 PMID: 12551939

77. Astapova I., Hollenberg A.N. The in vivo role of nuclear receptor corepressors in thyroid hormone action. Biochim Biophys Acta, 2013; 1830 (7), 3876–881. https://doi.org/10.1016/j.bbagen.2012.07.001 PMID: 22801336

78. Keeney D.S., Skinner C., Travers J.B., Capdevila J.H., Nanney L.B., King L.E., et al. Differentiating Keratinocytes Express a Novel Cytochrome P450 Enzyme, CYP2B19, Having Arachidonate Monooxygenase Activity. J Biol Chem, 1998; 273 (48), 32071–9. https://doi.org/10.1074/jbc.273.48.32071 PMID: 9822682

79. Zhou Z.., Hotchkissa S.A., Boobis A., Edwards R.J. et al. Expression of P450 enzymes in rat whole skin and cultured epidermal keratinocytes. Biochem Biophys Res Comm, 2002; 207 (1), 65–70.

80. Baron J.M., Holler D., Schiffer R., Frankenberg S., Neis M., Merk H. F., et al. Expression of multiple cytochrome p450 enzymes and multidrug resistance-associated transport proteins in human skin keratinocytes. J Invest Dermatol, 2001; 116(4), 541–8. https://doi.org/10.1046/j.1523-1747.2001.01298.x PMID: 11286621

81. Burk O., Koch I., Raucy J., Hustert E., Eichelbaum M., Brockmoller J., et al.The induction of cytochrome P450 3A5 (CYP3A5) in the human liver and intestine is mediated by the xenobiotic sensors pregnane X receptor (PXR) and constitutively activated receptor (CAR). J Biol Chem, 2004; 279 (37), 38379–85. https://doi.org/10.1074/jbc.M404949200 PMID: 15252010

82. Pavek P. Pregnane X Receptor (PXR)-Mediated Gene Repression and Cross-Talk of PXR with Other Nuclear Receptors via Coactivator Interactions. Front Pharmacol, 2016; 7 (456).

83. Smith S.A., Colley H.E., Sharma P., Slowik K.M., Sison-Young R., Sneddon A., et al. Expression and enzyme activity of cytochrome P450 enzymes CYP3A4 and CYP3A5 in human skin and tissue-engineered skin equivalents. Experimental dermatology, 2018; 27 (5), 473–5. https://doi.org/10.1111/exd.13483 PMID: 29227563

84. Leahy P., Crawford D.R., Grossman G., Gronostajski R.M., Hanson R.W. CREB Binding Protein Coordinates the Function of Multiple Transcription Factors Including Nuclear Factor I to Regulate Phosphoenolpyruvate Carboxykinase (GTP) Gene Transcription. J Biol Chem, 1999; 274 (13), 8813–22. https://doi.org/10.1074/jbc.274.13.8813 PMID: 10085123

85. Bolton E.C., So A.Y., Chaivorapol C., Haqq C.M., Li H., Yamamoto K.R. Cell- and gene-specific regulation of primary target genes by the androgen receptor. Genes Dev, 2007; 21 (16), 2005–17. https://doi.org/10.1101/gad.1564207 PMID: 17699749

86. Wilson S., Qi J., Filipp F.V. Refinement of the androgen response element based on ChIP-Seq in androgen-insensitive and androgen-responsive prostate cancer cell lines. Sci Rep, 2016; 6, 32611. https://doi.org/10.1038/srep32611 PMID: 27623747

87. Magee J.A., Chang L.W., Stormo G.D., Milbrandt J. Direct, androgen receptor-mediated regulation of the FKBP5 gene via a distal enhancer element. Endocrinol, 2006; 147 (1), 590–8.

88. Jakobs T.C., Schmutzler C., Meissner J., Kohrle J. The promoter of the human type I 5'-deiodinase gene—mapping of the transcription start site and identification of a DR+4 thyroid-hormone-responsive element. Euro J Biochem, 1997; 247 (1), 288–97.

89. Tagami T., Madison L.D., Nagaya T., Jameson J.L. Nuclear receptor corepressors activate rather than suppress basal transcription of genes that are negatively regulated by thyroid hormone. Mol Cell Biol, 1997; 17 (5), 2642–8. https://doi.org/10.1128/mcb.17.5.2642 PMID: 9111334

90. Katz D., Lazar M.A. Dominant negative activity of an endogenous thyroid hormone receptor variant (alpha 2) is due to competition for binding sites on target genes. J Biol Chem, 1993; 268 (28), 20904–10. PMID: 8407924

91. Jeon Y.J., You k, E S., Lee S.H., Suh J., Na Y.J., Kim H.M. Polychlorinated biphenyl-induced apoptosis of murine spleen cells is aryl hydrocarbon receptor independent but caspases dependent. Toxicol Appl Pharmacol, 2002; 181 (2), 69–78. https://doi.org/10.1006/taap.2002.9389 PMID: 12051990

92. Lesiak A., Zhu M., Chen H., Appleyard S.M., Impey S., Lein P.J., et al. The environmental neurotoxicant PCB 95 promotes synaptogenesis via ryanodine receptor-dependent miR132 upregulation. J Neurosci, 2014; 34 (3), 717–725. https://doi.org/10.1523/JNEUROSCI.2884-13.2014 PMID: 24431430

93. Kania-Korwel I., Lukasiewicz T., Barnhart C.D., Stamou M., Chung H., Kelly K.M., et al. Congener-specific disposition of chiral polychlorinated biphenyls in lactating mice and their offspring: Implications for PCB developmental neurotoxicity. Toxicol Sci, 2017; 158 (1), 101–115.

94. Sheedy C., Mooney C., Jimenez-Mateos E., Sanz-Rodriquez A, Langa E., Mooney C., et al. De-repression of myelin-regulating gene expression after status epilepticus in mice lacking the C/EBP homologous protein CHOP. Int J Physiol Pharmacol, 2014; 6 (4), 186–198.

95. Thornton M., Taylor A.H., Mulligan K., Al-Azzawi F., Lyon C.C., O'Driscoll J., et al. The Distribution of Estrogen Receptor β Is Distinct to That of Estrogen Receptor α and the Androgen Receptor in Human Skin and the Pilosebaceous Unit. J Invest Dermatol, 2003; 8 (1), 100–103.

96. Zouboulis C.C. Sebaceous gland receptors. Dermato-endocrinol, 2009; 1 (2), 77–80.

97. Soechitram S.D., Berghuis S.A., Visser T.J., Sauer P.J.J. Polychlorinated biphenyl exposure and deiodinase activity in young infants. Sci Total Environ, 2017; 574, 1117–1124. https://doi.org/10.1016/j.scitotenv.2016.09.098 PMID: 27710904

98. Berghuis S.A., Soechitram S., Sauer P.J., Bos A.F. Prenatal exposure to polychlorinated biphenyls and their hydroxylated metabolites is associated with neurological functioning in 3-month-old infants. Toxicol Sci, 2014; 142 (2), 455–62. https://doi.org/10.1093/toxsci/kfu196 PMID: 25246668

99. Chevrier J., Harley K.G., Bradman A., Gharbi M., Sjödin A., Eskenazi B. Polybrominated diphenyl ether (PBDE) flame retardants and thyroid hormone during pregnancy. Environ Health Perspect, 2010; 118 (10), 1444–49. https://doi.org/10.1289/ehp.1001905 PMID: 20562054

100. Tabuchi M., Veldhoen N., Dangerfield N., Jeffries S., Helbing C.C., Ross P.S. PCB-related alteration of thyroid hormones and thyroid hormone receptor gene expression in free-ranging harbor seals (Phoca vitulina). Environ Health Perspect. 2006; 114 (7):1024–31. https://doi.org/10.1289/ehp.8661 PMID: 16835054

101. Vos J.G, Strik J.J., van Holsteyn C.W., Pennings J.H. Polychlorinated biphenyls as inducers of hepatic porphyria in Japanese quail, with special reference to δ-aminolevulinic acid synthetase activity, fluorescence, and residues in the liver. Toxicol and Applied Pharmacol, 1971; 20 (2), 232–40.

102. Kimura-Kuroda J., Nagata I., Kuroda Y. Hydroxylated metabolites of polychlorinated biphenyls inhibit thyroid-hormone-dependent extension of cerebellar Purkinje cell dendrites. Dev Brain Res, 2005; 154 (2), 259–263.

103. Cheek A. O., Kow K., Chen J., McLachlan J. A. Potential mechanisms of thyroid disruption in humans: interaction of organochlorine compounds with thyroid receptor, transthyretin, and thyroid-binding globulin. Environ Health Perspect, 1999; 107 (4), 273–278. https://doi.org/10.1289/ehp.99107273 PMID: 10090705

104. Grimm F. A., Lehmler H.-J., He X., Robertson L.W., & Duffel M. W. Sulfated metabolites of polychlorinated Biphenyls are high-affinity ligands for the thyroid hormone transport protein transthyretin. Environ Health Perspect, 2013; 121 (6), 657–662. https://doi.org/10.1289/ehp.1206198 PMID: 23584369

105. Bassett J.H., Boyde A., Howell P.G., Bassett R.H., Galliford T.M., Archanco M., et al. Optimal bone strength and mineralization requires the type 2 iodothyronine deiodinase in osteoblasts. Proc Natl Acad Sci USA, 2010; 107 (16), 7604–9. https://doi.org/10.1073/pnas.0911346107 PMID: 20368437

106. Romero A.N., Herlin M., Finnila M., Korkalainen M., Hakansson H., Viluksela M., et al. Skeletal and dental effects on rats following in utero/lactational exposure to the non-dioxin-like polychlorinated biphenyl PCB 180. PLoS One, 2017; 12 (9), e0185241. https://doi.org/10.1371/journal.pone.0185241 PMID: 28957439

107. Gauger K.J., Giera S., Sharlin D.S., Bansal R., Iannacone E., Zoeller R.T. Polychlorinated biphenyls 105 and 118 form thyroid hormone receptor agonists after cytochrome P4501A1 activation in rat pituitary GH3 cells. Environ Health Perspect, 2007; 115 (11): 1623–30. https://doi.org/10.1289/ehp.10328 PMID: 18007995

108. Matthews J., et al., Co-planar 3,3',4,4',5-pentachlorinated biphenyl and non-co-planar 2,2',4,6,6'-pentachlorinated biphenyl differentially induce recruitment of oestrogen receptor alpha to aryl hydrocarbon receptor target genes. Biochem J, 2007; 406(2): p. 343–53. https://doi.org/10.1042/BJ20070585 PMID: 17511620

109. Sarin H. Conserved molecular mechanisms underlying the effects of small molecule xenobiotic chemotherapeutics on cells. Mol Clinical Oncol, 2016; 4: 326–368, 2016.

110. De S., Ghosh S., Chatterjee R., Chen Y.Q., Moses L., Kesari A., et al. PCB congener specific oxidative stress response by microarray analysis using human liver cell line. Environ Int, 2010; 36 (8), 907–17. https://doi.org/10.1016/j.envint.2010.05.011 PMID: 20638727

111. Hellal-Levy C., Couette B., Fagart J., Souque A., Gomez-Sanchez C., Rafestin-Oblin M. Specific hydroxylations determine selective corticosteroid recognition by human glucocorticoid and mineralocorticoid receptors. FEBS Lett, 1999: 464 (1–2), 9–13. https://doi.org/10.1016/s0014-5793(99)01667-1 PMID: 10611474

112. Loomis A. K., Thomas P. Binding Characteristics of Estrogen Receptor (ER) in Atlantic Croaker (Micropogonias undulatus) Testis: Different Affinity for Estrogens and Xenobiotics from that of Hepatic ER. Biol Reprod, 1999; 61 (1), 51–60. https://doi.org/10.1095/biolreprod61.1.51 PMID: 10377031

113. Eil C., Lippman M.E., Loriaux L.D. A dispersed-whole cell method for the determination of androgen receptors in human skin fibroblasts. Steroids, 1980; 35 (4), 389–404. https://doi.org/10.1016/0039-128x(80)90140-3 PMID: 7376228

114. Eil C., Gamblin G.T., Hodge J.W., Clark R.V., Sherins R.J. Whole cell and nuclear androgen uptake in skin fibroblasts from infertile men. J Androl, 1985; 6 (6), 365–71. https://doi.org/10.1002/j.1939-4640.1985.tb03295.x PMID: 3935634

115. Armanini D., Endres S., Kuhnle U., Weber P.C. Parallel determination of mineralocorticoid and glucocorticoid receptors in T- and B-lymphocytes of human spleen. Acta Endocrinol (Copenh), 1988; 118 (4), 479–482.

116. Eletxigerra U., Martinez-Perdiguero J., Merino S., Barderas R., Ruiz-Valdepeñas Montiel V., Villalonga R., et al. Estrogen receptor α determination in serum, cell lysates and breast cancer cells using an amperometric magnetoimmunosensing platform. Sens Biosensing Res, 2016; 7, 71–76.

117. Matsushima A., Liu X., Okada H., Shimohigashi M., Shimohigashi Y. Bisphenol AF is a full agonist for the estrogen receptor ERα but a highly specific antagonist for ERβ. Environ Health Perspect,2010; 118 (9), 1267–1272. https://doi.org/10.1289/ehp.0901819 PMID: 20427257

118. Zwergel T., Kakirman H., Rohde V., Wullich B., Unteregger G. Androgen receptor expression, proliferation index and aneuploidy in tissue explant cultures derived prostate carcinoma cells co-cultivated on membranes. Eur Urol, 1998; 33 (4): 414–23. https://doi.org/10.1159/000019628 PMID: 9612688

119. Dykstra K.D., Payne A.M., Abdelrahim M., Francis G.L. Insulin-like growth factor 1, but not growth hormone, has in vitro proliferative effects on neonatal foreskin fibroblasts without affecting 5-alpha-reductase or androgen receptor activity. J Androl, 1993; 14(2):73–8. PMID: 8514622

120. Martinez D.A., Zuscik M.J., Ishibe M., Rosier R.N., Romano P.R., Cushing J.E., et al. Identification of functional insulin-like growth factor-II/mannose-6-phosphate receptors in isolated bone cells. J Cell Biochem, 1995; 59 (2), 246–57. https://doi.org/10.1002/jcb.240590213 PMID: 8904318

121. Merrill M.J., Edwards N.A. Insulin-like growth factor-I receptors in human glial tumors. J Clin Endocrinol Metab, 1990; 71 (1), 199–209. https://doi.org/10.1210/jcem-71-1-199 PMID: 2164527

122. Muckom R, McFarland S, Yang C, Perea B, Gentes M, Murugappan A, et al. High-throughput combinatorial screening reveals interactions between signaling molecules that regulate adult neural stem cell fate. Biotechnol Bioengin, 2019; 116 (1), 193–205.

123. Piechota M., Korostynski M., Golda S., Ficek J., Jantas D., Barbara Z., et al. Transcriptional signatures of steroid hormones in the striatal neurons and astrocytes. BMC Neurosci, 2017; 18 (1), 32. https://doi.org/10.1186/s12868-017-0351-6 PMID: 28288585

124. Murani E., Trakooljul N., Hadlich F., Ponsuksili S., Wimmers K. Transcriptome Responses to Dexamethasone Depending on Dose and Glucocorticoid Receptor Sensitivity in the Liver. Front Genet, 2019; 10 (559).

125. Reddy T.E., Pauli F., Sprouse R.O., Neff N.F., Newberry K.M., Garabedian M.J., et al. Genomic determination of the glucocorticoid response reveals unexpected mechanisms of gene regulation. Genome Res, 2009; 19 (12), 2163–71. https://doi.org/10.1101/gr.097022.109 PMID: 19801529

126. Zennaro M.C., Le Menuet D., Lombes M. Characterization of the human mineralocorticoid receptor gene 5'-regulatory region: evidence for differential hormonal regulation of two alternative promoters via nonclassical mechanisms. Mol Endocrinol, 1996; 10 (12), 1549–60. https://doi.org/10.1210/mend.10.12.8961265 PMID: 8961265

127. Viengchareun S., Le Menuet D., Martinerie L., Munier M., Tallec L.P.-L., Lombès M. The Mineralocorticoid Receptor: Insights into its Molecular and (Patho)Physiological Biology. Nucl Recept Signal, 2007; 5, e012. https://doi.org/10.1621/nrs.05012 PMID: 18174920

128. Chuan-Dong G., Schwartz J.R., Vedeckis W.V. A Conserved Molecular Mechanism Is Responsible for the Auto-Up-Regulation of Glucocorticoid Receptor Gene Promoters. Mol Endocrinol, 2008; 22 (12), 2624–42. https://doi.org/10.1210/me.2008-0157 PMID: 18945813

129. Karmakar S., Jin Y., Nagaich A.K. Interaction of glucocorticoid receptor (GR) with estrogen receptor (ER) alpha and activator protein 1 (AP1) in dexamethasone-mediated interference of ERalpha activity. J of Biol Chem, 2013; 288 (33), 24020–34.

130. Rigiracciolo D.C., Scarpelli A., Lappano R., Pisano A., Santolla M.F., Avino S., et al. GPER is involved in the stimulatory effects of aldosterone in breast cancer cells and breast tumor-derived endothelial cells. Oncotarget, 2016; 7 (1), 94–111. https://doi.org/10.18632/oncotarget.6475 PMID: 26646587

131. Caroccia B., Seccia T.M., Campos A.G., Gioco F., Kuppusamy M., Ceolotto G., et al. GPER-1 and estrogen receptor-beta ligands modulate aldosterone synthesis. Endocrinol, 2014; 155 (11): 4296–304.

132. Ye P., Kenyon C.J., Mackenzie S.M., Nichol K., Seckl J.R., Fraser R., et al. Effects of ACTH, dexamethasone, and adrenalectomy on 11beta-hydroxylase (CYP11B1) and aldosterone synthase (CYP11B2) gene expression in the rat central nervous system. J Endocrinol, 2008; 196 (2), 305–11. https://doi.org/10.1677/JOE-07-0439 PMID: 18252953

133. Poulard C., Kim H.N., Fang M., Kruth K., Gagnieux C., Gerke D.S., et al. Relapse-associated AURKB blunts the glucocorticoid sensitivity of B cell acute lymphoblastic leukemia. Proc Natl Acad Sci USA, 2019; 116 (8), 3052–61. https://doi.org/10.1073/pnas.1816254116 PMID: 30733284

134. Altuwaijri S., Chuang K.H., Lai K.P., Lai J.J., Lin H.Y., Young F.M., et al. Susceptibility to autoimmunity and B cell resistance to apoptosis in mice lacking androgen receptor in B cells. Mol Endocrinol, 2009; 23 (4), 444–53. https://doi.org/10.1210/me.2008-0106 PMID: 19164450

135. Montesinos MM, Pellizas CG, Velez ML, Susperreguy S, Masini-Repiso AM, Coleoni AH. Thyroid hormone receptor beta1 gene expression is increased by Dexamethasone at transcriptional level in rat liver. Life Sci, 2006; 78 (22): 2584–94. https://doi.org/10.1016/j.lfs.2005.10.019 PMID: 16330054

136. Desdoits-Lethimonier C., Lesne L., Gaudriault P., Zalko D., Antignac J.P., Deceuninck Y., et al. Parallel assessment of the effects of bisphenol A and several of its analogs on the adult human testis. Human Reprod (Oxford, Eng), 2017; 32 (7), 1465–73.

137. Hercog K., Maisanaba S., Filipic M., Sollner-Dolenc M., Kac L., Zegura B. Genotoxic activity of bisphenol A and its analogues bisphenol S, bisphenol F and bisphenol AF and their mixtures in human hepatocellular carcinoma (HepG2) cells. Sci Total Environ, 2019; 687, 267–76. https://doi.org/10.1016/j.scitotenv.2019.05.486 PMID: 31207516

138. Wang C., Zhang J., Li Q., Zhang T., Deng Z., Lian J., et al. Low concentration of BPA induces mice spermatocytes apoptosis via GPR30. Oncotarget. 2017; 8 (30), 49005–15. https://doi.org/10.18632/oncotarget.16923 PMID: 28446726

139. Drobna Z., Henriksen A.D., Wolstenholme J.T., Montiel C., Lambeth P.S., Shang S., et al. Transgenerational Effects of Bisphenol A on Gene Expression and DNA Methylation of Imprinted Genes in Brain. Endocrinol, 2018; 159 (1), 132–144.

140. Moriyama K., Tagami T., Akamizu T., Usui T., Saijo M., Kanamoto N., et al. Thyroid hormone action is disrupted by bisphenol A as an antagonist. J of Clin Endocrin Metabol, 2002; 87 (11), 5185–90.

141. Sheng Z.G., Tang Y., Liu Y.X., Yuan Y., Zhao B.Q., Chao X.J., et al. Low concentrations of bisphenol a suppress thyroid hormone receptor transcription through a nongenomic mechanism. Toxicol Appl Pharmacol, 2012; 259 (1), 133–42. https://doi.org/10.1016/j.taap.2011.12.018 PMID: 22227104

142. Kundakovic M., Gudsnuk K., Franks B., Madrid J., Miller R.L., Perera F.P., et al. Sex-specific epigenetic disruption and behavioral changes following low-dose in utero bisphenol A exposure. Proc Natl Acad Sci USA, 2013; 110 (24): 9956–61. https://doi.org/10.1073/pnas.1214056110 PMID: 23716699

143. Ben-Jonathan N., Hugo E.R., Brandebourg T.D. Effects of bisphenol A on adipokine release from human adipose tissue: Implications for the metabolic syndrome. Mol Cell Endocrinol, 2009; 304 (1–2), 49–54. https://doi.org/10.1016/j.mce.2009.02.022 PMID: 19433247

144. Atlas E., Pope L., Wade M.G., Kawata A., Boudreau A, Boucher J.G. Bisphenol A increases aP2 expression in 3T3L1 by enhancing the transcriptional activity of nuclear receptors at the promoter. Adipocyte. 2014; 3 (3), 170–9. https://doi.org/10.4161/adip.28436 PMID: 25068083

145. Quesada I., Fuentes E., Viso-Leon M.C., Soria B., Ripoll C., Nadal A. Low doses of the endocrine disruptor bisphenol-A and the native hormone 17beta-estradiol rapidly activate transcription factor CREB. Faseb J, 2002; 16 (12), 1671–3. https://doi.org/10.1096/fj.02-0313fje PMID: 12207000

146. Kazemi S., Mousavi S., Aghapour F., Rezaee B., Sadeghi F., Moghadamnia A.A. Induction Effect of Bisphenol A on Gene Expression Involving Hepatic Oxidative Stress in Rat. Oxidat Med Cellul Longev, 2016; 5.

147. Somm E., Schwitzgebel V.M., Toulotte A., Cederroth C.R., Combescure C., Nef S., et al. Perinatal exposure to bisphenol a alters early adipogenesis in the rat. Environ Health Perspect, 2009; 117 (10), 1545–55.

148. Lee J.-E., Ge K. Transcriptional and epigenetic regulation of PPARγ expression during adipogenesis. Cell Biosci, 2014; 4, 29. https://doi.org/10.1186/2045-3701-4-29 PMID: 24904744

149. Al-Bader M, Ford C, Al-Ayadhy B, Francis I. Analysis of estrogen receptor isoforms and variants in breast cancer cell lines. Exper Therapeut Med, 2011; 2 (3), 537–44.

150. Pupo M., Pisano A., Lappano R., Santolla M.F., De Francesco E.M., Abonante S., et al. Bisphenol A induces gene expression changes and proliferative effects through GPER in breast cancer cells and cancer-associated fibroblasts. Environ Health Perspect, 2012; 120 (8), 1177–82. https://doi.org/10.1289/ehp.1104526 PMID: 22552965

151. Lapensee E.W., Tuttle T.R., Fox S.R., Ben-Jonathan N. Bisphenol A at low nanomolar doses confers chemoresistance in estrogen receptor-alpha-positive and -negative breast cancer cells. Environ Health Perspect. 2009; 117 (2):175–80. https://doi.org/10.1289/ehp.11788 PMID: 19270784

152. Alper O., Stetler-Stevenson W.G., Harris L.N., Leitner W.W., Ozdemirli M., Hartmann D., et al. Novel anti-filamin-A antibody detects a secreted variant of filamin-A in plasma from patients with breast carcinoma and high-grade astrocytoma. Cancer Sci, 2009; 100 (9): 1748–56. https://doi.org/10.1111/j.1349-7006.2009.01244.x PMID: 19594548

153. Hoover R.N., Hyer M., Pfeiffer R.M., Adam E., Bond B., Cheville A.L., et al. Adverse health outcomes in women exposed in utero to diethylstilbestrol. N Engl J Med, 2011; 365(14), 1304–1314. https://doi.org/10.1056/NEJMoa1013961 PMID: 21991952

154. Block K., Kardana A., Igarashi P., Taylor H.S. In utero diethylstilbesterol (DES) exposure alters Hox gene expression in the developing mullerian system. Faseb J, 2000; 14, 1101–1108. https://doi.org/10.1096/fasebj.14.9.1101 PMID: 10834931

155. Couse J.F., Dixon D., Yates M., Moore A.B., Ma L., Maas R., et al. Estrogen receptor-α knockout mice exhibit resistance to the developmental effects of neonatal diethylstilbesterol exposure on the female reproductive tract. Develop Biol, 2001; 238, 224–238. https://doi.org/10.1006/dbio.2001.0413 PMID: 11784006

156. Huang W-W., Yin Y., Bi Q., Chiang T-C., Garner N., Vuoristo J., et al. Developmental diethylstilbesterol exposure alters genetic pathways of uterine cytodifferentiation. Mol Endocrinol, 2005; 19(3), 669–682. https://doi.org/10.1210/me.2004-0155 PMID: 15591538

157. Lim W., Jeong W., Kim J-H, Lee J-Y., Kim J., Bazer F.W., et al. Differential expression of alpha 2 microglobulin in response to diethylstilbesterol and in ovarian carcinomas in chickens. Reprod Biol Endocrinol, 2011; 9: 137. https://doi.org/10.1186/1477-7827-9-137 PMID: 21978460

158. Grimm F.A., Hu D., Kania-Korwel I., Lehmler H.J., Ludewig G., Hornbuckle K.C., et al. Metabolism and metabolites of polychlorinated biphenyls. Crit Rev Toxicol, 2015; 45 (3), 245–72. https://doi.org/10.3109/10408444.2014.999365 PMID: 25629923

159. Sugino M., Hatanaka T., Todo H., Mashimo Y., Suzuki T., Kobayashi M., et al. Safety evaluation of dermal exposure to phthalates: Metabolism-dependent percutaneous absorption. Toxicol Appl Pharmacol, 2017; 328, 10–17. https://doi.org/10.1016/j.taap.2017.05.009 PMID: 28506834

160. Kirkup M.E., Murphy J., Beck M.H., Sansom J.E. Occupational contact sensitization to 1,2-diaminocyclohexane. Contact Derm, 2001; 45 (2), 121–122. https://doi.org/10.1034/j.1600-0536.2001.045002121.x PMID: 11553132

161. Ondrus A.E., Lee H.-l.D, Iwanaga S., Parsons W.H., Andresen B.M., Moerner W.E., et al. Fluorescent saxitoxins for live cell imaging of single voltage-gated sodium ion channels beyond the optical diffraction limit. Chem Biol, 2012; 19 (7), 902–912. https://doi.org/10.1016/j.chembiol.2012.05.021 PMID: 22840778

162. Fozzard H.A., Lipkind G.M. The tetrodotoxin binding site is within the outer vestibule of the sodium channel. Mar Drugs, 2010; 8 (2), 219–34. https://doi.org/10.3390/md8020219 PMID: 20390102

163. Dhar S.S., Johar K., Wong-Riley M.T.T. Bigenomic transcriptional regulation of all thirteen cytochrome c oxidase subunit genes by specificity protein 1. Open Biol, 2013; 3 (3), 120176. https://doi.org/10.1098/rsob.120176 PMID: 23516108

164. Orlowska K., Swigonska S., Sadowska A., Ruszkowska M., Nynca A., Molcan T., et al. Proteomic changes of aryl hydrocarbon receptor (AhR)-silenced porcine granulosa cells exposed to 2,3,7,8-tetrachlorodibenzo-*p*-dioxin (TCDD). Plos One, 2019; 14 (10), e0223420. https://doi.org/10.1371/journal.pone.0223420 PMID: 31584984

165. Lim Y., Traber M.G. Alpha-Tocopherol Transfer Protein (alpha-TTP): Insights from Alpha-Tocopherol Transfer Protein Knockout Mice. Nutr Res Pract, 2007; 1 (4): 247–53. https://doi.org/10.4162/nrp.2007.1.4.247 PMID: 20368946

166. Koh M., Takitani K., Miyazaki H., Yamaoka S., Tamai H. Liver X receptor up-regulates alpha-tocopherol transfer protein expression and alpha-tocopherol status. J Nutr Biochem, 2013; 24 (12), 2158–67. https://doi.org/10.1016/j.jnutbio.2013.08.008 PMID: 24231105

167. Johnson C.H., Bonzo J.A., Cheng J., Krausz K.W., Kang D.W., Luecke H., et al. Cytochrome P450 regulation by α-tocopherol in Pxr-null and PXR-humanized mice. Drug Metab Dispos, 2013 (eNov 2012); 41(2), 406–13. https://doi.org/10.1124/dmd.112.048009 PMID: 23160821

168. Kumar D., Yusuf M.A., Singh P., Sardar M., Sarin N.B. Modulation of antioxidant machinery in α-tocopherol-enriched transgenic Brassica juncea plants tolerant to abiotic stress conditions. Protoplasma, 2013; 250 (5), 1079–89. https://doi.org/10.1007/s00709-013-0484-0 PMID: 23361901

169. Park S.-K., Page G.P., Kim K., Allison D.B, Meydani, M. Weindruch, R., et al. Differential effect of α- and γ-tocopherol supplementation in age-related transcriptional alterations in heart and brain of B6/C3H F1 mice. J Nutr, 2008; 138 (6): 1010–1018. https://doi.org/10.1093/jn/138.6.1010 PMID: 18492827

170. Haase K., Pelling A.E. Investigating cell mechanics with atomic force microscopy. J. R. Soc Interface, 2015; 12, 20140970: 1–16.

171. Kamm R.D., Bashir R., Arora N., Dar R.B., Gillette M.U., Griffith L.G., et al. Perspective: The promise of multi-cellular engineered living systems. APL Bioengineering, 2018; 2, 040901. https://doi.org/10.1063/1.5038337 PMID: 31069321